



Norwegian University of
Science and Technology

Influence from Asperities

Modelling of Laboratory Test

Sigurd Sætherø Steen

Civil and Environmental Engineering

Submission date: June 2017

Supervisor: Leif Lia, IBM

Co-supervisor: Gabriel Sas, NORUT
Dipen Bista, IBM

Norwegian University of Science and Technology
Department of Civil and Environmental Engineering



MASTER THESIS

Student: SIGURD SÆTHERØ STEEN

Title: INFLUENCE FROM ASPERITIES
– MODELLING OF LABORATORY TESTS

1 BACKGROUND

Concrete dams are used for forming reservoirs for more than 300 years and still the mechanisms keeping them same are still not fully discovered and good models to predict the stability of the structures are still during development. Concrete dams for most research purposes divided into two groups; massive structures based on gravity and lightweight structures based on static forces. The resistance against sliding is most significant for lightweight concrete dams and this thesis will focus on such structures.

Sliding resistance for lightweight concrete dams such as Ambursen dams (In Norwegian: platedam), buttress dams and gated dams is of outmost importance for the global safety of the dams. For lightweight concrete dams, this is an issue to be mentioned related to the low ratio between the normal force and horizontal forces. Available and accepted methods are not satisfactory solving the problem with realistic determination of shear strength between concrete and rock.

In the period from 2014 – 2018 a research program StableDams are initiated to develop better models to predict sliding resistance and shear capacity in the interface between concrete and rock foundations. In the spring semester of 2017 an intensive laboratory test program has been

developed at Luleå Tekniska Universitet LTU in Luleå to investigate both samples from current dams and artificial samples designed specifically to this research program. This master thesis will focus on FEM modelling to simulate the tests performed in the LTU lab and to describe how this model can be used to predict resistance on full-scale dams.

2 MAIN ISSUES IN THE THESIS

To be done:

- 1) Finite element modelling of shear tests from LTU in the finite element program Atena. A feasible model should be developed with the right material parameters from material tests and literature. The model will be useful for predicting the right failure modes, and it should have similar work diagram and shear capacity as the lab test sample.
- 2) Experiences from the FEM must be used to model a full-scale Ambursen dam pillar from Dam Kalhovd in Telemark. This includes how to discover how scale effects best should be handled, and to make a reasonable representation of the shear capacity of the interface between rock and concrete with respect to geometry and roughness. The result will be compared with analytic methods. A core point is to investigate how the shear capacity of the interface changes with size and position of roughness elements (asperities).
- 3) Proposals for calculation procedures for shear capacity for concrete dams should be developed based on FEM, or other models or methods the candidate find feasible.

Based on experiences from models, the work with scale effects and discussions with the involved parties, the candidate shall give advices on the carrying out of a large-scale shear test.

3 SUPERVISION, DATA AND INFORMATION

Main supervisor at NTNU will be Professor Leif Lia and the co-supervisors will be PhD-student Dipen Bista and Researcher Gabriel Sas in NORUT/LTU. Further collaboration will be organized with LTU (Luleå), KTH (Stockholm), Norut (Narvik), NVE and Statkraft.

The candidate is encouraged to search information through colleges and employees at NTNU, SINTEF, Energy Norway, Authorities and other companies or organizations related to this topic. Contributions from other partners must always be referred in a legal way.

4 THESIS REPORT, FORMAT, REFERENCES AND DECLARATION

The report should be written with a text editing software, and figures, tables, photos etc. should be of good quality. The report should contain an executive summary, a table of content, a list of figures and tables, a list of references and information about other relevant sources. The report should be submitted electronically in B5-format .pdf-file in DAIM, and three paper copies should be handed in to the institute.

The executive summary should not exceed 450 words, and should be suitable for electronic reporting.

The master thesis must be submitted in DAIM not later than the date given in the contract.

Trondheim, March 24. 2017

Leif Lia

SUMMARY

Traditional stability analysis of concrete dams is based on the Mohr-Coulomb failure criteria with a peak friction angle to find the shear capacity. The peak friction angle is often in the range between 40 and 50 degrees, and is highly dependent on the foundation roughness. It is either assumed or set by expert judgement from literature. This method is highly inaccurate, and gives a high error margin. More advanced methods exist, but there is to the authors knowledge no analytical models that takes the deformation in the dam into account.

The aim of this thesis is to find out how well use of the finite element method can describe the shear capacity of a concrete dam, by applying the real geometry of the foundation together with a basic friction angle. The biggest challenge with failure of concrete dams, is that there are so many possible combinations of failure modes. The idea is to let the model calculate all possible failure modes, to find the weakest block in the chain. The simulations were run in the finite element software Atena.

When doing this investigation, it has been important to benchmark the models against a real case. It was therefore decided to model the shear box tests done by Dipen Bista at LTU at the same time as this thesis was made. There were done 22 shear tests of samples of concrete casted on rock, and done material tests. This provided valuable material parameters and test results for the benchmarking of the numerical models made in this thesis.

It was soon made clear that the modelling of the shear test was not straight forward, and it proved hard to get results that matched the tests. Due to lack of time and good test results, only 4 of the 22 tests were modelled. Of these, only two represent the shear tests in a good way, although the two others also give valuable insight, and have many similarities to the shear tests modelled. A parametric study shows that a probable explanation for the differences are the rotational stiffness of the test setup.

At the end, a case study is carried out on one pillar of Dam Kalhovd. The pillar is assessed with finite element analysis, and the real geometry of the foundation with a resolution of about 20 cm. For this section, this increases the factor of safety against sliding from 1.14 with the traditional approach to 1.98 with the new approach. Use of the FEM seems to be a better description of reality than the traditional method. This seems to be a promising way of assessing old dams that are deemed unsafe by new regulations.

SAMMENDRAG

Tradisjonell likevektsanalyse av betongdammer baserer seg på Mohr-Coulombs skjærkriterium med maks friksjonsvinkel for å finne skjærkapasiteten. Maks friksjonsvinkel er ofte mellom 40 og 60 grader, og er veldig avhengig av fundamentets ruhet. Friksjonsvinkelen er enten antatt, eller satt ut ifra tolkning av litteratur. Denne metoden er unøyaktig, og gir en høy feilmargin. Mer avanserte metoder eksisterer, men det er så vidt undertegnede vet ingen av disse metodene som tar deformasjonen i dammen i betraktning.

Målet med denne oppgaven er å finne ut hvor bra endelig elementmetode (FEM) kan beskrive skjærkapasiteten til en platedam ved å bruke den korrekte geometrien til fundamentet og en friksjonsvinkel for flatt skjærplan. Den største utfordringen ved glidebrudd i betongdammer er at det er så mange mulige kombinasjoner av mekanismer. Ideen er å la modellen regne ut alle mulige kombinasjoner for å finne det svakeste leddet i kjeden. Beregningene ble utført i elementmetodeprogrammet Atena.

Når en ny metode brukes er det viktig å kvalitetssikre den. Det ble derfor besluttet å modellere en serie med skjærbokstester som ble utført av Dipen Bista ved LTU samme semester som denne oppgaven ble skrevet. Det ble gjort 22 tester av betong støpt på stein, og det ble utført tester for å finne materialegenskaper. Dette ga verdifulle testresultater for sammenlikning av de numeriske modellene som ble utviklet i denne oppgaven.

Det ble snart klart at det å modellere skjærtesten ikke var rett fram, og det var vanskelig å få resultater som passet med testresultatene. På grunn av mangel på tid og testresultater ble bare fire av testene modellert. Av disse var det bare mulig å få resultater som passet med lab-resultatene for to, selv om de andre to også gav godt innblikk i lab-testenes oppførsel, og hadde mange likheter med lab-testene. En parametrisk studie viser at en sannsynlig årsak til forskjellene er rotasjonsstivheten i testoppsettet.

En casestudie ble utført på pilar 59 fra Dam Kalhovd. Pilaren ble analysert med endelig elementmetode på den reelle geometrien med en oppløsning på omkring 20 cm. For denne seksjonen ble sikkerhetsfaktoren økt til 1.98, sammenliknet med 1.14 med den tradisjonelle metoden. Bruk av endelig elementmetode og reel geometri virker å være en bedre beskrivelse av virkeligheten enn den tradisjonelle metoden, og burde dermed tas i bruk. Dette virker å være en lovende metode for å vurdere gamle dammer som har blitt beregningsmessig usikre på grunn av nye forskrifter.

PREFACE

This thesis is the final part of my master degree at the Department of Civil Engineering at the Norwegian University of Science and Technology (NTNU).

It all started with me studying hydropower engineering and becoming interested in the *finite element method*. Originally it was the problem with the effect of stress concentration at the corners of the dam on the cohesion that got me interested. When I did my project on *reliability based methods in the analysis of concrete dams*, we discussed how to include the friction. I got the idea (which I am not the first to get) that use of the *finite element method* could solve the problem of representing the roughness without any complicated shear criterion. Through this work I have got a good understanding of the problem and a good experience with use of nonlinear finite element analysis.

I want to express special thanks to my co-supervisor Dr. Gabriel Sas at NORUT. He has always been there when I have needed something, kept me motivated and been a good friend. I would like to thank my other co-supervisor Dipen Bista at NTNU/NORUT for letting me use his experimental results for the benchmarking of my models. The experimental results are the property of the Stable Dams project hosted at NORUT, and I claim no intellectual property rights to it. I would also like to thank Dr. Dobromil Pryl at Cervenca consulting for giving good answers to all my questions regarding the finite element software.

I thank Energi Norge for the financial support, which has enabled me to be two weeks in Luleå and one week in Narvik for supervision. The thesis would not have been the same without these stays.

Trondheim, June 11th 2017

Sigurd Sætherø Steen

TABLE OF CONTENT

SUMMARY	i
SAMMENDRAG	ii
PREFACE	iii
1. INTRODUCTION	1
2. THEORETICAL BACKGROUND	2
2.1. State of the art of research on concrete dams	2
2.2. Scale effects.....	7
2.3. Summary of previous work at NTNU.....	12
3. THE STABLE DAMS PROJECT	16
3.1. Why do we need more knowledge of concrete dams?.....	16
4. DESCRIPTION OF THE SHEAR TESTS	18
4.1. General info about the test program	18
4.2. Setup.....	18
4.3. Overview of test samples	19
4.4. Measurements	21
5. PRELIMINARY ANALYSIS OF SHEAR TESTS.....	22
5.1. Hand calculation of sample M5.....	22
5.2. Hand calculation of sample F1	23
5.3. Hand calculation of sample E8	23
5.4. Hand calculation of sample E11	26
6. FEA OF SHEAR TESTS	28
6.1. Introduction.....	28
6.2. Choice of idealization	28
6.3. Building the model in GiD.....	28
6.4. Material properties	40
6.5. Models and results	42
7. CASE STUDY DAM KALHOVD	59
7.1. Introduction.....	59
7.2. Defining the factor of safety.....	59
7.3. Material parameters.....	60
7.4. Model	60
7.5. Results	64
7.6. Parametric study	65
7.7. Assessment of scale effects.....	66

8.	ADVICE ON THE LARGE-SCALE SHEAR TEST	68
8.1.	Introduction.....	68
8.2.	Location of the large-scale test	68
8.3.	Load case	69
8.4.	How to apply loads.....	69
8.5.	Monitoring.....	71
8.6.	Project risks	71
9.	CONCLUSIONS	73
9.1.	Findings.....	73
9.2.	Suggestions for future work	74
10.	SOURCES.....	75
	Appendix A – Derivation of the Mohr-Coulomb formula for inclined sliding	77
	Appendix B – Work diagrams based on LVDT measurements	78
	Appendix C – Results from stability assessment of Dam Kalhovd	86

1. INTRODUCTION

The Norwegian Dam Safety Regulations states that dams in consequence class 2 – 4 shall be reassessed every 15 years, and dams in class 1 every 20 years. The reassessment shall document if the dam is in accordance with the given regulations. These regulations change. The first Norwegian regulation for dams came in 1981 (Konow, 2017). A figure showing construction years for Norwegian dams is shown in figure 1.1:

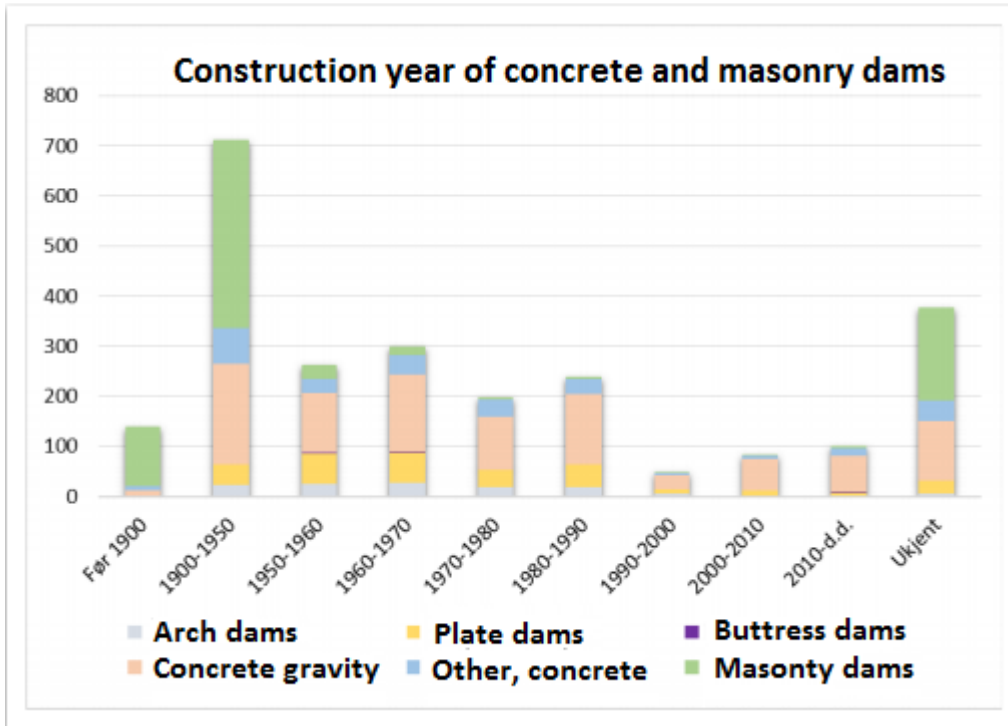


Figure 1.1 Construction years for Norwegian dams from the NVE register (Konow, 2017)

Figure 1.1 shows that almost all Norwegian concrete dams are built before the first regulation. Before 1981, NVE assessed the plans for each dam separately (Konow, 2017). A general trend is that today’s regulations are stricter/different than the NVE practice when the dams were built. The Norwegian dams were built to be safe enough when they were built. The problem now is that “safe enough” has changed. It is not so easy or cheap to change the dams.

This has made a need to prove that many existing dams are still safe enough, using other methods than the traditional methods. For global stability, the traditional method for plate dams is to find a safety factor against sliding and overturning (see equation 2.4). After the new guidelines from 2002, this safety factor must be larger than 1.4 for plate dams and 1.5 for gravity dams (for sliding).

The aim of the thesis is to develop new methods for assessment of the sliding stability of concrete dams. The method used is based on finite element analysis of the dam with the real geometry of the foundation. The hypothesis is that using the real foundation geometry will give a contribution to the resistance capacity large enough that it will be sufficient to only strengthen some pillars on most plate dams.

The objectives of the thesis are to first benchmark the method on some shear box tests with known resistance, and then apply the method to a real size plate dam pillar.

2. THEORETICAL BACKGROUND

2.1. State of the art of research on concrete dams

2.1.1. General stability formulations

The purpose of a dam is to retain water. To obtain this it must be watertight, and be able to resist the loads. Only the load resisting property is of interest for this thesis. A concrete dam can fail in three principle ways, sliding, overturning and material failure. A dam failure is usually a combination of these three. For a dam to resist the loads, all forces and the moment must be in global and local equilibrium. The general way of expressing force and moment equilibrium in 2D is:

$$\sum F_H = 0 \quad (2.1)$$

$$\sum F_V = 0 \quad (2.2)$$

$$\sum M = 0 \quad (2.3)$$

For Norwegian conditions, the most important forces acting on a dam is:

W – hydrostatic pressure. On an inclined surface this is often decomposed into a horizontal and vertical part, W_h and W_v .

I – Ice load

G – Self-weight of the dam

U – Uplift, from the hydraulic pressure under the dam

F_f – Maximum capacity of the friction force under the dam

C – Maximum capacity of the cohesion force under the dam foundation

N – Normal force

Sediment load, earthquake load and hydrostatic back pressure is here neglected for simplicity.

The forces that acts on a concrete dam can be divided into two categories, independent forces and dependent forces. By independent forces are here meant forces which values are given from the other forces. There are two such forces, the friction and the normal force. Given that they have high enough capacity, these forces balance the other forces, both in magnitude and resultant position, to give force and moment equilibrium.

The dimensioning criterion for dams is not that they should be stable, according to the assumptions that are made, but that they should be stable with a margin. For sliding safety this margin is called a factor of safety, FS. A simple way to express this safety factor is that it is the ratio between driving and stabilizing forces. The definition of the FS in the Norwegian guidelines for concrete dams for a horizontal foundation are (NVE, 2005):

$$FS = \frac{c * A + \sum F_V * \tan(\varphi)}{\sum F_H} \quad (2.4)$$

φ is the friction angle, c is the cohesion, and A is the foundation area with compression.

$$\sum F_V = W_v + G - U \quad (2.5)$$

$$\sum F_H = W_h + I \quad (2.6)$$

The correct way to interpret $\sum F_V$ and $\sum F_H$ in dam engineering is thus not the sum of forces acting on the dam, because that should be zero, but the compression and friction forces on the dam foundation. This neglects the normal force, since the normal force is equal to the other vertical forces acting on the foundation. This neglect is ok as long as the capacity of the rock foundation is not exceeded.

2.1.2. Methods for calculating sliding stability

Equation (2.4) is also called *the shear friction method*. A simpler form of *the shear friction method* is the sliding resistance method, which is basically the same, only without cohesion, and slightly different expressed. Both these methods are force equilibrium methods, where the dam is seen as a rigid body. A more accurate way of assessing the sliding stability is to use stress equilibrium instead of force equilibrium, which is called *the limit equilibrium method* (Johansson, 2009):

$$FS = \frac{\tau_f}{\tau} \quad (2.7)$$

Here τ_f is the available shear capacity and τ is the required shear stress to have stress equilibrium in a point. Equation # applies to all parts of the concrete rock interface. To be able to benefit from the use of *the limit equilibrium method*, one need to be able to express spatial stress - strain and stress capacity variation, or at least express the distribution of forces with high resolution. One way to express this is through a Finite Element Method, FEM.

2.1.3. Shear criteria

2.1.3.1. Mohr-Coulomb's shear criterion

To find the sliding stability of a concrete dam, one needs to have an expression for the friction capacity under the dam. The classical formula for the friction capacity is the Mohr-Coulomb criterion (Johansson, 2009):

$$\tau_f = c + \sigma'_n * \tan(\varphi) \quad (2.8)$$

σ'_n is the effective normal stress.

This criterion can be traced back to Leonardo Da-Vinci (Johansson, 2009), and is the most used expression for the friction capacity. It is popular due to its simplicity. Often, the cohesion is hard to find, so it is neglected. The friction capacity formula is then only dependent on one parameter, the friction angle φ , which can be found from guidelines or other literature.

2.1.3.2. Advanced shear criteria

Unfortunately, science has shown that nature is not always that simple. In 1966, Franklin Patton published a book containing a bi-linear shear capacity criterion (Patton, 1966). Doing shear tests on "saw-tooth" samples he derived that there are two possible failure modes for a rock joint, sliding over the asperities, or shearing through. Bonding is not included in Patton's criterion as it is here presented. Patton's criterion is illustrated with the following diagram (Patton, 1966):

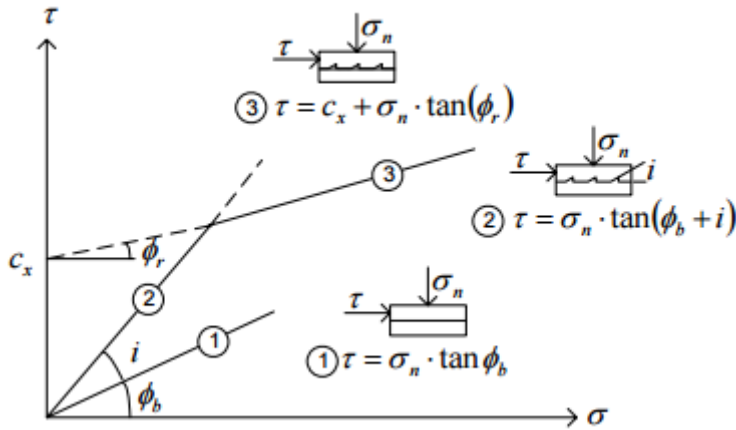


Figure 2.1 Bilinear failure criterion from Patton (1966)

For low normal loads, the sample will have to slide over the asperities, and thus the asperity angle, which in this case is the same as the dilatation angle, is added to the friction angle in the expression. Since there is no bonding, and no material failure, there is no cohesion:

$$\tau_{peak} = \sigma_n * \tan(\varphi_b + i) \quad (2.9)$$

For high normal loads, the peak shear load will exceed the shear capacity of the asperities, and they will be sheared off. Then there is no dilatation, and thus i disappears. Since the surface will have another texture after the asperities have been sheared off, the residual friction angle, φ_r , is used instead of the basic:

$$\tau_{residual} = c_x + \sigma_n * \tan(\varphi_r) \quad (2.10)$$

- τ_{peak} is the peak friction capacity
- $\tau_{residual}$ is the residual friction capacity after sliding has occurred
- σ_v is the normal stress on the interface
- φ_b is the basic friction angle, meaning the peak friction angle of a plain interface
- i is the dilatation
- φ_r is the friction angle when the roughness is cut off.

Between full dilatation and “residual sliding” there is a transition zone, making a curved envelope (Johansson, 2009). One should be careful with using Mohr-Coulomb’s criterion with a literature peak friction angle, since Patton’s criterion shows that it is dependent on the normal load. For samples without asperities, Patton’s criterion is reduced to Mohr-Coulomb’s criterion.

One drawback with Patton’s criterion is that the basic and residual friction angle is dependent on the surface roughness. For a mathematically perfect plain, there is no roughness, so the basic friction angle comes from the micro-roughness, which varies with the preparation of the surface. This makes it important to be consistent when doing shear tests, so that the roughness on the sample reflects the roughness that will be on the actual surface when sliding occurs. Another drawback is that it is made for a man-made idealized joint surface (Johansson, 2009). To make a criterion for a natural rock joint is a much harder task. Some good attempts of this has been made. Among these can be mentioned Barton’s criterion (Barton, 1973), Ladanyi and Archambault’s criterion (Ladanyi and Archambault, 1969), Kulatilake’s criterion (Kulatilake et al., 1995), Grasselli’s criterion (Grasselli, 2001) and Johansson’s criterion (Johansson, 2009). Barton’s and Johansson’s criteria will here be further discussed.

2.1.3.3. Barton's criterion

Barton's criterion is similar to Patton's criterion, only with a curved envelope. The advantage with Barton's criterion compared to Patton's is the ability to calibrate the friction angle to both the surface geometry and the material strength. The criterion was proposed in (Barton, 1973), and further developed in (Barton and Choubey, 1977). Barton's criterion is formulated as:

$$\tau_f = \sigma'_n * \tan \left[JRC * \log_{10} \left(\frac{JCS}{\sigma'_n} \right) + \varphi_b \right] \quad (2.11)$$

JCS – Joint compressive strength. For unweathered surfaces, this equals the compressive strength of the materials. For weathered joints, it is not that simple. The JCS is proposed set by use of a Smith hammer (Barton and Choubey, 1977). If nothing else is known, $\frac{1}{4}$ of the compressive strength could be used (Barton and Choubey, 1977).

JRC – Joint roughness coefficient. This parameter reflects the surface roughness, and could be set by visual comparison with some typical roughness profiles presented in (Barton and Choubey, 1977), or from tilt tests on small samples by formula (2.12) (Barton and Choubey, 1977):

$$JRC = \frac{\varphi' - \varphi_r}{\log \left(\frac{JCS}{\varphi'_n} \right)} \quad (2.12)$$

φ' is the basic friction angle found from tilt tests.

If the surface is weathered, it is proposed to use the residual friction angle instead of the basic, and if nothing else is known, this can be estimated to 20° (Barton and Choubey, 1977).

One of the main advantages with Barton's criterion is that shear capacity scale effect can be implemented, which will later be explained.

2.1.3.4. Johansson's criterion

Johansson made a conceptual model to find the shear capacity of a triangular asperity (Johansson, 2009). What is interesting with Johansson's criterion is that it is built on an understanding of the real process, and not just curve-fitting. An important keyword is the matedness of the joint surfaces, which expresses the relative size of the contact area between two surfaces (Johansson, 2009). Even though it is not perfect, it provides a foundation to build a good general model on. The roughness part of the model is based on a triangular asperity, exposed to shear load, and a normal load equal to the compressive strength of the rock. The explanation of the high normal load is that for a real surface, there will be few contact points when the sample starts to slide, and the force on each contact will crush the contacts with highest stress, until all contact points has a normal load equal to the compressive strength. The model is based on Patton's criterion, identifying three possible failure modes:

- 1) sliding over the asperity. The formula for this is given in eq. (2.9) in Patton's criterion.
- 2) Shearing through the asperity at the base. The formula is the same as eq. (2.10) in Patton's criterion.
- 3) Tensile failure of the asperity. A new formula is here introduced (Johansson, 2009):

$$T = \frac{(3 * \sigma_{ci} + 4 * \sigma_{ti}) * L_{asp}^2}{2 * \tan(i)} \quad (2.13)$$

T – Shear resistance of the asperity

σ_{ci} – Uniaxial compressive strength of the asperity material

σ_{ti} – Tensile strength of the asperity material

L_{asp} – Dimension of the asperity (assumed quadratic shape in the interface plain)

i – Asperity angle

The principle is that the failure mode giving the smallest capacity will be the failure mode happening, and for a standard hard rock ($\sigma_{ci} = 100 \text{ MPa}$, $\sigma_{ti} = 10 \text{ MPa}$ and $\varphi_b = 30^\circ$), the following diagram can be calculated:

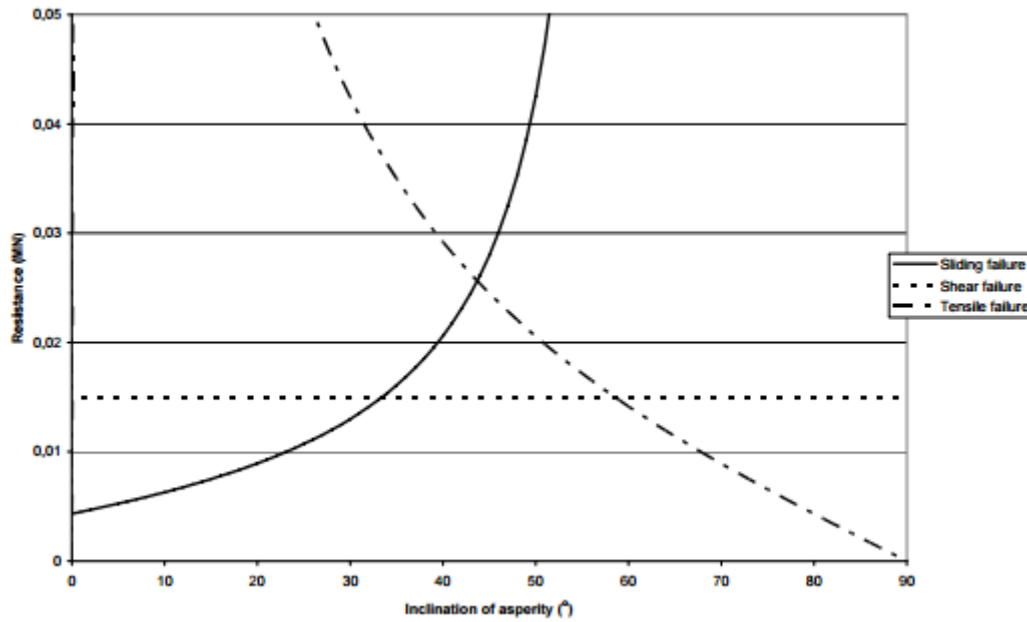


Figure 2.2 Resistance capacity for different failure modes from (Johansson, 2009)

Figure 2.2 shows that for asperities with angles up to 34 degrees, the failure mode will be sliding over the asperities, for 34 to 68 degrees, the failure mode will be shear failure, and from 68 degrees it will be tensile failure of the asperities.

Equation (2.13) is made by taking moment equilibrium about the toe of the asperity, as shown in figure 2.3:

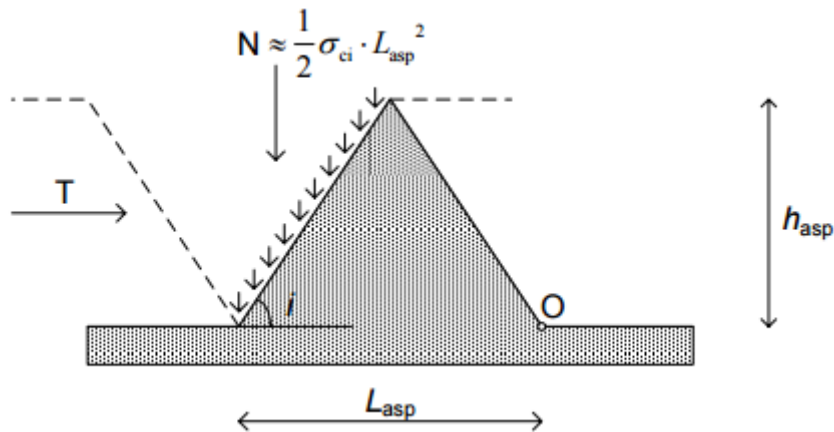


Figure 2.3 Illustration of the conceptual model from (Johansson, 2009)

The formula for the moment equilibrium is formulated as:

$$T * \frac{L_{asp} * \tan(i)}{4} - N * \frac{3}{4} * L_{asp} = \sigma_{ti} * L_{asp}^2 * \frac{L_{asp}}{2} \quad (2.14)$$

(2.14) can be rearranged to (2.13). But there is a problem with (2.14), it overestimates the capacity from the tensile strength by a factor of two. It is reasonable to assume that rock behave similar to concrete in tensile failure, and standard construction concrete is linear elastic until tensile failure (see figure 6.3). If the asperity overturns as a rigid body, the stress should not be equal to the tensile stress capacity over the whole base, but distributed linearly from σ_{ti} at the front of the asperity to zero at the toe. The average stress should then be $\frac{\sigma_{ti}}{2}$, but the arm should be $\frac{2 * L_{asp}}{3}$ instead of $\frac{L_{asp}}{2}$, making the contribution from the tensile strength $\sigma_{ti} * L_{asp}^2 * \frac{L_{asp}}{3}$, giving a reduction of 16.6 % ($\frac{1}{6}$).

(2.13) can then be re-written as eq. (2.15):

$$T = \frac{(9 * \sigma_{ci} + 8 * \sigma_{ti}) * L_{asp}^2}{6 * \tan(i)} \quad (2.15)$$

Johansson's shear criterion was compared with shear test on split core samples and a large-scale test. The average friction angle found with the shear criterion were in average 55.6°, while the shear test found an average friction angle of 45.8°.

2.2. Scale effects

2.2.1. Scale effect from literature

Scale effects exists for many properties. In this section will be treated scale effects in the shear capacity of rock joints. Scale effects of mesh size is treated in section 6.3.3.1. The presentation of scale effects in the shear capacity of rock joints will be based on Barton's shear strength criterion, for which a scale effect theory is developed.

Bandis, Lumsden and Barton investigated the scale effect of different roughness scales of rock joints (Bandis, 1980). Rock joints in a medium hard rock ($\sigma_c = 80\text{MPa}$) where simulated by a weak ($\sigma_c = 0,75 - 4,45\text{MPa}$), concrete-like brittle material. This made it possible to scale down the length scale so that it was possible to simulate prototype joints of 2 – 12 meters. A casting mould of the rock joint of interest was made, and a brittle material was casted into the casting mould to create multiple similar replicas. The replicas where tested in shear with different sample length and size.

Some of the conclusions from Bandis (1980) are listed here:

- Large samples have lower shear capacity/friction angle than small ones. This effect is asymptotic, meaning that the reduction in friction angle with the increase in sample size goes towards zero as the sample size goes towards infinity. The friction angle converges to the residual friction angle as the size increase.
- The contact area decreases with increasing sample size. At the same time the size and number of contact areas increase with increasing sample size. This can be explained by that larger samples have larger asperities, and the contact areas will therefore be larger and fewer relative to size.
- The intrinsic strength of rock is inverse proportional to sample size, but this effect is decreasing in the same way as the friction coefficient. This effect will cause smaller roughness elements to have a higher average limit stress than large ones, and can explain the decrease in friction angle with increasing sample size, since larger samples also have larger contact points.

- Large samples have higher peak shear displacement. Rule of thumb is that peak shear deformation is equal to 1 % of the sample length, but less for large samples (>3 m). Mark that Grasselli (2001) has related this to the crystal size.

If we relate this to Barton's shear criterion, increased block size tends to decrease JRC and JCS. In (Barton and Bandis, 1982) is presented formulas for the size effect on JCS and JRC:

$$JRC_n = JRC_0 * \left(\frac{L_n}{L_0}\right)^{-0.02JRC_0} \quad (2.16)$$

$$JCS_n = JCS_0 * \left(\frac{L_n}{L_0}\right)^{-0.03JRC_0} \quad (2.17)$$

The formulas are based on curve fitting from 137 shear tests on rock joints.

A scale dependent expression for the peak strength displacement δ is made (Barton and Bandis, 1982):

$$\delta = \frac{L}{500} * \left(\frac{JRC}{L}\right)^{0.33} \quad (2.18)$$

Johansson (2009) states that for perfectly mated joints, there should be no scale effects. According to Johansson (2009), the scale effect increases with the decreasing degree of matedness.

It should be mentioned that none of the scale effect theories known to the author includes the degree of stress mobilization. An example of such a scale effect is the tensile strength of a paper when ripping it from one side. The tensile strength of the paper is then independent of the length of the paper, since the stress is only mobilized around the edge of the crack. For a paper, this effect is due to the out-of-plane bending of the paper, but a similar effect would be there also with only in-plane-deformation, for example in a concrete dam, or in a concrete plug in hydropower tunnels. The crack starts at the front of the dam, and propagates. This effect increases, the larger the structure is, since the peak strength deformation is not proportional to the scale of the structure (Grasselli, 2001). This effect is tried quantified through an example, applying data from Liahagen (2012) on a section of a typical concrete dam.

2.2.2. Quantification of the scale effect from flexibility

The E-modulus of concrete is about 30 GPa. A large plate dam is 30 m high and with 30 m bottom width. The pillars are 0,6 m wide at the bottom (B_W) and there is 6 m c/c between the pillars. This gives a water pressure of 300 kPa on the dam at the bottom. The static situation that gives the largest deformation of the dam is if the dam is hinged at the toe with no friction under the dam. The displacement of the front of the dam could then be estimated by eq. (2.19):

$$\Delta x = \frac{\sigma_x * B_W * \frac{c}{c}}{E * t} = \frac{300 \text{ kPa} * 30\text{m} * 6\text{m}}{30 \text{ GPa} * 0.6\text{m}} = 3 \text{ mm} \quad (2.19)$$

If the uptake of forces is distributed equally over the length, the deformation is halved to 1,5 mm. For a real dam loaded to its capacity for sliding the situation will be something between, since the normal forces will be largest near the toe and small near the upstream side. It is important to keep this order of magnitude in mind when transferring knowledge from shear tests to a large-scale interface. The problem is if the deformation in the upstream part of the dam can pass the peak stress deformation before this capacity is reached in the downstream part of the dam. A rigid body approach will thus underestimate the real capacity, but how much? If the dam is infinitely stiff the

rigid body approach will be a perfect estimation. The worst case is the situation where the dam is hinged at the toe, with a deformation through the dam of 3 mm. Whether this is a problem will depend on the shape of the asperities. For a perfectly plane and smooth foundation, there is no problem since there will then be no peak stress, but only the residual strength the whole time. For asperities with 20 degrees, the load diagram of test 2.2 from Liahagen (2012) is shown in figure 2.4, and can be used to investigate whether this is a problem. What makes the results from this test useful, is that the deformation is measured close to the concrete rock interface. Else rotation and shear deformations tend to give increasing displacements with increasing height over the interface. Sample 2.2 had a normal stress of 0.83 MPa, which is in the same order of magnitude as would be found in such a dam as here is of interest.

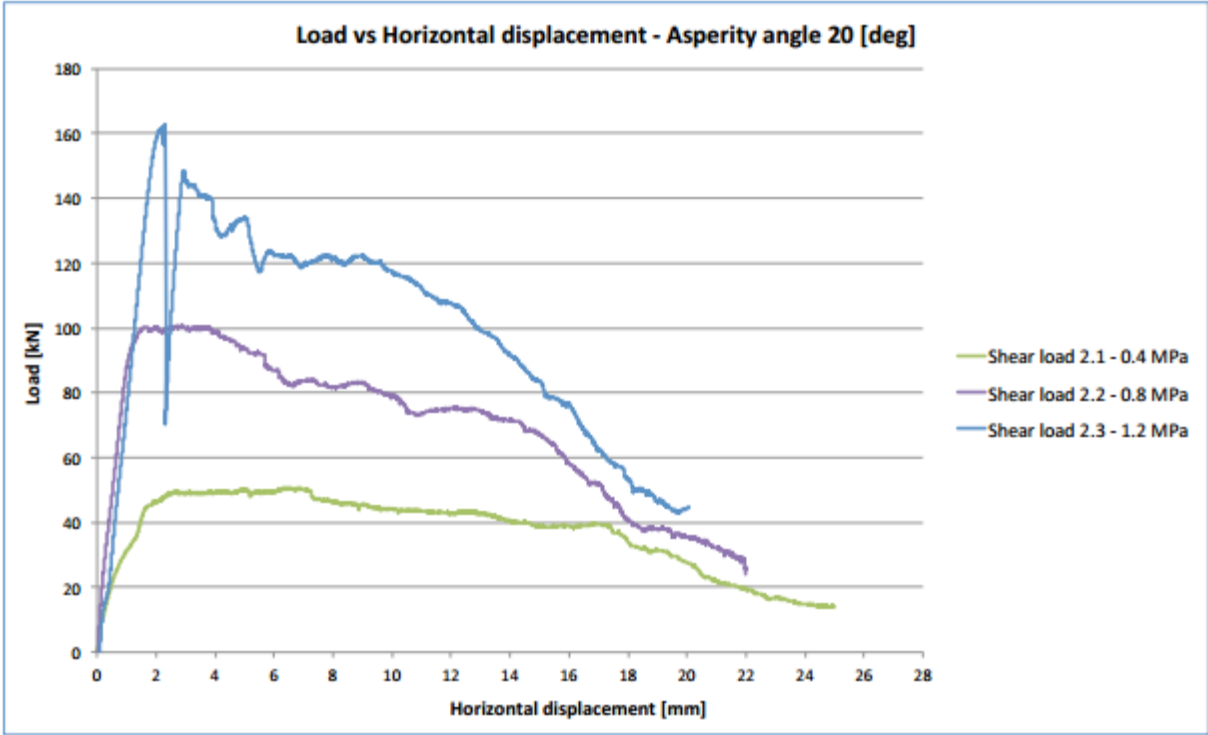


Figure 2.4 Shear stress - strain diagram for saw teeth samples of concrete on rock with asperity angle 20° from (Liahagen, 2012)

As can be seen from figure 2.4, the zone of peak stress deformation is about 4 mm, making it possible for the whole dam to have peak stress at the same time, and justifying the use of a rigid body approach.

But what happen if the asperity angle is increased or the size of the dam is larger? The work diagrams for the tests by Liahagen, with 40 degrees asperity angle, is given in figure 2.5:

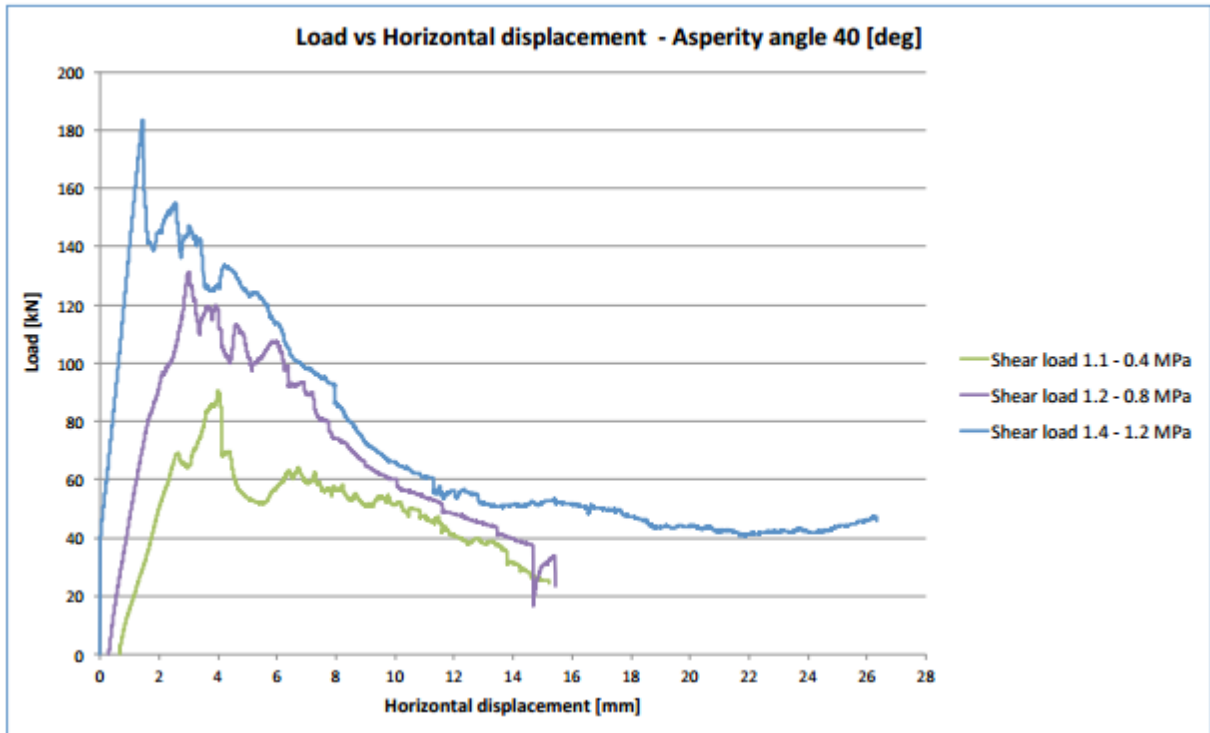


Figure 2.5 Shear stress - strain diagram for saw teeth samples of concrete on rock with asperity angle 40° from (Liahagen, 2012)

If the load diagram for test 1.2, shown in figure #, were transferred to a real dam, the maximum capacity would be reached when the dam toe reaches its peak, because the load diagram is flatter after the peak. The peak average stress would then be the average of the peak stress of the work diagram and stress with 3 mm more deformation, as shown in figure 2.6:

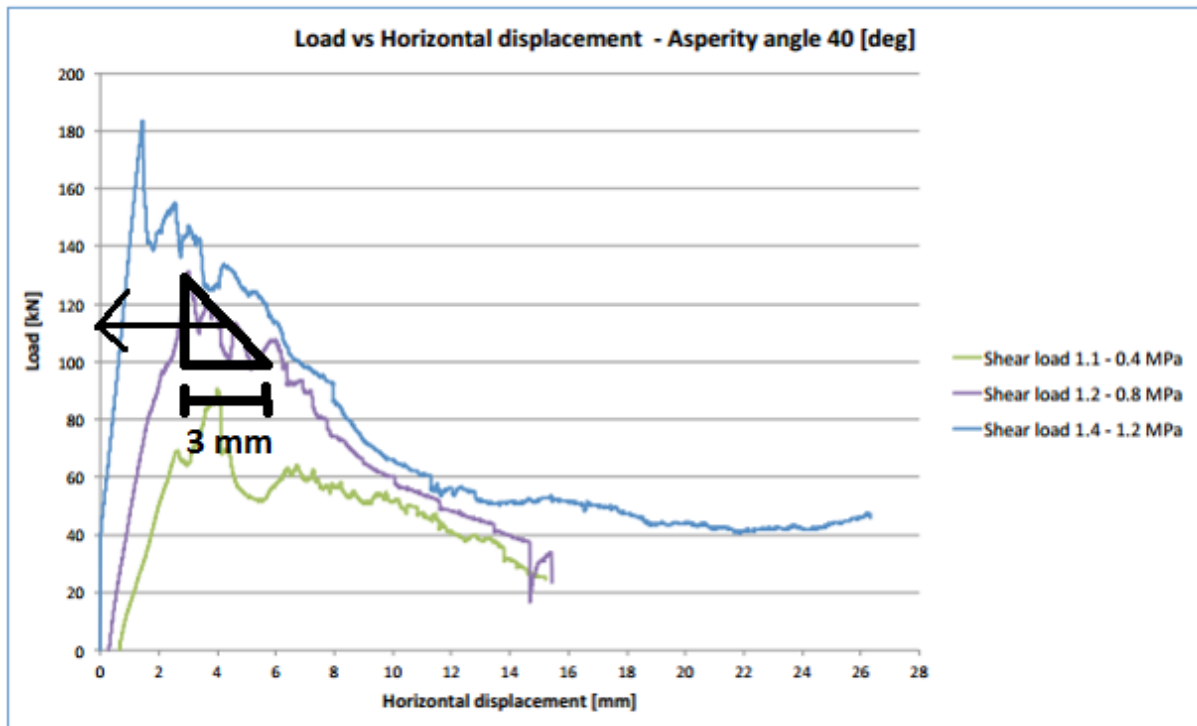


Figure 2.6 Shear capacity as a function of the interface displacement, giving an average shear capacity for a structure with 3 mm maximum displacement

The peak load is 130 kN, the load with 3 mm more deformation is 100 kN, giving an average peak load of 115 kN for the dam hinged at the toe. Using the peak capacity directly from the shear test would then underestimate the capacity by about 12 %. The amount of underestimation by not taking the deformation in the dam into account would increase with the angle of the asperities and the size of the dam. Since a concrete gravity dam will deform by about one tenth of a plate dam, the problem will not be so big for similar dams, but gravity dams are often larger. If this methodology should be applied in a real case, one should use the same load value to find the deformation of the dam, as the one found from the work diagram, which makes it in principle an iterative methodology. If this would be an issue would depend on if the safety factor is used to increase the load or reduce the shear capacity. It should be noted that in (Liahagen, 2012) it is used LVDT measurements of displacement (see section 4.4). In section 4.4 is found that the LVDT measured displacements are much larger than for the other measurement system. It is therefore reasonable to assume that the average peak displacement for the dam should be smaller than what is found here.

One factor that helps the dam is that also the rock mass under the dam deforms. That is why one include a large rock foundation when making FEMs of dams. This effect is larger for gravity dams than for plate dams, since plate dam pillars have about 10 times as much rock foundation per m pillar than gravity dams.

For the flexibility scale effect to be included in a FEA, it would need to be used a non-linear shear criterion for the peak stress behavior. Such a shear criterion is not available in the software used in this thesis.

2.3. Summary of previous work at NTNU

This master thesis is one in a row at the Department of Civil Engineering at NTNU, on the shear capacity of concrete dams. In this section, a brief summary of previous works is presented.

2.3.1. Stølen's master thesis

(Stølen, 2012). The goal with the thesis is to calculate the stability for dam Målset through the use of FEA, and through that work develop procedures that could be used also for other dams. Atena was chosen for the FEA, and a model was made of a plate dam pillar with real geometry. Since there was lack of good material data the model could not say anything sure about the stability of the dam, but compared to hand calculations done with the same material data it gave good insight into the behavior of the dam.

2.3.2. Liahagen's master thesis

(Liahagen, 2012). The topic for this master thesis is what factors influence the shear capacity of concrete dams, and more specifically to do shear tests to quantify the influence of asperity angle and normal stress. 12 shear tests were done on samples of concrete casted on granite blocks, at the rock mechanics lab at Luleå University. It is shown that steeper asperities give higher peak strength, and that the failure mode changes from sliding over the asperities at low asperity angles, to shearing through the asperities at high asperity angles. A picture of a sample in the test apparatus is shown in figure 2.7, and the shape of the interface between concrete and rock in the samples are shown in figure 2.8:



Figure 2.7 One of the samples from Liahagen in the testing machine

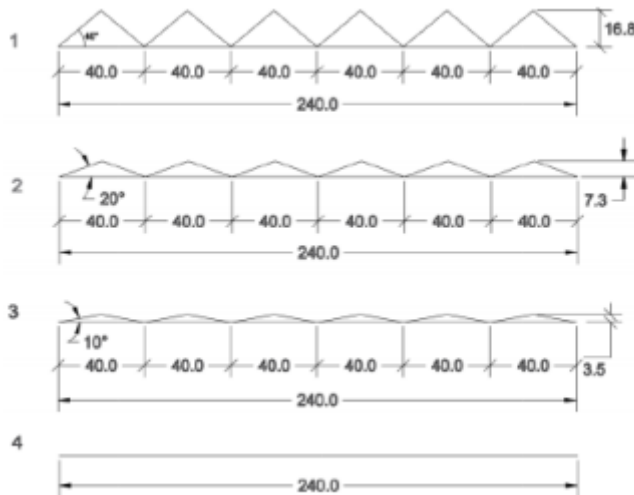


Figure 2.8 The shape of the samples from (Liahagen, 2012)

The width of the samples is 240 mm. The surface is smooth, but not polished. Because of this, micro-roughness is present, and the macro-roughness is the triangular asperities. The results from the tests are given in table 2-1:

Table 2-1 The results from (Liahagen, 2012)

Sample	i	N	V	δ_{II}	σ_n	τ_{max}	ϕ_{max}	$\delta_{II_{max}}$	Notes
	[°]	[kN]	[kN]	[mm]	[MPa]	[MPa]	[°]	[mm]	
1.1	40	27.52	90.53	4.00	0.48	1.57	73.08	15.23	
1.2	40	46.91	131.19	3.03	0.81	2.28	70.32	15.44	
1.3H	40	72.47	299.17	3.58	1.26	5.20	76.41	5.07	Bond
1.4	40	68.49	183.42	1.44	1.19	3.18	69.52	26.34	
2.1	20 ²	27.57	50.74	6.39	0.48	0.88	61.48	24.99	
2.2	20	47.77	100.59	2.86	0.83	1.75	64.60	21.98	
2.3	20	68.36	162.83	2.30	1.19	2.83	67.23	20.07	
3.1	10	24.82	35.38	9.78	0.43	0.61	54.95	33.16	
3.2	10	45.98	58.70	6.55	0.80	1.02	51.93	32.94	
3.3	10	67.65	85.43	2.83	1.17	1.48	51.63	33.23	
4.1H	0	67.85	240.00	2.49	1.18	4.17	74.24	14.59	Bond
4.2	0	67.23	52.04	33.23	1.17	0.90	37.74	33.23	

The load is applied as a pure shear load, and the normal load is applied in the middle of the top side. The failure modes of most of the samples are sliding over the asperities, with damage to the top of the asperity before it slides over. Pictures of the samples after testing shows that the amount of damage to the asperity increase with the asperity angle and the normal force. All the samples with a 40 degree asperity angle fails by material fracture with almost no sliding, and the higher the normal force, the more damage. The cohesion of the bonded tests can be found from test 4.1H and 4.2 as the difference between the shear capacities, and can thus be quantified to 3,3 MPa. This is far less than the estimated concrete material cohesion of 8,2 MPa, which is an indication that the interface between concrete and rock would be a probable failure plane for a concrete dam on a smooth foundation, even with bonding.

The most interesting conclusion from this thesis is that the asperity angles have much larger influence on the capacity of the samples than the normal load. If this is transferred to concrete dams

it gives the possibility of preparing the foundation with a large roughness and use less concrete in the dam for weight. This will require good tools and methods for verifying the shear capacity.

2.3.3. Eltervaag’s master thesis

(Eltervaag, 2013). The topic of this thesis is to model the shear tests from Liahagen (2012) in the finite element program Atena (Cervenca Consulting, 2017), and apply the experience from these models to make a model of a full-scale dam section. Material data was taken from material tests, literature and the Atena manual (Cervenca et al., 2013).

In Atena, the model for resistance against sliding is based on the Mohr-Coulomb shear criteria. Eltervaags approach was based on Patton’s criteria for sliding, which he was able to implement in Atena by use of cohesion softening. Patton’s criterion is given in (2.9) and (2.10).

For the friction coefficient is used the residual friction angle, found from shear test 4.2, which had a flat interface (see table 2-1). For catching the peak capacity is used the cohesion parameter in Mohr-Coulomb. This can be seen in figure 2.9, where the cohesive parameter is gradually reduced over a distance of 15 mm. It has no physical meaning as cohesion, but it seems to be a good way of representing the gradual wearing of micro-roughness.

A large part of the work was to do a parametric study of the stiffness of the interface material. The problem was that the recommended stiffness created an ill-conditioned system (Eltervaag, 2013). The following figure shows how much the interface stiffness can mean for the resulting work diagram:

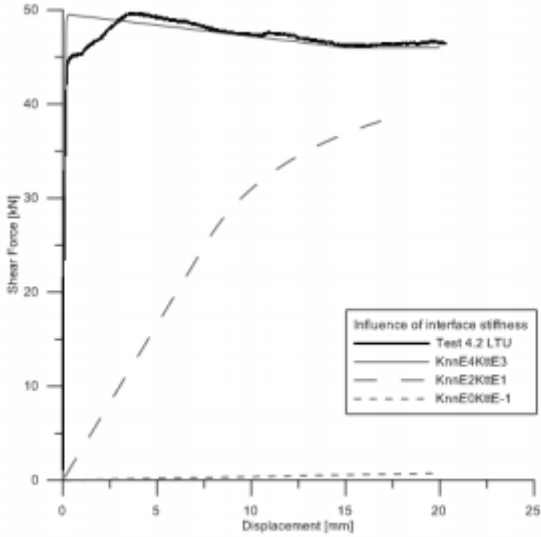


Figure 2.9 Influence of the interface material stiffness (Eltervaag 2012)

The figure shows the result from test 4.2. This test has a flat interface and a normal stress of 1,2 MPa. The right tangential stiffness was found to be $6 \cdot 10^3 \frac{MN}{m^3}$. The best fit tangential stiffness for the other samples ranged between $6 \cdot 10^2 \frac{MN}{m^3}$ and $6 \cdot 10^3 \frac{MN}{m^3}$.

After the parametric study of the interface material stiffness, the result from the FEM fitted the results from the shear test very well, with an average error on the peak stress of about 2 % and a

maximum error of 6 %. The experience from test sample modelling was used to model a part of a full-scale dam. An interesting comment from Eltervaag is that when trying to model a test where the failure mode consists of shearing through the asperities the model crashes before failure is reached. This problem is solved by using a flat interface, and treat the asperities as roughness through the friction angle, which gives a good result.

2.3.4. Nymo's master thesis

(Nymo, 2016). The main finding in this thesis is that the beam formula underestimates the zone of compression in the dam, while it is quite straight forward to find it with a FEM. The zone of compression is important to find, since it is a common assumption that bonding only occur in this zone.

3. THE STABLE DAMS PROJECT

This thesis is written in collaboration with NORUT, as a part of the Stable Dams project. The project is financed by the Norwegian state, the hydropower producers and the main consultant companies. It is hosted at NORUT Narvik, which is a North-Norway research institute working with northern technology. The background for the project is that there are some thousand concrete dams in Norway, and new guidelines have deemed many of them unsafe, creating a need for investments of billions in upgrading to meet the requirements.

3.1. Why do we need more knowledge of concrete dams?

There are many assumptions in the capacity assessment of concrete dams. These assumptions rise from the fact that there are a lot of variables, of which statistical distributions and relations are not known. In a perfectly deterministic world one could, given enough data, predict exactly future events. For the purpose of designing concrete dams, this means that one would be able to calculate the necessary capacity exactly, and do the design to meet the requirements. There are two problems with this, the world is not deterministic, and even if it were, there is not enough data. This can be proven through respectively the use of Heisenberg's uncertainty principle, and the fact that the elementary building blocks, the atoms, are so small and numerous that no computer model could be able to hold all their unique positions, relations, velocities, and other relevant properties. To design concrete dams, one must therefore use statistics. The simplest way to do this is to have one parameter: The dam. This is the same as using historical data, saying that "the dam will be safe enough if we do it like this, because we have done it like this before, and it worked". Since no dam is built exactly like another, this requires some classifications into separate groups, f. ex "concrete gravity dams lower than 15 meters built after 1950". The problem with this method is that it does not give enough information to use it in the design process for a particular dam. To have better data we need to use more parameters. This reduces the uncertainty related to each parameter, since they then become more general and cheaper to test, but it requires better knowledge of the relation between the parameters, and it requires more data. It seems to be a general law that the accuracy of a prediction increases with the amount of data that are being utilized, given that the data is relevant and correct, and used in the right way. This can be illustrated with trying to find the statistical distribution of a data set from point observations. One point says nothing, two points can give a straight line, three points can give a parabola, and so on. Three points can also give a straight line, but it can also be a higher order function, or random. The more points added that fits the straight line, the higher the probability that the hypothesis is correct, but one can never be sure, even if all the data fits, because it can be a higher order function, it can be random, or there could be errors in the data set.

So, what does this have to do with dam construction? If more data about the material properties can be utilized, the capacity prediction can come closer to the true capacity, reducing the uncertainty margins and the construction costs. And what is more relevant for the Norwegian hydropower industry, it can prove that dams that are deemed unsafe after new regulations are safe enough, or reduce the required rehabilitation. But with increasing complexity, the chance of errors increases. The more complex methods therefore require increased knowledge of both the true relations between parameters and the computational tools. To get this knowledge is an investment that will hopefully spare construction and rehabilitation costs and/or structural collapses. As all other investments, there is a relation between the size of the investment and the return on the investment. The marginal rate of return on an investment decrease to zero as the size of the investment goes towards infinity. In the case of concrete dam knowledge, the maximum possible benefit is to build a dam that exactly meet the required capacity to withstand the loads through its

lifetime with 100 % certainty. This is a limited gain given a limited time span, while the expenditure required to achieve it is infinite. Between the simple “one parameter approach” (general dam statistics) as described earlier, and “the correct solution”, there seems to be an economic optimum, where the marginal cost of more research equals the marginal benefit.

The problem with using this approach to find the optimal amount of knowledge is that the relation between investment and return is very unsure. But one thing that can be done is to give reasonable arguments that an investment in knowledge is or is not feasible.

In a survey done by Jensen in 1998, it was concluded that the cost of bringing all the dams up to the required standard was 2,5 billion NOK (Jensen and Skoglund, 2000). The price of a new 15 m high and 100 m long concrete dam is about 50 million NOK, according to (Norconsult, 2016). As a comparison, the budget of the Stable Dams project is 17 million NOK. If Stable dams can spare more than 1 % of the costs related to dam upgrading, or translated to a more practical case, if Stable Dams has more than a 40 % chance of avoiding the unnecessary replacement of one medium sized dam, it is an economic success.

4. DESCRIPTION OF THE SHEAR TESTS

4.1. General info about the test program

The shear tests carried out at Luleå Tekniska Universitet in the spring of 2017 are a part of the Stable Dams Project, which is carried out by NORUT, in cooperation with the Norwegian hydropower sector. The planning and experimental work was done by Mr. Dipen Bista at NORUT. The main motive of the Stable Dams project is to investigate the mechanisms that occur in the failure of a concrete dam, and in this test program, the role of the positions of asperities in the interface between dam and concrete is investigated.

4.2. Setup

Shear tests were carried out on approximately cubic samples of the interface between concrete and rock with different location of asperities. The test setup is shown in figure #, and a simplified sketch is shown in figure #. It must be pointed out that the simulation models, and also figure # is mirrored compared to figure #.

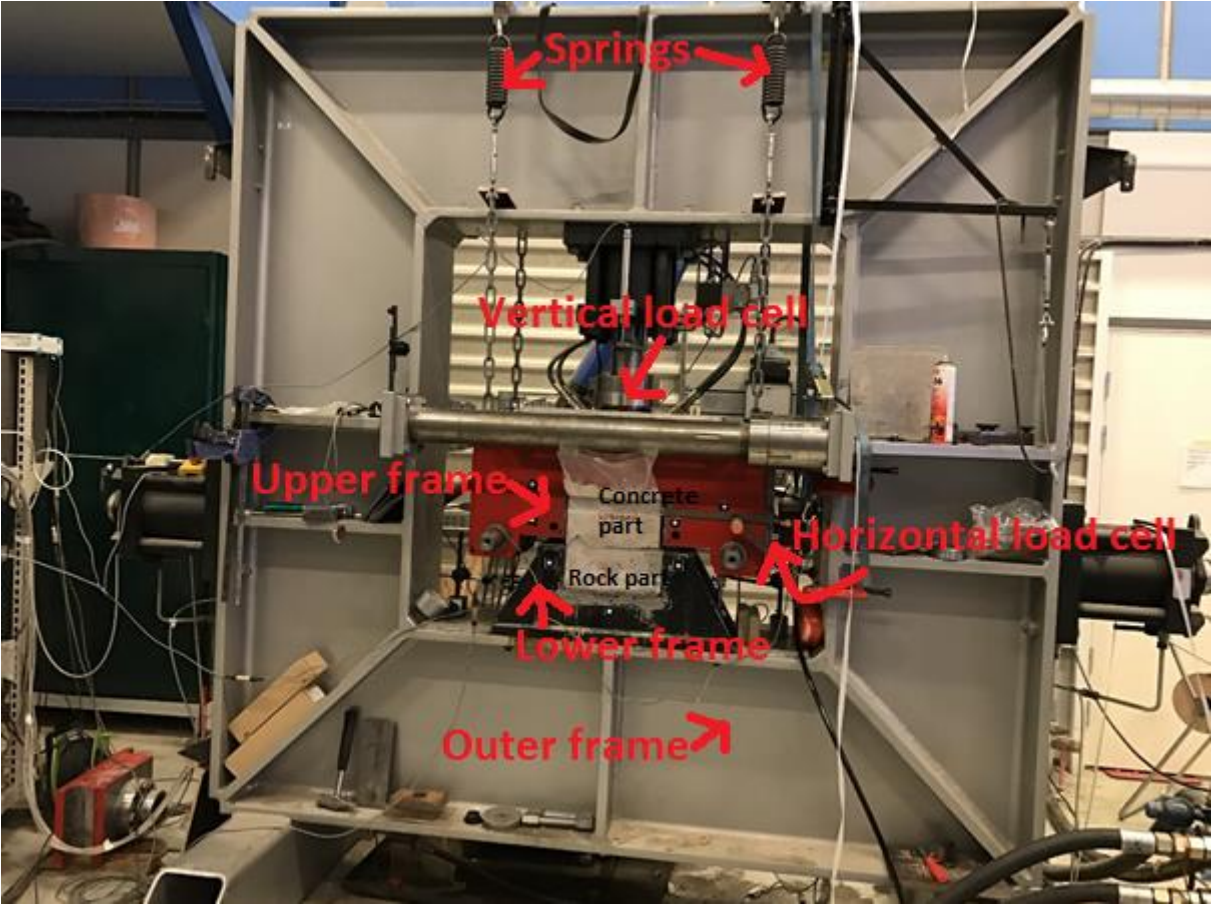


Figure 4.1 Test setup for the shear box tests on man-made asperities done at LTU in the spring 2017

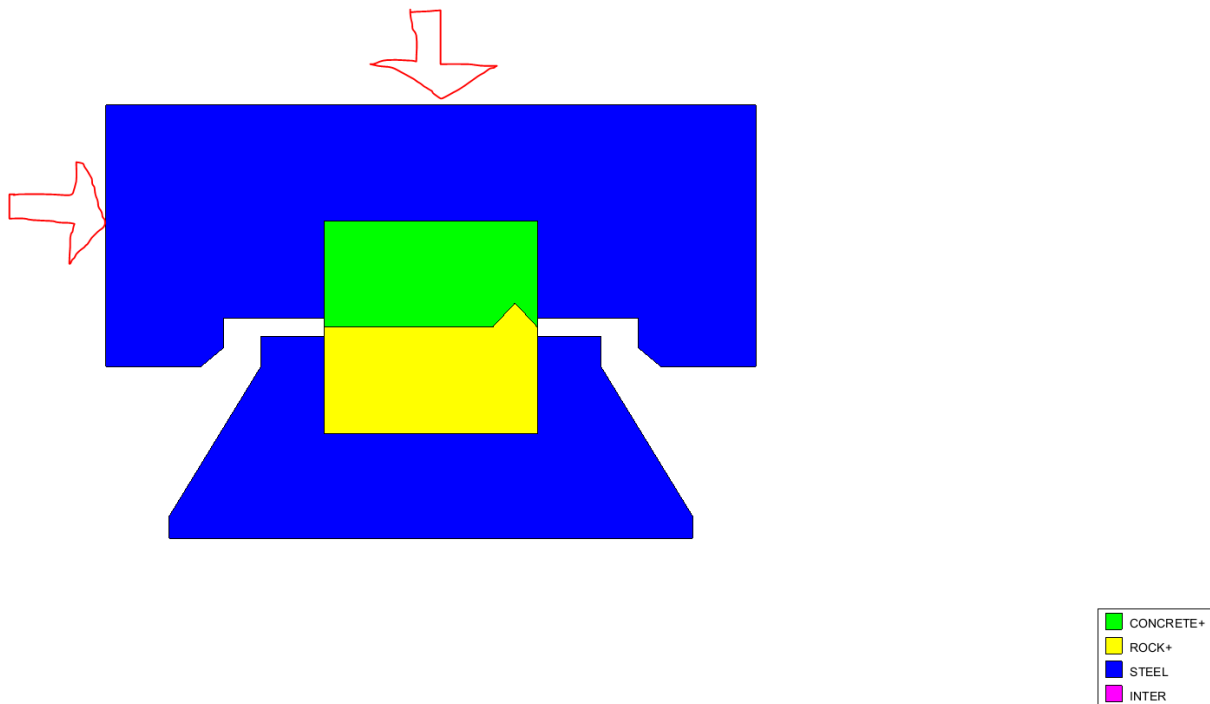


Figure 4.2 A principle sketch of the test setup from figure 4.1. Note that this sketch is mirrored.

To investigate the effect of asperities there are done three types of samples, one with an asperity placed at the toe (as in figure 4.2), one with an asperity placed in the middle and one with the asperity at the heel (the load side). The samples are named respectively A, B and C, and sample A is shown in the setup in figure 1. There were also done some samples without asperities. The dimension of the samples is approximately 280 mm X 280 mm X 270 mm.

The samples are made by cutting of high quality gneiss rock into the right shape, and casting of the concrete directly at the rock sample. To avoid bonding between the layers, a thin rubber sheet is sprayed on the surface of the rock before casting of the concrete. The rubber is scraped of before the tests are made, so that the interface is clean. The interface between concrete and rock (hereafter referred to as the interface) is flat but not polished. This gives an artificially low roughness, but it is a technical necessity to be able to produce an un-bonded sample and still be able to scrape away the rubber sheet. An alternative could be to use a viscous substance that can washed of, f. ex. fat, but such substances would also severely affect the properties of the concrete.

4.3. Overview of test samples

Two types of tests were done, tests with the load placed as in figure 4.2 which allows rotation, and a setup with the load placed further down where the rotation is blocked, making it a pure shear test. These types are hereafter referred to as respectively samples with eccentric and non-eccentric load.

Both load cases with all three asperity positions is tested with three different normal loads of 1 MPa, 0.6 MPa and 0.2 MPa. The details on all the tests are shown in table 4-1:

Table 4-1 Test matrix from shear box tests done on man-made asperities at LTU in the spring of 2017

Name	Load case	Asperity position	Vertical load [MPa]	Shear load capacity [MPa]
E1	Non-eccentric	Heel	1	2.8
E2	Non-eccentric	Heel	0.6	1.9
E3	Non-eccentric	Heel	0.2	1.0
M2	Non-eccentric	Middle	1	2.8
	Non-eccentric	Middle	0.6	Test failed
M3	Non-eccentric	Middle	0.2	1.2
E8	Non-eccentric	Toe	1	2.6
E9	Non-eccentric	Toe	0.6	2.1
E10	Non-eccentric	Toe	0.2	0.8
F1	Non-eccentric	None	1	0.9
F6	Non-eccentric	None	0.6	0.6
E4	Eccentric	Heel	1	0.7
E5	Eccentric	Heel	0.6	0.4
E6	Eccentric	Heel	0.2	0.3
M7	Eccentric	Middle	1	1.4
M5	Eccentric	Middle	0.6	1.1
M6	Eccentric	Middle	0.2	0.4
E11	Eccentric	Toe	1	2.4
E12	Eccentric	Toe	0.6	1.8
E13	Eccentric	Toe	0.2	0.5
F3	Eccentric	None	1	0.8
F4	Eccentric	None	0.6	0.3

The justification of having these two different load cases is that the eccentric load case has stresses similar to a scaled model of a dam, with a combination of sliding and overturning. If one instead looks at the failure mode of a small part of a dam foundation, the failure mode will be sliding and/or lifting/crushing (from the global rotation). This is represented in the tests as the non-eccentric load case.

The size of the asperities is set from scaling down terrain roughness, meaning asperities of some meters in the dam interface, for a typical height for a Norwegian plate dam. The asperity angle of 45 degrees is set so that the failure mode shall be shearing through the asperity, and not sliding over it, as it would be with low asperity angles. Figure 2.2 shows this clearly.

Of the twenty-two tests, four were modelled in the work with this thesis, M5, F1, E8 and E11. The results from these models are described in section 6.5.

4.4. Measurements

There were done three types of measurements:

- 1) Loads were measured by the load cells applying the hydraulic pressure for the load pistons.
- 2) Direct measurements of displacements were done on the test machine with the LVDT measurement system, which is an electromechanical system that translates movement into electrical signals to a control unit.
- 3) Displacement were measured using the ARAMIS Digital Image Correlation System, which consist of a high-resolution camera making a video of the shear test, and a powerful data program that post processes the video to find the displacement at a given time.

The challenge was to coordinate these three systems. It was discovered that the LVDT measurements and the ARAMIS measurements of displacements did not match. The displacements measured by the LVDT system was up to ten times the ones measured by the ARAMIS system. It was decided that the ARAMIS system should be trusted. Due to an error done in the lab, the ARAMIS system was not correlated against the load measurements. Therefore, this correlation had to be done manually by the researcher, which was a very time-consuming task, and was therefore only done for four samples, M5, F1, E8 and E11.

The Aramis system can be used to find the displacement of every point on the sample. For the samples where it was used, it was found the displacement for two points, one on each side of the concrete – rock interface, near the sample toe, and the relative displacement was found from subtracting one from the other. Measurements and loads were calibrated by adjusting the initial value to zero.

5. PRELIMINARY ANALYSIS OF SHEAR TESTS

The aim of this section is to give some estimates of the capacity of the modelled samples towards different failure modes. Depending on the assumptions used, the estimates could give lower limit, higher limit, or be an estimation of the expected capacity. This is useful to assess both numerical model results and lab results. For example, if the calculation shows that a sample should overturn at a shear load of 100 kN, while the lab test failed by shearing through the asperity at 200 kN, there must be something wrong with the lab test, and/or with the data used in the hand calculation and the numerical models. For description of the samples, see table 4-1.

5.1. Hand calculation of sample M5

5.1.1. Sliding over the asperity

Since sample M5 is free to rotate, the failure mode with sliding over the asperity will include overturning. It is not possible to calculate the capacity of sample M5 by hand because it has two contact points, one at the asperity and one at the toe, and it is not straight forward to find the distribution of forces between these points by hand calculation.

5.1.2. Overturning

The forces at peak strength is drawn in figure 5.1:

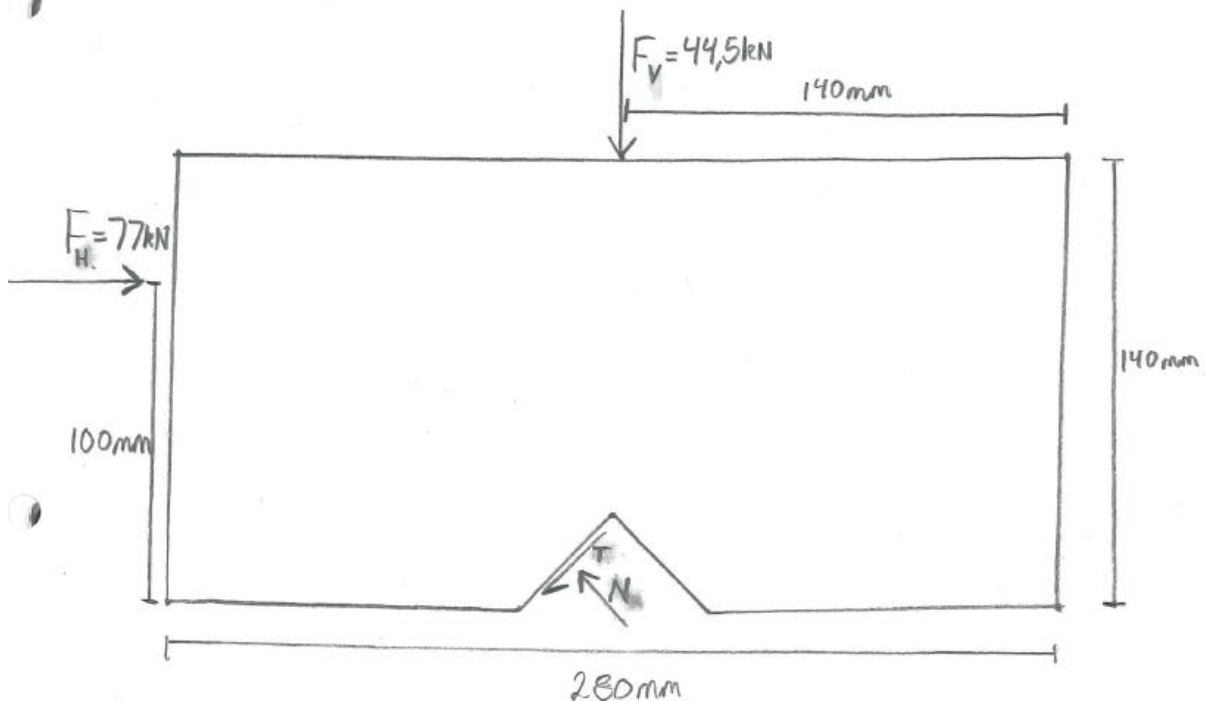


Figure 5.1 Principle drawing of sample M5 with acting forces

From equation (5.1) can then be shown that sample M5 should be unstable against overturning long before peak strength:

$$FS_{\text{overturning}} = \frac{F_V * a_V}{F_H * a_H} = \frac{44.5 * 140}{77 * 100} = 0.81 \quad (5.1)$$

So why is not the failure mode of M5 overturning? The answer could be the contribution from the asperity. In a dam stability assessment, the stabilizing moment from interface friction is not recognized, since it is assumed a straight plain. Here comes the same problem as in the section with sliding over the asperity. It is not possible to find the distribution of shear forces between the asperity and the rest of the interface, since the sample is free to rotate.

From figure 5.1 can be seen that the normal force on the asperity is contributing with a de-stabilizing moment and the asperity friction is contributing with a stabilizing moment. If the friction angle on the asperity is 45° , the two forces will be equal, and since the asperity angle is 45 degrees, the moments from the two forces would also be equal. That means the net contribution to the moment equilibrium from the asperity is zero. If the asperity angle or the friction angle had been larger, the asperity would have given a contribution to the stability. This should be considered for overturning stability on foundations with steep asperities.

There are at least 19 % of the stabilizing moment against overturning that cannot be explained from the measured forces. This is thought-provoking and leads to the conclusion that there may be something wrong with the test-setup or the measured forces.

The real failure mode of the sample is compression induced tensile failure by splitting of the sample from the asperity to the point of load application. This is not straight forward to calculate by hand.

5.2. Hand calculation of sample F1

Since this sample is fixed against rotation and has no asperity, only sliding is relevant. The capacity against sliding can be found by Mohr-Coulombs criterion. But this requires a friction angle. Maybe more interesting is therefore to use the capacity from the shear tests to find the basic friction angle, to be used for calculation on the other samples:

$$\varphi_b = \tan^{-1} \left(\frac{F_H}{F_V} \right) = \tan^{-1} \left(\frac{60}{74} \right) = 39^\circ \quad (5.2)$$

5.3. Hand calculation of sample E8

5.3.1. Sliding over asperity

It was observed in the lab test that the E8 sample has only one contact point at the time of failure, at the asperity. This makes it statically determined, and thus it is possible to calculate its capacity against sliding, given that this is the failure mode.

The calculation starts with force equilibrium in the direction perpendicular to the asperity surface to find an equation for the normal force, as shown in figure 5.2:

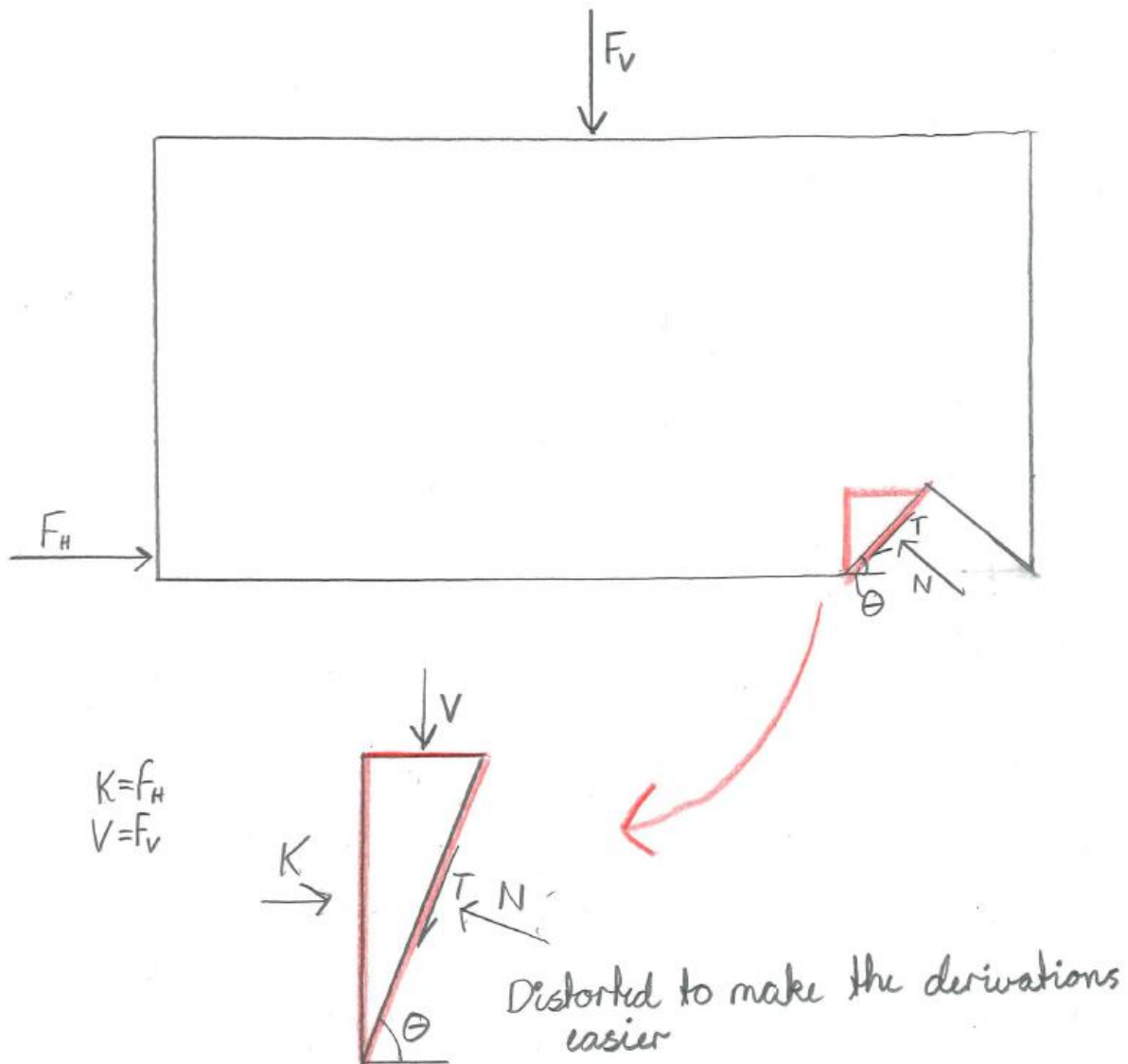


Figure 5.2 Principle drawing of sample E8 with acting forces

Then the global equilibrium must be found by either taking the force equilibrium in the direction parallel to the asperity surface, or to take equilibrium in the horizontal and vertical direction, of which both should give the same result. It is here chosen to take force equilibrium in the horizontal and vertical direction, so that the results could be checked.

$$N = K * \sin(\theta) + V * \cos(\theta) \quad (5.3)$$

$$T = N * \tan(\varphi) \quad (5.4)$$

$$\sum F_x = K - N * \sin(\theta) - T * \cos(\theta) \quad (5.5)$$

$$\sum F_y = N * \cos(\theta) - T * \sin(\theta) - V \quad (5.6)$$

The full derivation can be found in appendix A. The resulting formula for the required shear force to give sliding over the asperities is found to be:

$$K = V * \frac{\cos(\theta) * \tan(\varphi) + \sin(\theta)}{\cos(\theta) - \sin(\theta) * \tan(\varphi)} \tag{5.7}$$

When this function is drawn, it can be shown that (5.7) can be further simplified to:

$$K = V * \tan(\theta + \varphi) \tag{5.8}$$

For sample E8 the following values are given:

- Vertical force: $V = 74 \text{ kN}$
- Asperity angle: 45°
- Friction angle: 39°

To have sliding over the asperity, (5.8) gives a horizontal force of 703 kN, which is far larger than the peak capacity. At such large asperity angles, the result is very sensitive to differences in friction angle. If the friction angle were 45° and the asperity angle also 45° , it would not in theory be possible to get sliding over the asperity for any shear force, since $\tan(90^\circ)$ is infinity.

5.3.2. Shearing through the asperity

Multiple shear surfaces are possible, but only one is straight forward to check by hand, cutting through as a straight plain. This is similar to the failure surface observed in the lab test. The assumption giving the highest capacity is a rigid body assumption, giving an even stress distribution along the failure surface, while a linear elastic stress distribution gives only half the capacity of the rigid body assumption. The rigid body assumption can be seen as a higher limit. The linear elastic assumption cannot be seen as a lower limit, as there could be geometrical effects in the asperity, making a less beneficial stress distribution. The assumed stress distributions can be seen in figure 5.3:

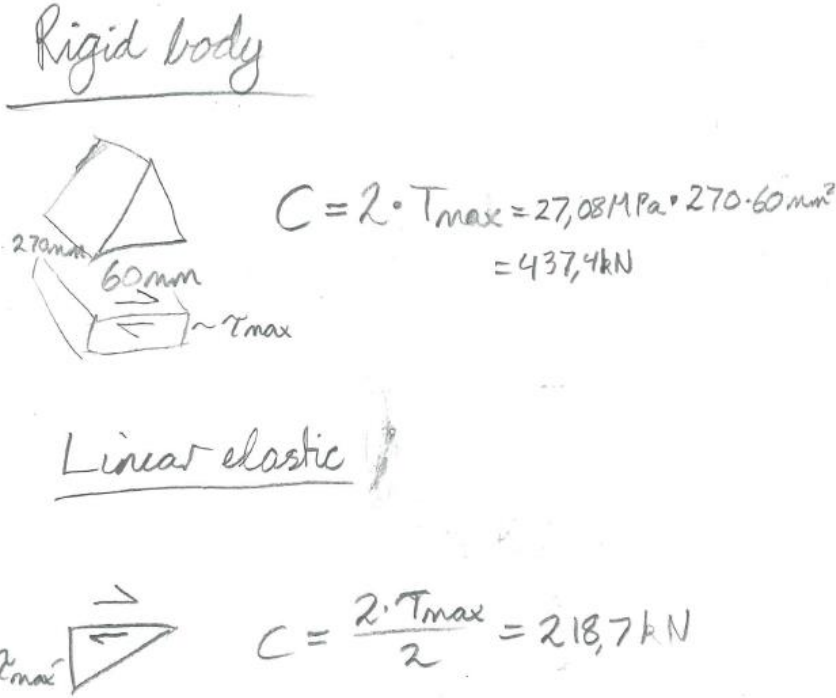


Figure 5.3 Drawing of a constant and a triangular (linear elastic) stress distribution

If the same material model is used as in the numerical model, the capacity is only governed by the material cohesion. With a material cohesion of 13.54 MPa, the shear capacity of this failure mode is 437 kN for rigid body, and 219 kN for linear elastic stress distribution, as can be seen in figure #. The capacity of the sample in the lab test was 191 kN, giving a quite good fit to the linear elastic assumption. The Atena simulation gave a capacity of 288 kN, which is between the linear elastic and the rigid body assumption.

5.4. Hand calculation of sample E11

5.4.1. Sliding over the asperity

Given that the sample does not overturn, the shear force needed for sliding over the asperity should be the same for this sample as for E8.

5.4.2. Overturning

The shear load required for the sample to overturn is dependent on the point of overturning. In the lab test is observed that the point of overturning is very close to the dam toe, after the undercutting of the asperity. If it is assumed that the sample overturns without any friction against the asperity, the required shear load can be found by the formula:

$$F_H = F_V * \frac{a_{Fv}}{a_{Fh}} = 74 \text{ kN} * \frac{135}{100} = 100 \text{ kN} \quad (5.9)$$

This value can thus be viewed as a lower limit of the capacity against overturning.

5.4.3. Undercutting and overturning

In figure # can be seen that the failure mode is a combination of undercutting and overturning. If a straight shear plain through the asperity is assumed, the tensile capacity of the asperity can be included as a stabilizing load. Given that the sample overturns as a rigid body, the stress distribution will be linear, as shown in figure 5.4:

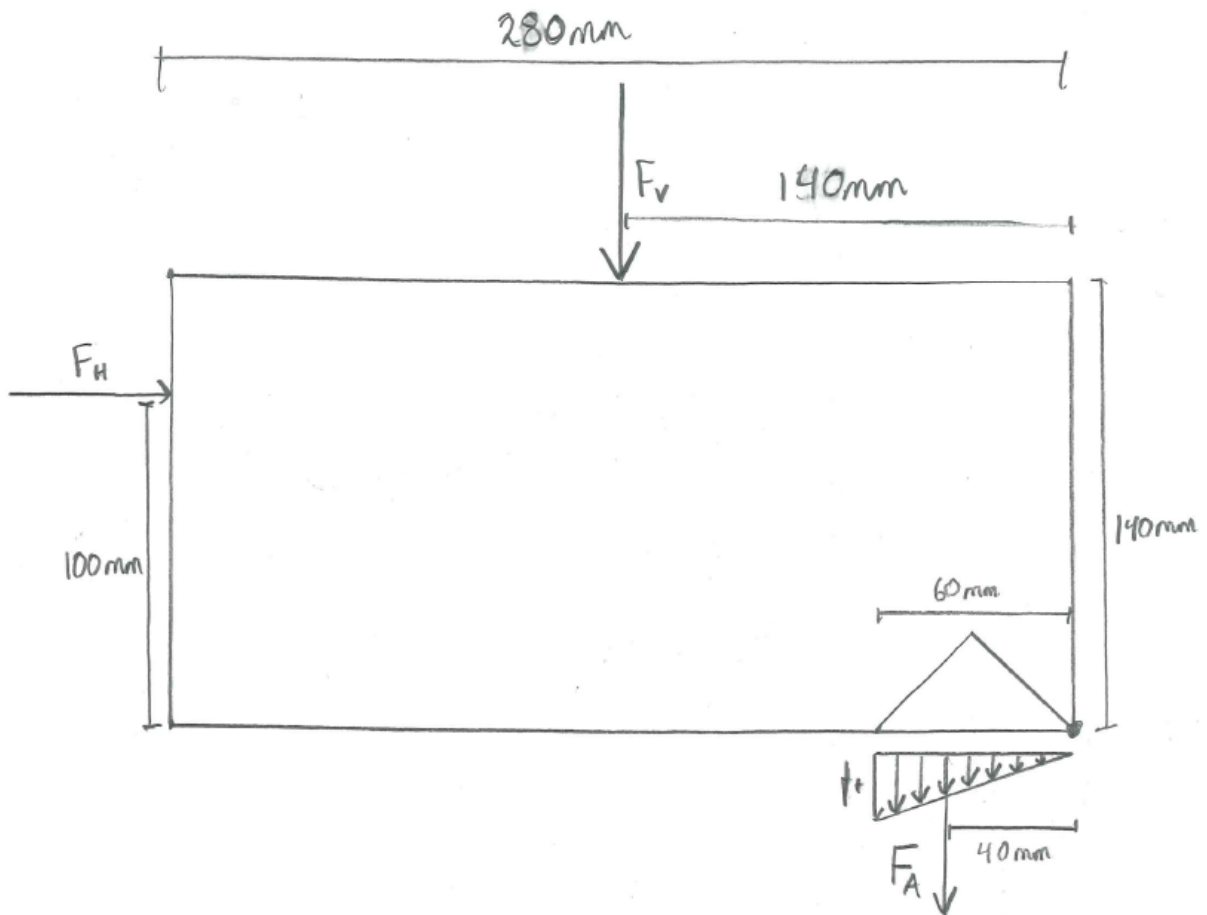


Figure 5.4 Principle drawing of sample E11 with forces when the sample overturns and ripping off the asperity

The force needed to rip of the asperity F_A can be calculated as:

$$F_A = A_{As} * \frac{f_t}{2} = 60\text{mm} * 170\text{mm} * \frac{13.54 \text{ MPa}}{2} = 69\text{kN} \quad (5.10)$$

The required shear load to have overturning can then be found as:

$$F_H = \frac{F_V * a_{Fv} + F_A * a_{Fa}}{a_{Fh}} = \frac{74\text{kN} * 140 + 69\text{kN} * 40}{100} = 131 \text{ kN} \quad (5.11)$$

As a comparison, the test result was 176 kN, and the Atena simulation gave a capacity of 125 kN, with a similar failure mode to the one calculated here.

6. FEA OF SHEAR TESTS

6.1. Introduction

The objective of this thesis is to make numerical models of shear box tests done in the rock mechanics lab at Luleå University (LTU), and apply the experience from the modelling for making a full-scale numerical model of a dam section. In this thesis, two kinds of tests are modelled, tests with pure shear load, fixed against rotation, and tests with the shear load applied at a distance from the interface, without any rotation constrains. The tests without rotation is somewhat similar to the tests done by Liahagen (2012), except these tests have only one asperity, and an asperity angle of 45 degrees for all tests. The asperity angle of 45 degrees was designed so that the failure mode will be undercutting of the asperities. As observed by Eltervaag (2013) it is hard to model a material failure due to the nature of tensile failure (see section 6.5.5.), and to capture the post-peak behavior is therefore not an important topic of this thesis.

6.2. Choice of idealization

A 2D model with *plain stress* was used, meaning that the model can expand freely in the third direction by the Poisson effect, in contrast to *plain strain*, where the material expansion is blocked, and therefore takes expansion forces in the third direction. *Plain stress* is thus a good approximation of a thin layer, and *plain strain* for a cross section with “infinite” thickness, like a concrete gravity dam. In (Eltervaag, 2013), the tests were first tried simulated in 3D, but this was soon abandoned, as the models were computationally expensive. The hypothesis of 2D behavior can be defended because the samples have the same geometry for a xy-plane for all z values.

6.3. Building the model in GiD

Atena is a finite element program (Cervenca Consulting, 2017). That means that it can model a structure that is loaded, and find the structural response to the applied forces in the form of stresses and strains in the structure. Atena Studio is a simulation program, and require input files with geometrical and material data, and other important problem characteristics such as solution methods, iteration and error limits and iteration method. This input file must be made by another program, in this case the creation of the input file is made in the program GiD, which is a general purpose modeler and pre-processing tool for FEA (CIMNE, 2017). First a brief overview is presented. Then a more detailed description is given. The models for the individual samples modelled is described in section 6.5.

6.3.1. Overview of the process

The layout in GiD can be seen in figure 6.1:

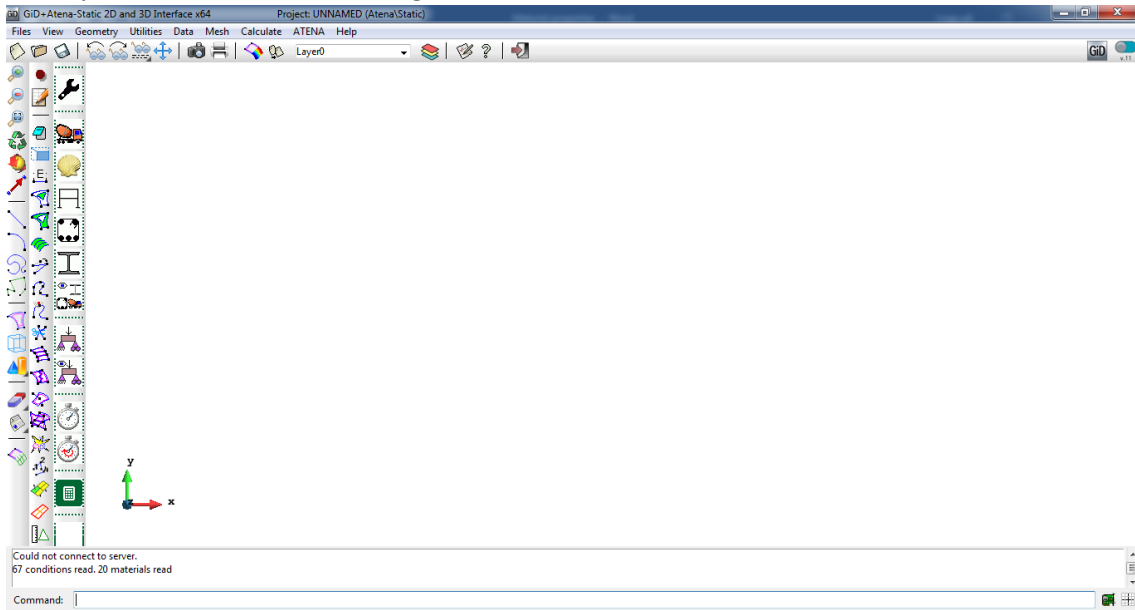


Figure 6.1 The GiD interface

In this project, the models are built through the following steps:

- 1) The geometry is drawn. This is done by first creating all the points. Then lines are drawn between the points, and surfaces are created from lines. When modelling in 2D plain stress, the 3rd dimension is managed by assigning a thickness to the material.
- 2) If there shall be sliding between materials in the model, a contact surface must be created, so that the characteristics for the interface can be defined. This is done by first duplicating the interface line such that the each of the two neighbor surfaces has its own line, with the line normal in opposite directions. Then a contact area is defined between these two lines. The contact area has no thickness, and the properties will be defined when an interface material is assigned to it. If two parts are fixed to each other, or if it is known that they will not move, a solid contact can be defined. The easiest way to do this is to let the two surfaces share the contact line.
- 3) The materials are defined from a material model, values are chosen for the material parameters, and materials are assigned to each surface.
- 4) Supports are defined, monitors for displacements, loads, stresses or other characteristics is defined. The function of monitors is to give important results in table form. For example, can a work diagram be made by plotting an external force monitor against a deformation monitor.
- 5) If many loads are applied one after another, the loads must be defined in different load intervals. The first interval contains the boundary conditions, the monitors and the first load to be applied. In the second interval and so on, the first load and the monitors are removed, while the supports remain, and a new load is applied. Loads can be defined as force, or as forced displacement. To avoid that the model becomes singular when the capacity is reached, the load that we are interested in measuring, in this case the shear load, should be given as forced displacement.

A number of load steps should be chosen for each load interval according to the assumed stability of the model. If the system is well conditioned, few load steps are needed. This is much about trial and error.

- 6) Problem data are adjusted.
- 7) The model is run, and the results evaluated.

6.3.2. Geometry and boundary conditions

The most important part of all numerical modelling is how to discretize reality into geometry. The discretization is based on the following assumptions:

- 1) It was clear from the beginning that the frame was too complex to be modelled directly. It is hollow, the wall thickness is not known, and it has internal stiffening in the loading direction. To model the frame was therefore chosen the same model as in Eltervaag (2013), where the frame was modelled as a massive rectangular frame, with geometry as shown in figure 6.2:

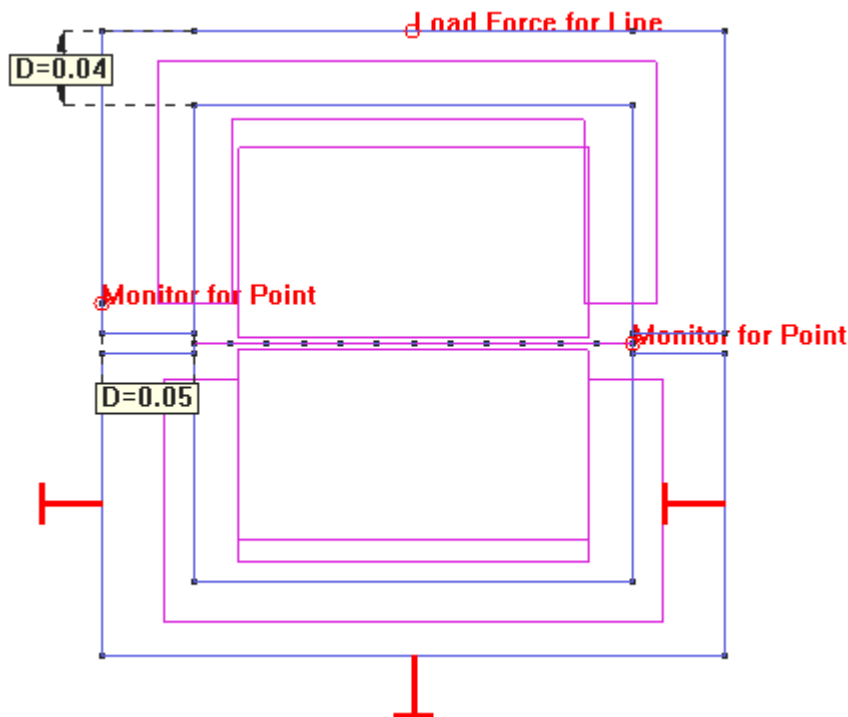


Figure 6.2 The model used as a starting point for the numerical model development

Regarding figure 6.2, and all other GiD figures must be explained the meaning of the pink lines. The Pink lines represents the surfaces. To make it possible to edit surfaces and lines independently of each other, the symbols for the surfaces and lines are placed so that they do not overlap. This has nothing to do with the real behavior of the model.

- 2) The interfaces steel – concrete, and steel – rock are fixed together. It is reasonable to assume that this gives a higher degree of clamping than in the prototype. This gives the following effects:
 - 2.1) Both the concrete and rock part of the sample is seriously prevented from bending due to the unbendable steel frames. This makes it less likely to see the failure mode of breaking of the concrete part that were observed during the laboratory tests on some samples.
 - 2.2) The lower half of the sample is prevented from rotating inside the frame. This will probably reduce the absolute displacement compared to the prototype. This problem

can be circumvented by using the relative displacements between the two sample halves.

- 3) All surfaces are perfectly even. This means that all interfaces are perfectly mated. This is hard to achieve in the laboratory, even though the concrete is casted directly on the rock with only a thin rubber sheet between. Perfectly mated surfaces give a stiffer transferring of forces between the model parts compared to if the mating is poorer, because a larger contact area gives lower stress levels and therefore less deformation. The lower stresses due to larger contact area also gives less local stress concentration. The small margins involved can be illustrated by that the peak strength displacement for the sample is in the order of magnitude 0,3 mm.

6.3.3. Material models

6.3.3.1. The concrete and rock material models

The materials used to model rock and concrete in Atena is based on the same material model, a material called *nonlinear cementitious 2* (Cervenca et al., 2013). This material uses a fracture-plastic model, which combines the Rankine-fracture Model for concrete cracking with a plasticity model for concrete crushing. It would also be possible to use a rock material model to model the rock, but this material model is more useful for modelling soil and weak rock masses with discontinuities and weathered cracks, as it is based the Drucker-Prager plasticity model, which is a modified version of the Mohr-Coulomb failure criterion. It was decided that this material model cannot represent the rocks that are used in these laboratory test, as there was used high strength rock which strength is governed more by the material strength, and less by the discontinuities. The stress-strain diagram for the Cementitious 2 material is shown in figure 6.3:

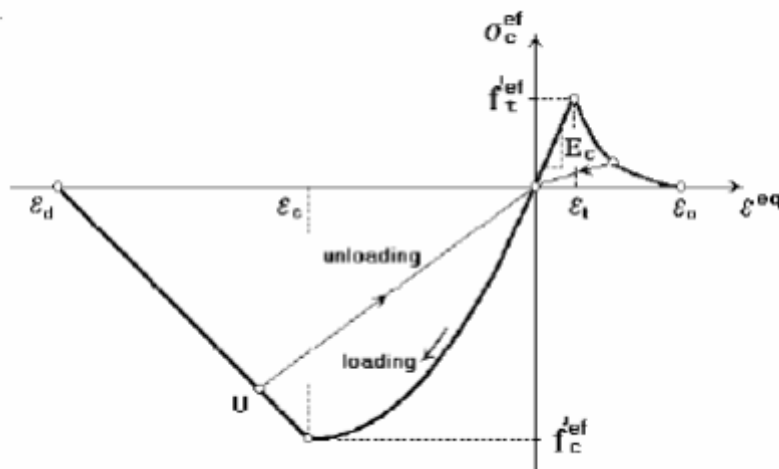


Figure 6.3 The stress - strain diagram for the Cementitious 2 material model from (Cervenca et al., 2013)

For biaxial stresses, the following failure criterion is used:

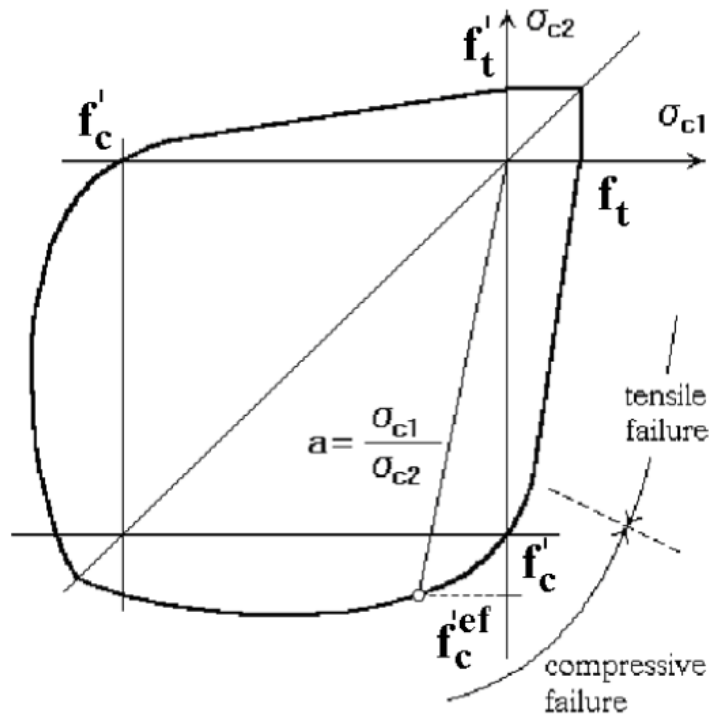


Figure 6.4 Failure surface for 2D stress for the Cementious 2 material model from (Cervenca et al., 2013)

Figure 6.3 and 6.4 shows that the rock and concrete is strong in compression and weak in tension, and that there is softening of the compressive strength in crushing. According to (Cervenca et al., 2013), this is a good description of the real behavior in concrete.

Crack model and fracture mechanics

For low stresses the material model is simple and linear, and is quite easy to implement. The advanced part of the material model is the non-linear fracture part. Concrete cracks before it fractures. The cracks are very thin, and they govern the material behavior. If this were to be modelled directly, the element size would have to be very small. The complexity of the stress situation in front of a crack can be illustrated with figure 6.5 from (Bažant and Oh, 1983):

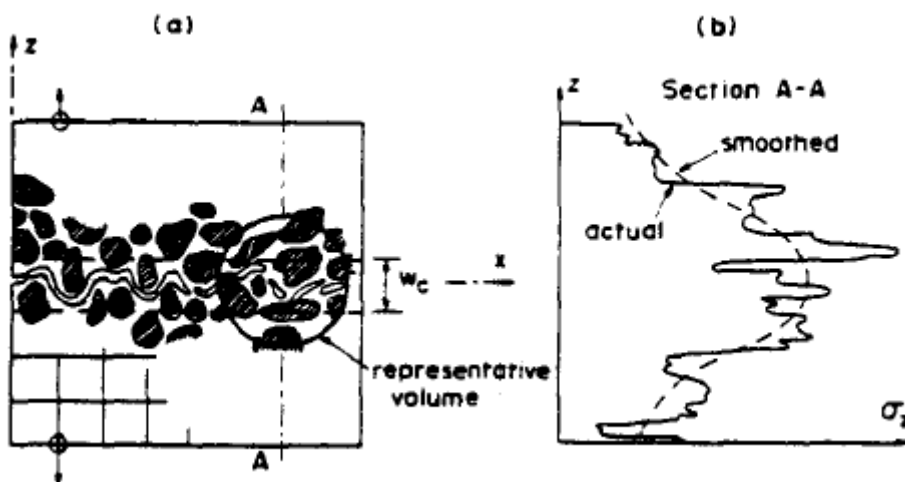


Figure 6.5 The stress state in front of a crack from (Bažant and Oh, 1983)

according to the direction of the crack. The material model is weakened both in stiffness and strength when cracking (Cervenca et al., 2013).

6.3.3.2. The steel material model

To model steel is chosen the material model *solid elastic* (Cervenca et al., 2013). This material model is simple and linear, with only two parameters relevant for this setup, the E-modulus of 500 GPa and the poisson ratio 0,2. The assumption of linearity is satisfied because the steel frame is dimensioned to have stresses in the linear area. The fact that the steel material model has no fracture mechanics is very beneficial for the model, as it avoids local fracture as a result of point loads on the concrete part. It was first tried to apply the loads between the steel and concrete, but this caused severe local damage, which slowed the model down and created errors.

6.3.3.3. The interface material model

The set-up with the most important parameters and the material model for the interface material model can be seen in figure 6.7:

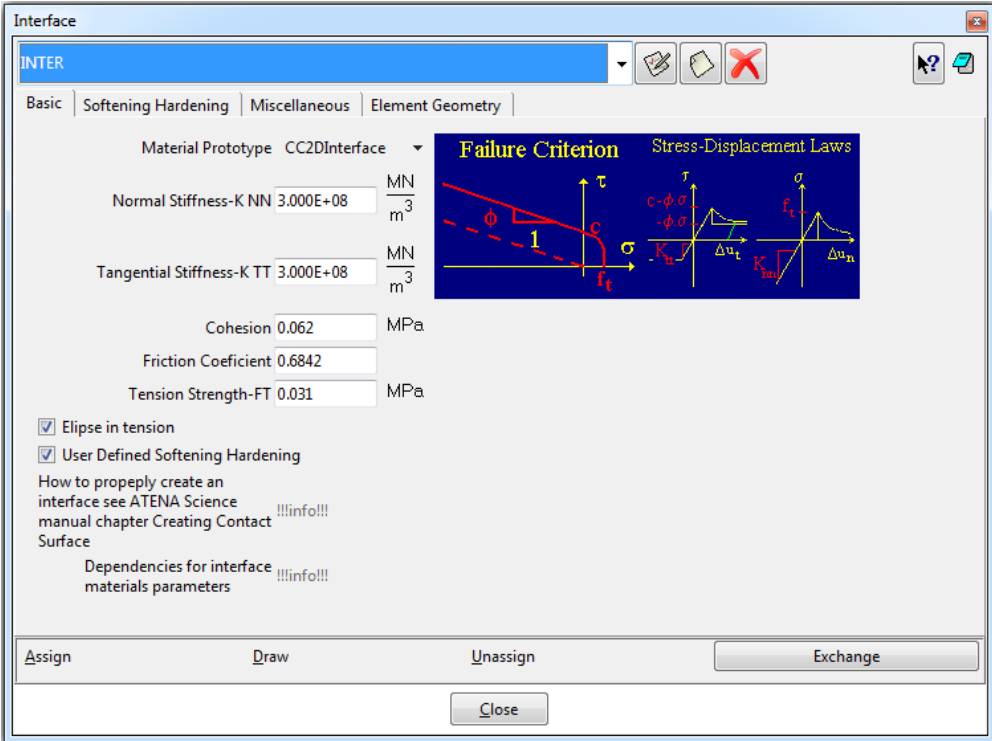


Figure 6.7 The interface material model in GiD (CIMNE, 2017)

The key role of the interface in this project has been to govern the sliding behavior. In Atena, this is governed by the Mohr-Coulomb failure criteria with a curved envelope in tension, as seen in figure 6.7.

Friction factor

The friction factor can be found by re-arranging the Mohr-Coulomb shear failure criterion from equation (2.4) into equation (6.1):

$$k_f = \tan(\varphi) = \frac{F_x}{F_y} \tag{6.1}$$

F_x is the peak shear force, and F_y is the normal force.

Interface material stiffness

Principally there are two approaches to calibration of the interface, it is a choice between using the interface stiffness to calibrate the model to the observed work diagram, or to set the interface stiffness according to some reasonable value according to some criterion. With the first approach, one hopefully gets a model that fits the laboratory test, but if the deviations between model and prototype is due to something else than difference in interface stiffness, one risk to make a miss-calibrated model that cannot be used for anything because it will give wrong results for all other problems. Here is derived the formulas needed for calibration of the interface stiffness.

For calibration of the interface stiffness is used measurements A1 and A2 from the F1 sample, showed in figure 6.8. The difference between these gives the relative displacement of the interface.

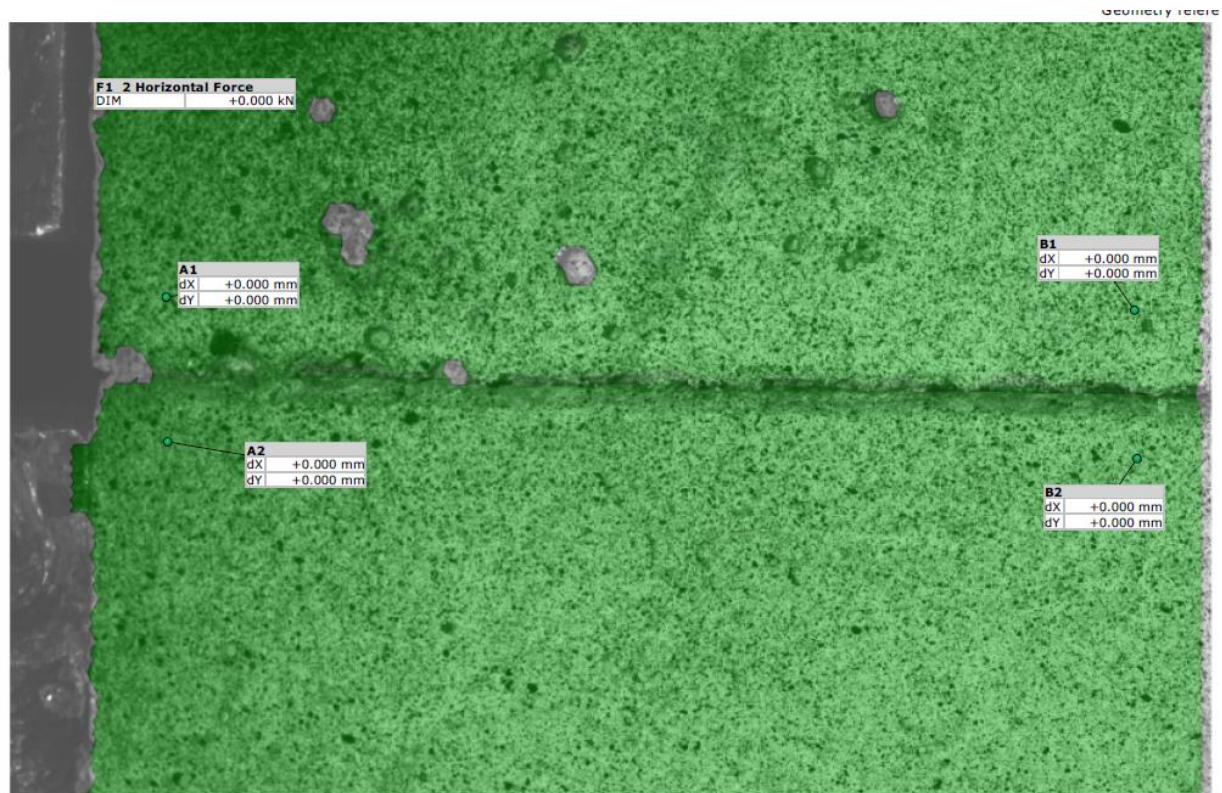


Figure 6.8 The measurement points for displacement on the surface of the F1 sample from Aramis

In most basic mechanics books can be found eq. (6.2) – (6.8) (Hibbeler and Fan, 2011):

$$\sigma = E * \varepsilon \quad (6.2)$$

$$\tau = G * \gamma \quad (6.3)$$

$$G = \frac{E}{2(1 + \nu)} \quad (6.4)$$

$$\varepsilon_y = \frac{\Delta y}{y_0} \quad (6.5)$$

$$\gamma_{xy} = \frac{\Delta x}{y_0} \quad (6.6)$$

$$\sigma_y = \frac{F_y}{A_{xz}} \quad (6.7)$$

$$\tau_{xy} = \frac{T_x}{A_{xz}} \quad (6.8)$$

The symbols are explained in figure 6.9, showing the load situation on the interface of the F1 sample:

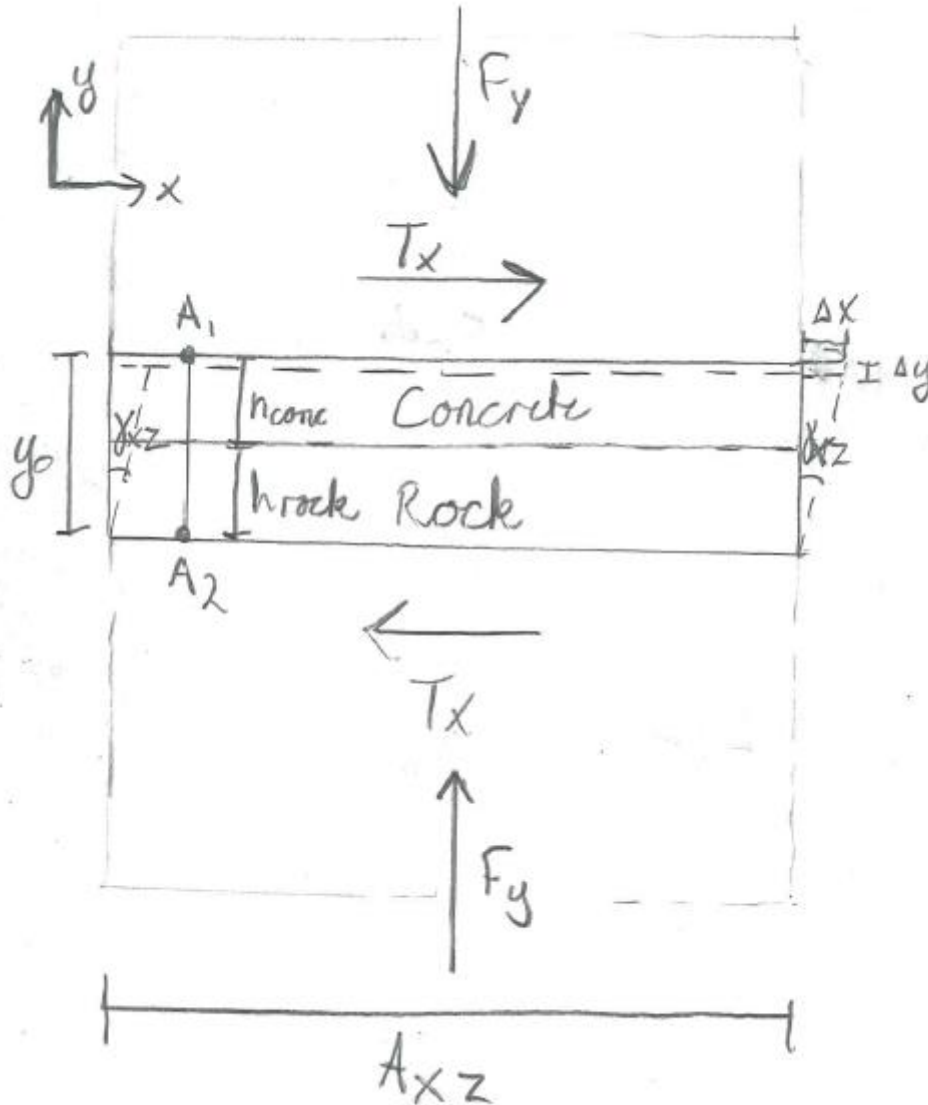


Figure 6.9 The forces acting on the interface of the F1 sample

Formula (6.2) – (6.8) can be re-arranged into:

$$E_y = \frac{\sigma_y}{\varepsilon_y} = \frac{F_y * y_0}{A_{xz} * \Delta y} \quad (6.9)$$

$$G_{xy} = \frac{\tau_{xy}}{\gamma_{xy}} = \frac{T_x * y_0}{A_{xz} * \Delta x} \quad (6.10)$$

The stiffness of the interface material is given in Atena in the units $\frac{MN}{m^3}$. Stiffness is usually given in force per area, but since the interface layer has no thickness, this would give no deformation or a singular stiffness matrix. By giving the stiffness in force per volume, the thickness of the boundary layer is accounted for. If it is assumed that all the deformation between the two measurement points

A1 and A2 in figure 6.9 is happening in the interface (no elastic deformation), this gives equation (6.11) and (6.12):

$$K_{NN} = \frac{E_y}{y_0} = \frac{F_y}{A_{xz} * \Delta y} \quad (6.11)$$

$$K_{TT} = \frac{G}{y_0} = \frac{T_x}{A_{xz} * \Delta x} \quad (6.12)$$

The elastic deformations in the sample can be checked by modifying formula (6.11) and (6.12) into formula (6.13) and (6.14), and inserting the stiffness for rock and concrete:

$$\Delta y = F_y * \left(\frac{h_{concrete}}{A_{xz} * E_{concrete}} + \frac{h_{rock}}{A_{xz} * E_{rock}} \right) \quad (6.13)$$

$$\Delta x = T_x * \left(\frac{h_{concrete}}{A_{xz} * G_{concrete}} + \frac{h_{rock}}{A_{xz} * G_{rock}} \right) \quad (6.14)$$

If the height of concrete and rock between A1 and A2 is assumed to be 10 mm each, the elastic deformation for the F1 sample should be $\Delta y = 0.0004 \text{ mm}$ and $\Delta x = 0.0002 \text{ mm}$. Principally, these numbers should be subtracted from the deformation in equation (6.11) and (6.12), but the values are considered neglectable.

That the stiffness of the interface material is different from the material stiffness is not necessary true literally speaking, but the boundary layer would be weaker since it is not perfectly mated on the micro scale, and therefore the contact area is smaller. A smaller area with high stiffness could thus be simulated by a larger area with lower stiffness, giving the same result as a complicated simulation of the real geometry. This is similar to using a friction coefficient for sliding resistance in the way that a complicated mechanism is translated to a simple parameter.

A reasonable interpretation of the interface layer thickness could for example be the height of the largest roughness elements, and a reasonable way to find the stiffness could be the material stiffness of the weakest material multiplied with the ratio between the real contact area and the sample area. Unfortunately, it is hard to find the real contact area on a micro scale since it requires high resolution scanning of the two adjoining plains, and computer analysis on how the two parts fit together at the given vertical stress levels. For a perfectly mated joint with zero height, the interface stiffness as it is defined should be infinitely high. This will not work from a computational point of view. The experience from the modelling is that if the interface stiffness is set too high, the model crashes. It is observed that using too low interface material stiffness is making the model too soft and smooth. This can best be illustrated with the attempts to calibrate the model of the M5 sample to the LVDT measurements, as seen in figure 6.10:

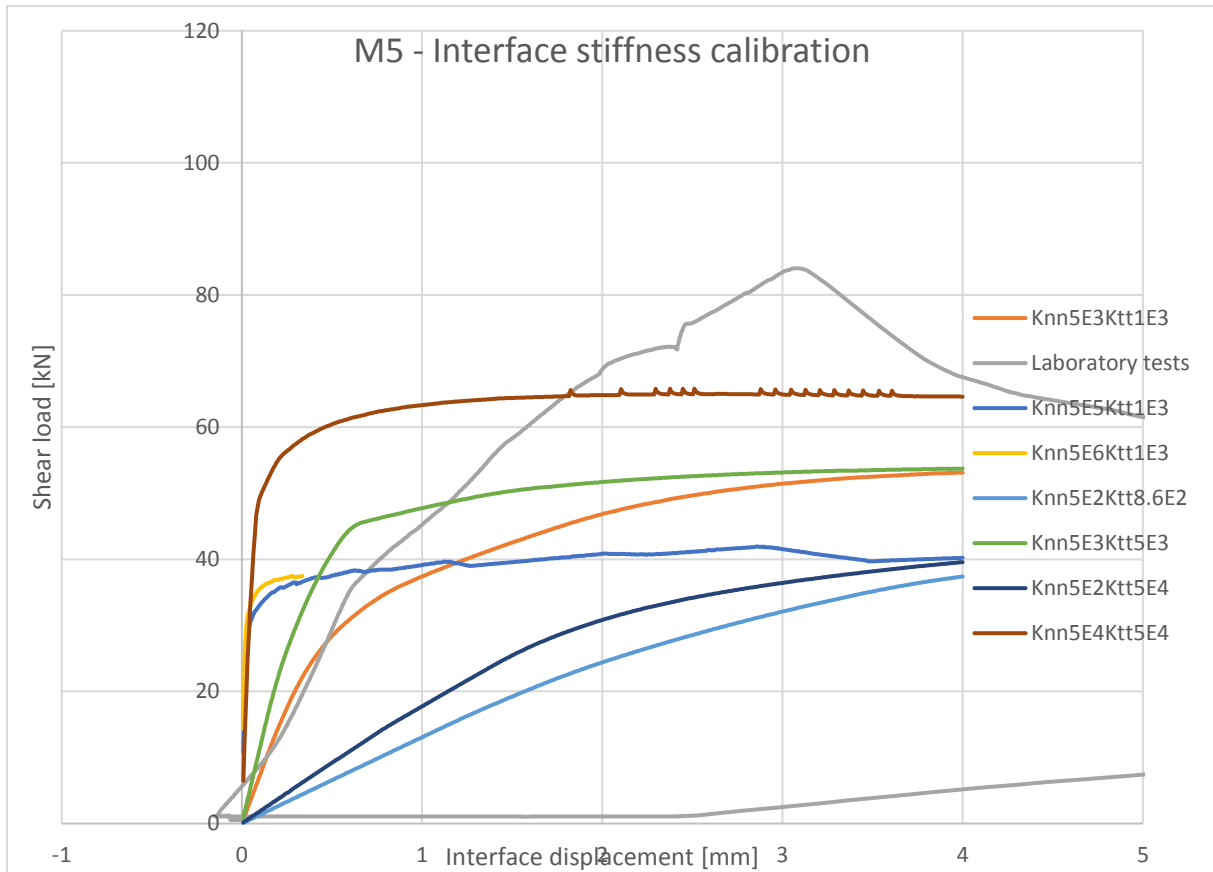


Figure 6.10 Calibration of the interface material stiffness to the LVDT measurements for the M5 sample. The figure is an example of the unnatural soft behavior when the interface material stiffness is set too low

It can be described as putting a thick rubber mattress between the concrete and the rock part. It will allow the interface to deform far more than what has physical meaning, and therefore the concrete can rotate around the asperity without any damage. Since the failure mode is not described correctly, it will be challenging to get the correct post-peak behavior.

6.3.4. Meshing

It is used triangular, linear elements, after the advice of Dobromil Pyl at Cervenca Consulting, since these perform better when distorted, than higher order elements. When applying linear elements, it is important to have some elements over the thickness of a cross section exposed to bending, since linear elements cannot replicate a varying strain field within the element. The asperities we are dealing with in this project is exposed to heavy bending, and to get good results, there need to be some elements over the thickness. Since there is only one large asperity in the models in this project, this is not the dimensioning criterion for the number of elements anywhere, but it would be an issue for small roughness elements, for example on a real rock surface geometry. The need to have some elements over the thickness is dimensioning for the steel frame, since it is exposed to bending, and are thin compared to the test specimen. The dimensioning criterion for the concrete and rock mesh seems to be to be able to meet the spatial variations in stresses along the concrete - rock interface. Bažant and Oh (1983) pointed out that to satisfy the hypothesis of homogeneous properties within an element, the mesh should not be refined to more than some multiples of the largest aggregate. The largest aggregate size is in this case 16 mm, but probably smaller along the boundaries. When the mesh in this thesis to a large extent is set smaller than this, it is because it is used 2D elements,

meaning that the size of the elements is the area of the element times the depth of the structure. So even a 1 mm triangular element has a volume of 135 mm³.

6.3.5. Interval data

The basic function of interval data is to be able to apply more than one load, one after another. For each interval is defined loads and boundary conditions. This option also allows for varying load increments and solution parameters through the simulation.

6.3.6. Solution parameters

The function of these is to decide how Atena shall do the analysis. An illustration of the setup can be seen in figure 6.11:

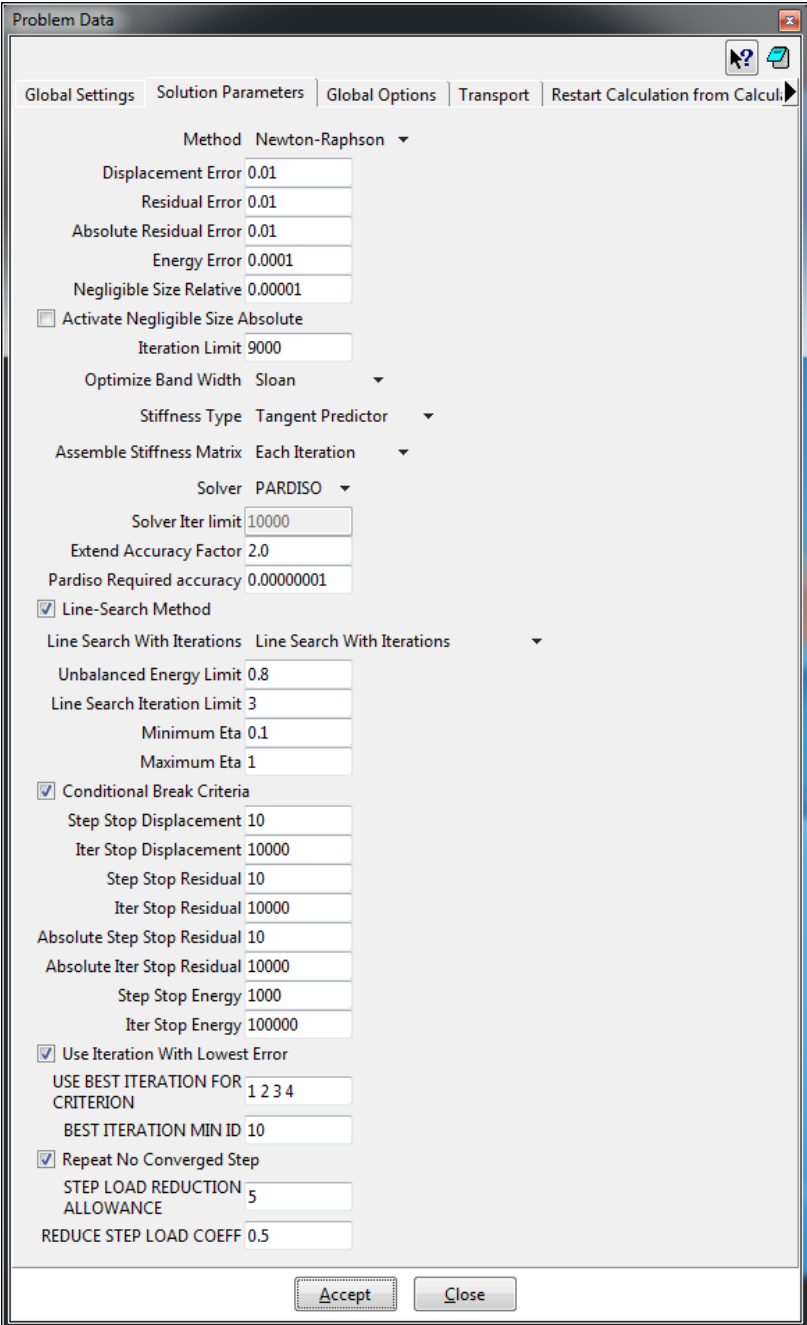


Figure 6.11 The solution parameters from GiD (CIMNE, 2017)

6.3.6.1. Iteration method

It is not practically possible to calculate the solution to a large set of non-linear equations directly. Therefore, an iteration method is needed. In Atena one has the choice between the Newton-Raphson method and the Arc Length method. The Newton-Raphson method is recommended for most cases, while the Arc-length method is recommended for cases with rapid changes, such as sudden failures causing snapbacks (Cervenca et al., 2013). This makes the Newton-Raphson suited for pre-peak simulation and the Arc-length method suited for post-peak simulation. Within the Newton-Raphson method one has a choice between Full Newton-Raphson and Reduced Newton-Raphson. This choice is governed by the Stiffness Type and how often the stiffness matrix is assembled. In a reduced method, the stiffness matrix is not updated for each iteration, only for each step. The stiffness type for a reduced method is the elastic predictor, which in contrast to the tangential predictor, is more robust but not so efficient. Because of this, a good strategy is to start with the Full Newton-Raphson, and switch to a reduced Newton-Raphson in difficult areas.

6.3.6.2. Equation solver

One has the choice between several different solvers. A solver is a script to implement the equation solver method. They differ in what tricks and shortcut they take to save computational time. Each solver will have its pros and cons for particular types of problems. As long as the iteration criteria is fulfilled when reaching a solution, it does not matter which solver was used, so it is only a matter of computational time. Two solvers were used in this project, the Paradiso and the LU solver. The LU solver is more robust than the Paradiso solver, but it is also slower and more memory intensive. It is recommended to start with the Paradiso solver, and switch to the LU solver when the Paradiso solver do not give any solution (Cervenca et al., 2013). With reference to section 6.3.6.1. about iteration methods, it is smart to use the Paradiso solver together with the Full Newton-Raphson method, and the LU solver together with the Modified Newton-Raphson and the Arc-length method.

6.3.6.3. Iteration criteria

These settings give the required accuracy for an iteration to be good enough. The default values of 1 % error in displacement and 0.01 % in energy are used.

6.4. Material properties

6.4.1. Concrete material properties

6.4.1.1. Concrete compressive strength

The concrete is designed to be a C40, which means it has a characteristic strength of 40 MPa, and a medium strength of 48 MPa after 28 days according to EC2 (Standard Norge, 2010). In this simulation, the medium strength is used as input to Atena, since this is the most probable value.

The compressive strength is dependent on the curing time. For the M5 sample, the curing time was 31 days. In the Eurocode, the strength is given after 28 days. The strength development for the extra three days can be calculated with formula 3.1 and 3.2 in EC2 (Standard Norge, 2010).

$$f_{cm}(t) = \beta_{cc}(t) * f_{cm} \quad (6.15)$$

$$\beta_{cc}(t) = \exp \left\{ s \left[1 - \left(\frac{28}{t} \right)^{\frac{1}{2}} \right] \right\} \quad (6.16)$$

s is dependent on the cement type, and is between 0,20 and 0,38. The formula is not valid beyond 28 days for construction purposes, but for scientific purposes it should be possible to extrapolate the formula for some days.

Assuming it is a normal class (N) cement gives an s of 0,25, which gives a $\beta_{cc}(31) = 1,01$, meaning that the real strength is 1% higher than the 28 day strength. This is considered neglectable, and in the calculations a compressive strength of 48 MPa are used.

6.4.1.2. Concrete tensile strength

The tensile strength can be found from the compressive strength, applying table 3.1 in EC2 (Standard Norge, 2010). A C40 concrete has a medium tensile strength f_{ctm} of 3,5 MPa according to table 3.1 in EC2.

6.4.1.3. Other concrete parameters

The Atena manual (Cervenca et al., 2013) gives suggested values for the input parameters for concrete. It is not full consistency between these suggestions and the Eurocode, and no information is available to make an informed choice. To represent C40 is chosen the column with compressive strength of 50 MPa, since the values for the compressive and tensile strength and E-modulus seems to have the best fit to the values from the Eurocode. Parameters, abbreviations and values are listed in table 6-1:

Table 6-1 Concrete material parameters from (Cervenca et al., 2013)

Parameter	Short form	Value	Unit
Compressive strength	f_c	48	MPa
E-modulus	E_c	33	GPa
Tensile strength	f_{ct}	3,5	MPa
Poisson ratio	ν	0.2	-
Compressive cracking initiation stress	F_{c0}	23.63	MPa
Tensile fracture energy	G_f	$9.26 \cdot 10^{-5}$	MN/m

6.4.2. Rock material properties

6.4.2.1. Rock compressive and tensile strength

The compressive strength was set according to Eltervaag (2013) to 280 MPa, since it is a similar rock type. The tensile capacity was found with the Brazilian Test to 13.5 MPa. The E-modulus is set according to Eltervaag (2013) to 100 GPa.

6.4.2.2. Rock fracture energy

The fracture energy G_f is the amount of energy needed to open a new unit crack area ($=>J/m^2$). When doing tensile strength tests, the fracture energy is the area under the work diagram from the top point until failure, as shown in figure 6.12:

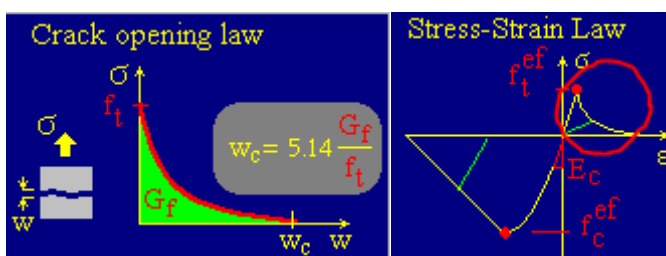


Figure.6.12 Illustration of the fracture energy, from Atena (CIMNE, 2017)

Suggested values for concrete are given by Cervenca et al. (2013), but these are not applicable for rock. According to Bažant and Oh (1983), the fracture energy G_f for a rock can be found from equation (6.17):

$$G_f = \frac{f_u^2}{c_n^2 * A * E} * g(\alpha_0) \quad (6.17)$$

For a particular granite with tensile strength 4,8 MPa and E-modulus 29,4 GPa for core samples with diameter 30 mm and length 50 mm, the fracture energy was calculated to 94 J/m² (Bažant and Oh, 1983). Since in this case we do not have data on the geometric parameter $g(\alpha_0)$, we must assume this to be constant and representative to our case. If we disregard c_n and A we can simplify equation (6.17) to (6.18):

$$G_f \propto \frac{f_u^2}{E} \quad (6.18)$$

The fracture energy for our gneiss should then be approximately:

$$G_f = 94 \frac{J}{m} * \frac{13,5^2}{\frac{100}{4,8^2} * \frac{100}{29,4}} = 219 \frac{J}{m} \quad (6.19)$$

6.4.3. Interface material parameters

During the modelling process, it was clear that the measurements of basic friction angle was not consistent with the results from the shear box tests. It was therefore chosen to calibrate the friction angle to sample F1 (see section 6.5.2).

Sliding tests done on sawed drill samples of the rock indicates a basic friction angle of 32,86 degrees. When doing such sliding tests, it was clear that the basic friction angle found from this test was too dependent on the preparation of the samples. It was therefore decided to instead use one of the flat samples with the same normal stress for calibration, in this case the F1 sample. A tensile strength and cohesion of zero is used for the interface, because there is no bonding. It was decided to avoid using to cohesion parameter as an expression for the dilatancy as in Eltervaag (2013), since the dilatancy is a part of the friction factor, while the cohesion is independent of the normal stress.

In the program manual for Atena can be found a recommended value for the interface stiffness, given by equation (6.20) (Cervenca et al., 2013):

$$K_{NN} = K_{TT} = \frac{E}{t} * 10 \quad (6.20)$$

E – Youngs modulus of the weakest material

t – Element size of the weakest material

For a concrete with E = 30 GPa and element sizes of 10 mm along the interface, the resulting stiffness is $3 * 10^7$ MN/m³.

Note that equation (6.20) is not very exact, the accepted range is from 0.1 to 100 times the value from (6.20). E is set to 30 000 MPa.

6.5. Models and results

The goal was to model all the shear tests. Due to miscommunication, the gap between the frames were believed to be 25 mm instead of 10 mm. This lead to an early cutoff of the toe corner of the samples. Due to this and other mistakes, several weeks were spent trying to calibrate a not representative model of sample M5 to the LVDT measurement results (see section 4.4). These problems were solved quite late in the project. Then a choice had to be made for which samples to

model. Since the results from the digital image correlation system Aramis were so time consuming to extract, it was not possible to get reliable results from all the samples, which is necessary for evaluating the results of the numerical models. It was therefore decided to model three samples, one sample with a flat interface, to calibrate the interface stiffness, and then one sample with and one sample without rotation. The aim of the modelling of the shear tests is then to evaluate how accurately the FEM can replicate the tests, and the implications of the degree of rotational freedom on the shear strength.

6.5.1. Sample M5

Sample M5 had the asperity in the middle, and a normal pressure of 0.6 MPa. The test sample failed by a tensile failure through the concrete part of the sample, initiated at the tip of the asperity. At the same time, the rock part fails by splitting of the top part of the asperity. An illustration of these failure modes can be seen in figure 6.13:

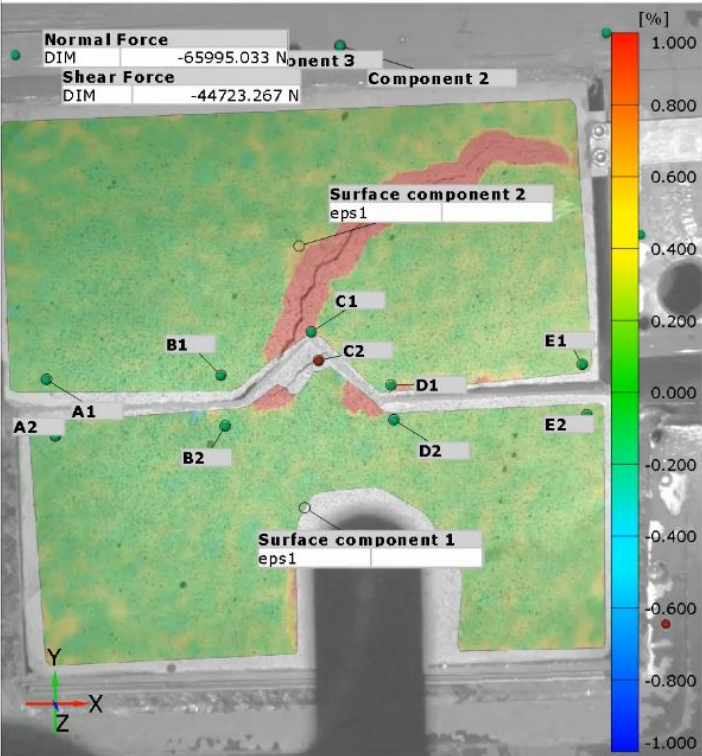


Figure 6.13 The failure modes of the M5 sample

Initially, the M5 model was built with the wrong geometry, which gave wrong results. At the end of the project, a new model was built for the M5, and the result from this model is presented here. The model geometry is shown in figure 6.14:

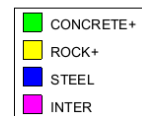
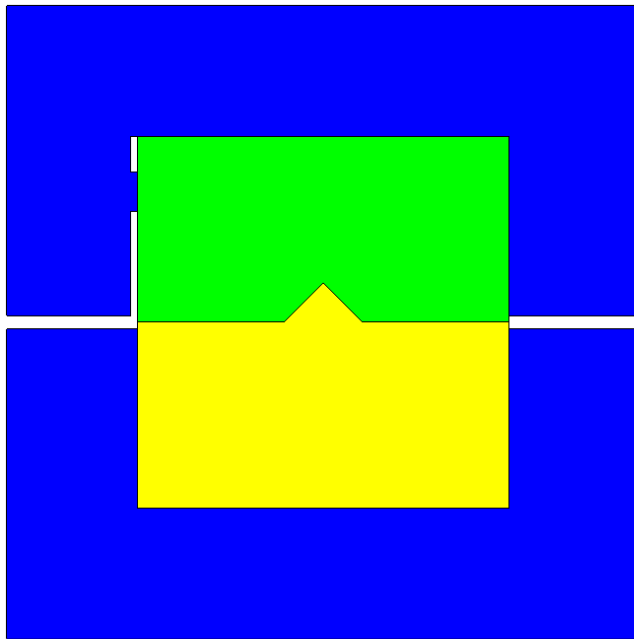


Figure 6.14 The geometry of the numerical model of the M5 sample

The vertical load is applied as a line load on the top edge, and the shear load is applied 100 mm over the interface.

The model predicted the capacity exactly (1% off), but it failed by the wrong failure mode. It failed by overturning, without any material damage. The results are presented in figure 6.15:

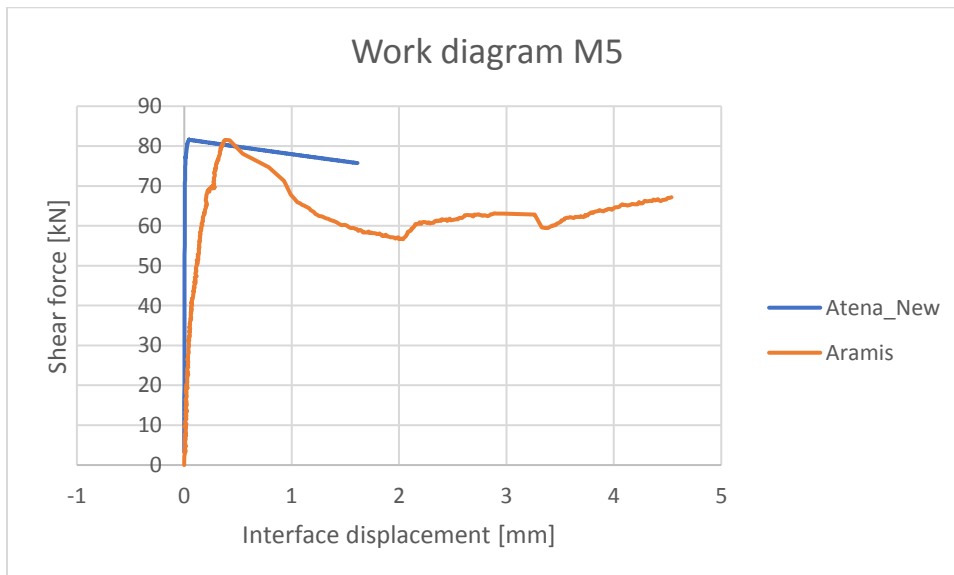


Figure 6.15 Resulting work diagram from the simulation of the M5 sample (blue) together with the test results (orange)

A reasonable explanation of the different failure modes but correct capacity is that the found capacity is the capacity where the sample becomes unstable against overturning. This could affect the structural strength, and it is reasonable to believe that a beginning overturning has initiated the

observed structural collapse. It should be noted that the hand calculations for sample M5 showed that it should be unstable against overturning. Therefore, it is reasonable to believe that there is something with the boundary conditions that is not represented correctly in the numerical model.

6.5.2. Sample F1

The F1 sample has a normal load of 1 MPa, and a flat interface. The failure mode of the F1 sample was sliding, without any material failure. The purpose of modelling the F1 sample is to calibrate the interface parameters. This is not possible to do from the samples with asperities, since it is not possible to separate between normal and shear load at the interface, or between normal and shear displacement on the interface when the interface angle is not constant.

First, the friction coefficient was calculated from equation (6.1) to 0.80.

The load was applied on the model in two load steps, first a step with the vertical loads, then a step with the horizontal loads. In the second step, the sample was fixed against rotation by use of master – slave conditions on the top edge, as shown in figure 6.16:

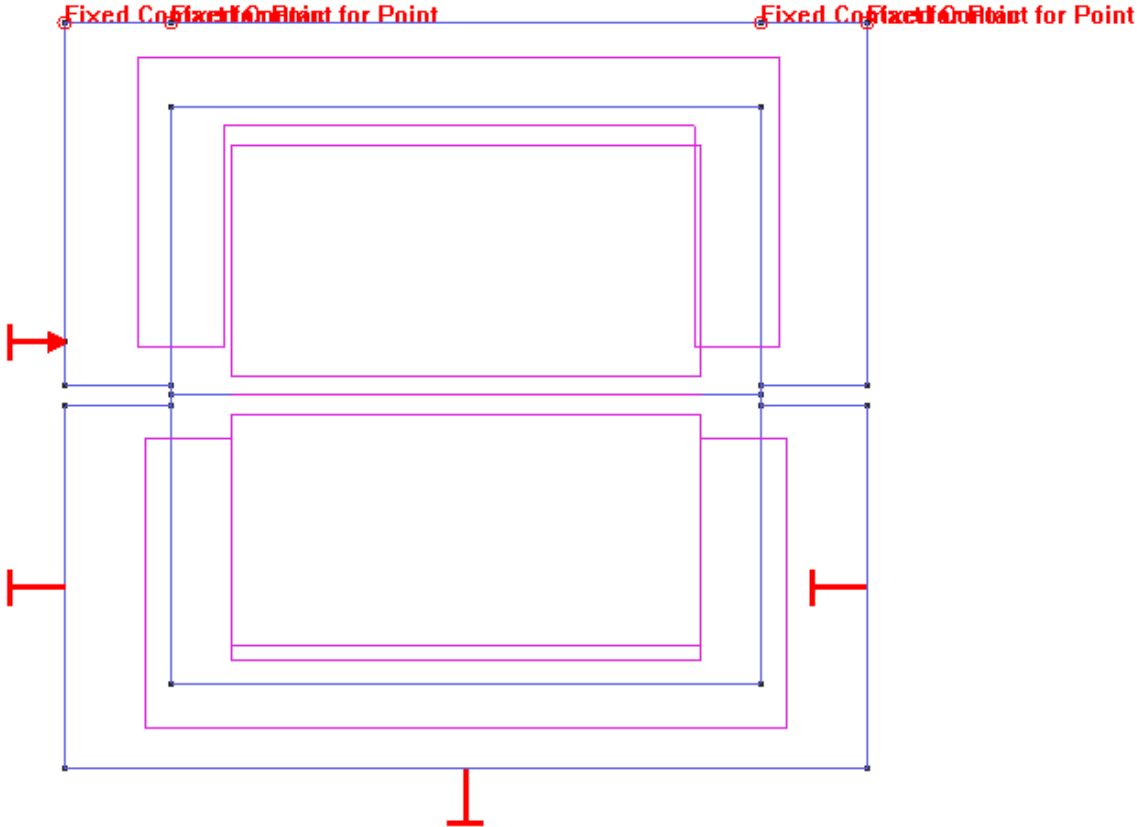


Figure 6.16 The geometry of the numerical model for the F1 sample

The way the master – slave condition works is that the degrees of freedom in the vertical direction is merged for the four points, so that if one points moves in the vertical direction, the others move the same distance. This prevents rotation. The points are free to move independently in other directions.

The mesh was drawn with 1 mm elements along the interface, and the initial simulation was run with interface material stiffness of $3 \cdot 10^8$ MN/m³, as recommended in Cervenca et al. (2013). When the resulting work diagram of relative displacements of the interface was compared with the interface displacement from Aramis, it was found that the model was too stiff, as shown in figure 6.17:

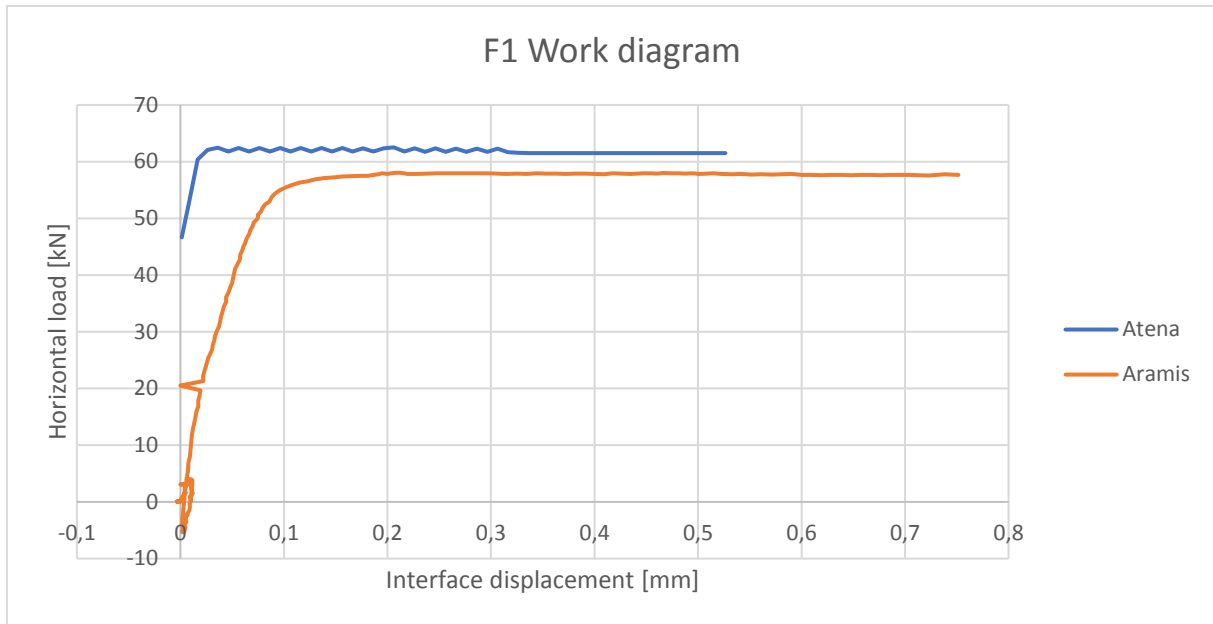


Figure 6.17 First result for the F1 sample

Since it was observed that the initial slope was far too steep, the interface material stiffness was reduced to fit the test results. The new stiffness was found by reading off load and displacement for two points, on the linear part of the work diagram from Aramis:

Table 6-2 Values of shear load and interface displacement for the F1 sample from Aramis for calibration of the tangential interface material stiffness

Displacement [mm]	Shear load [kN]
0	0
0.02	19.65

The tangential stiffness of the interface material can then be found from eq. (6.12):

$$K_{TT} = \frac{\tau_{xy}}{\Delta x} = \frac{T_x}{A * \Delta x} = \frac{19.65 * 10^{-3} MN}{0.27m * 0.27m * 0.02 * 10^{-3}m} = 13477 \frac{MN}{m^3} \quad (6.12)$$

For calibration of K_{NN} we must look at the work diagram for the application of the normal load. The work diagram for the normal load is shown in figure 6.18:

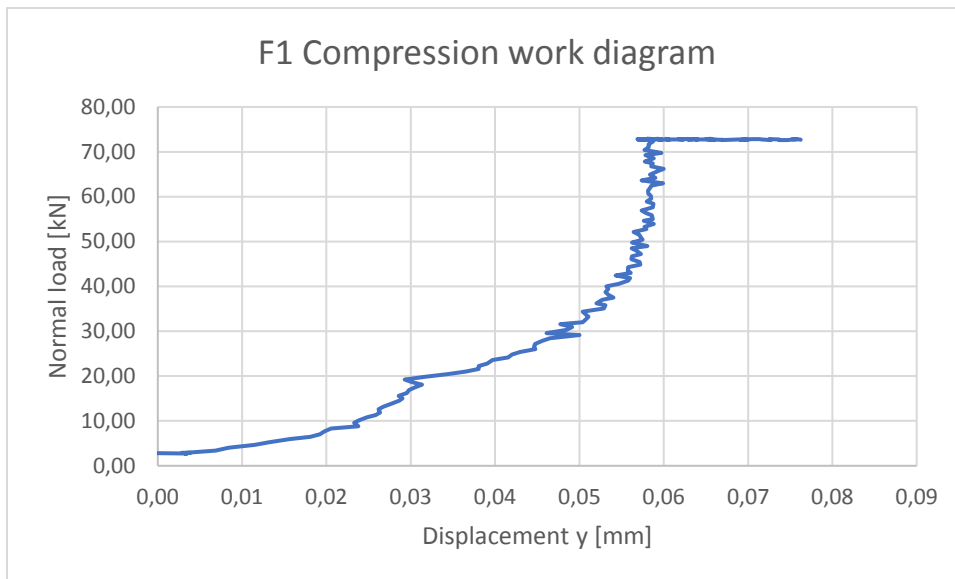


Figure 6.18 Normal load - displacement diagram for the F1 sample for calibration of the normal interface material stiffness

Figure 6.18 shows that the relationship between compression and deformation is not linear. So, when calibrating a linear parameter from figure 6.18, it must be calibrated in the same area of normal forces as may be expected in the test. That means that it should be calibrated in the upper area, where the diagram is linear. A new diagram was therefore made for this area, and is showed in figure 6.19:

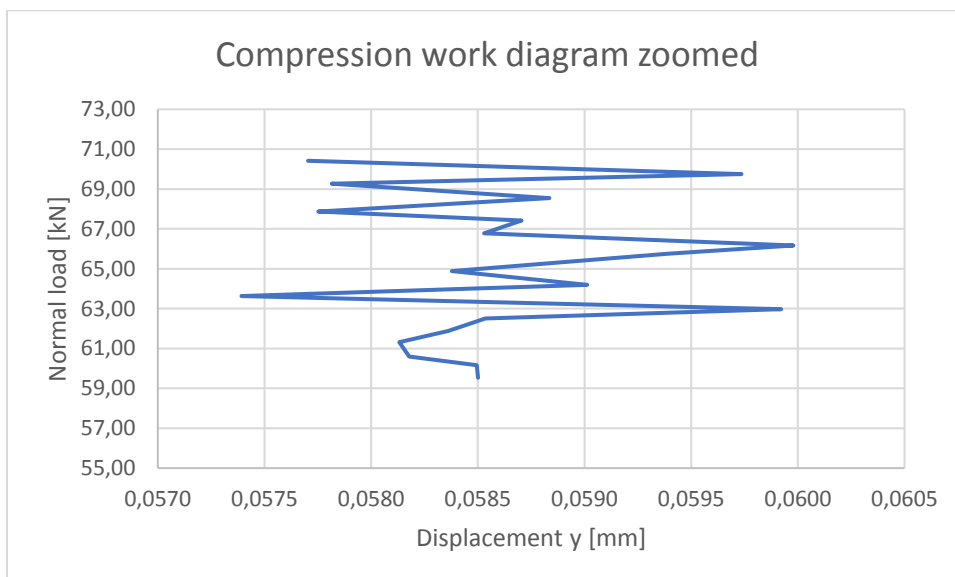


Figure 6.19 Zoomed version of figure 6.18 for calibration of the normal interface material stiffness for the F1 sample

As can be seen from diagram 6.19, it is not possible to interpolate a stiffness from this diagram. It seems to be as good as vertical. This is also as could be expected from the initial value, and the normal stiffness is therefore kept at $3 \cdot 10^8 \text{ MN/m}^3$.

When running the model with these values of tangential stiffness and friction coefficient, the following fit was obtained:

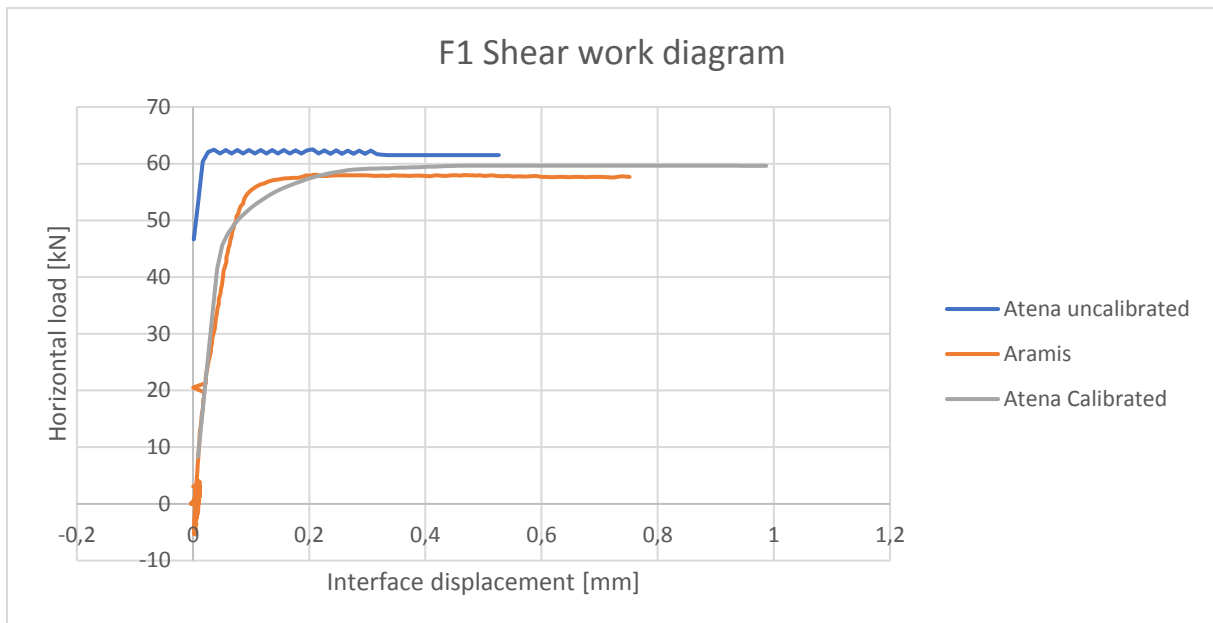


Figure 6.20 Shear work diagram from the un-calibrated and the calibrated model of the F1 sample, together with the test results from Aramis

The initial slope and the capacity is ok. The deficit in capacity between the test and the Atena model after the calibration is due to that the interface stiffness in Atena also affects the capacity to some extent, such that a higher stiffness gives a higher capacity. If cohesion was used, the opposite result should have been expected, since a soft interface would distribute the stresses better over the interface. This relation makes the interface stiffness more important when having cohesion, and also more complex to calibrate. It can be observed that the elastic part of the test is not fully linear. This is hard to replicate by the use of a linear parameter. The curvature of the FEM is smoother than the test in the transition from elastic deformation to sliding. This is observed to be the case for most Atena models, and can have something to do with the constitutive material models.

6.5.3. Sample E8

The E8 sample is a pure shear test with an asperity at the end. It was blocked towards rotation such that the sample could deform in the x- and y- direction. The failure mode of sample E8 is cutting through the asperity. The precise path of the crack is different at the two sides, as shown in figure 6.21:



Figure 6.21 The failure modes of the E8 sample from the front side and the back side. The failure modes are slightly different

Since the E8 sample is constrained against rotation, the same master - slave conditions as for the F1 sample was used. The geometry and parameters are equal, except for the asperity. The model was

first run with the calibrated interface stiffness from the F1 model. This led to a too soft behavior with too low strength, as explained in section 6.3.3.3. After this was made clear, the simulation was run with an interface stiffness according to eq. (6.20), of $3 \cdot 10^8$, since it was used 1 mm elements along the interface. The model then became very stiff, and with very high peak strength as shown in figure 6.22:

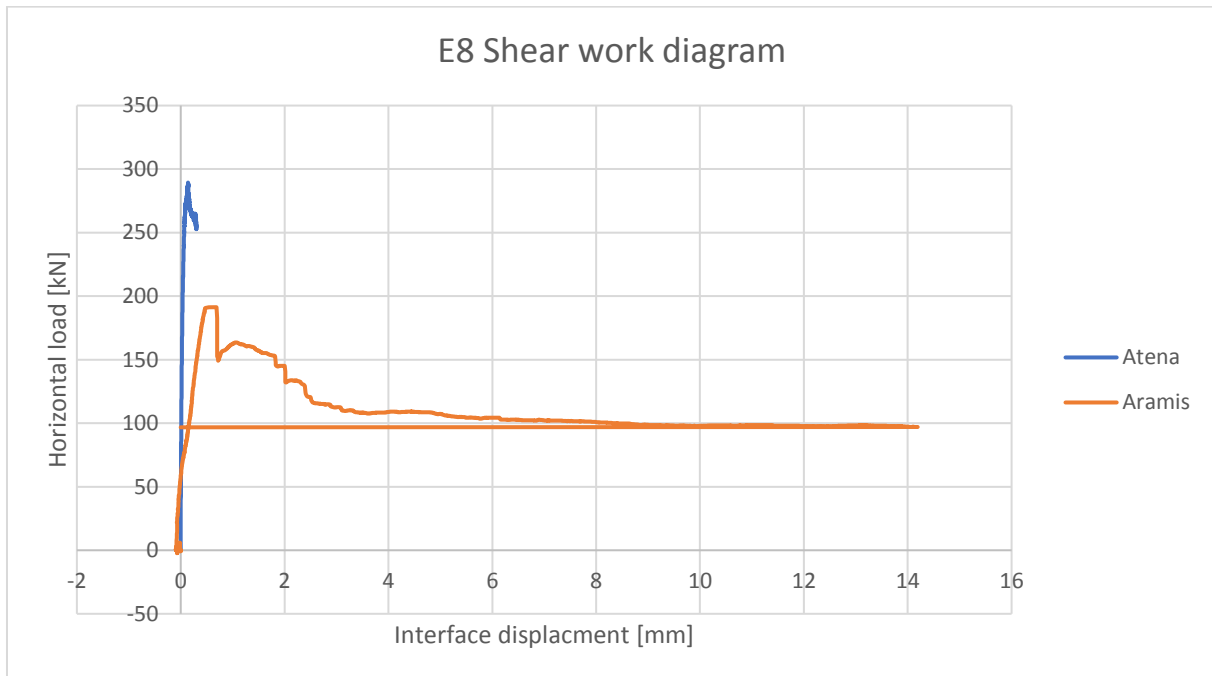


Figure 6.22 The resulting work diagram from the simulation of the E8 sample (blue) and the test result from Aramis (orange)

In figure 6.22, it is seen that the FEM capacity is 288 kN, while the lab test capacity is 191, and that the FEM interface is far too stiff.

After this was tried a model which had 10 times higher tangential stiffness than the first one. This gave negligible difference in shear stiffness. It was therefore clear that the shear stiffness of the E8 sample to a large extent is governed by the normal stiffness of the interface. This makes sense, since most of the force is on the asperity, and the force resultant is almost perpendicular to the surface.

Here could have been done a parametric study of the normal and tangential stiffness to find the best fit. Experiences from the M5 samples have shown that this is not straight forward. Due to the bad conditioning (Eltervaag, 2013), it can take up to 6 hours for one model to run, and many runs are required. It is not acceptable to modify the model with the wrong parameter, just to fit the results. It was therefore decided to instead investigate the differences in behavior between lab test and simulation, to see if there were other problems with the model. As can be seen from figure 6.22, a larger problem with the model than the stiffness is the strength, which is far too high in the Atena model.

Investigation of boundary conditions

From the digital image processing tool Aramis, a video was made of the deformation in the frame, with the displacement in the x- and y- direction quantified for eight points. Two pictures from this video is shown in figure 6.23 and 6.24:

E8 frame displacement

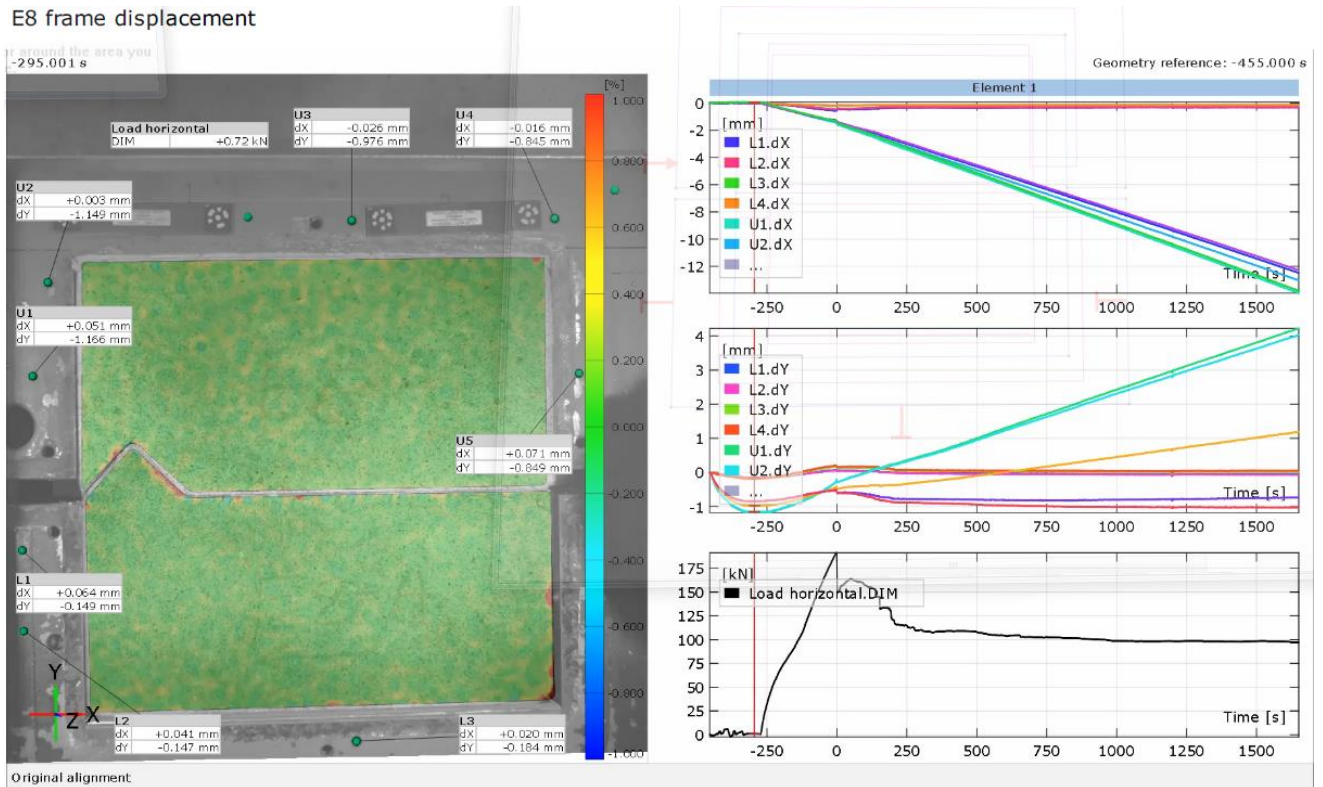


Figure 6.23 Frame displacements of the E8 sample initially

Generated with GOM Correlate Professional 2016



E8 frame displacement

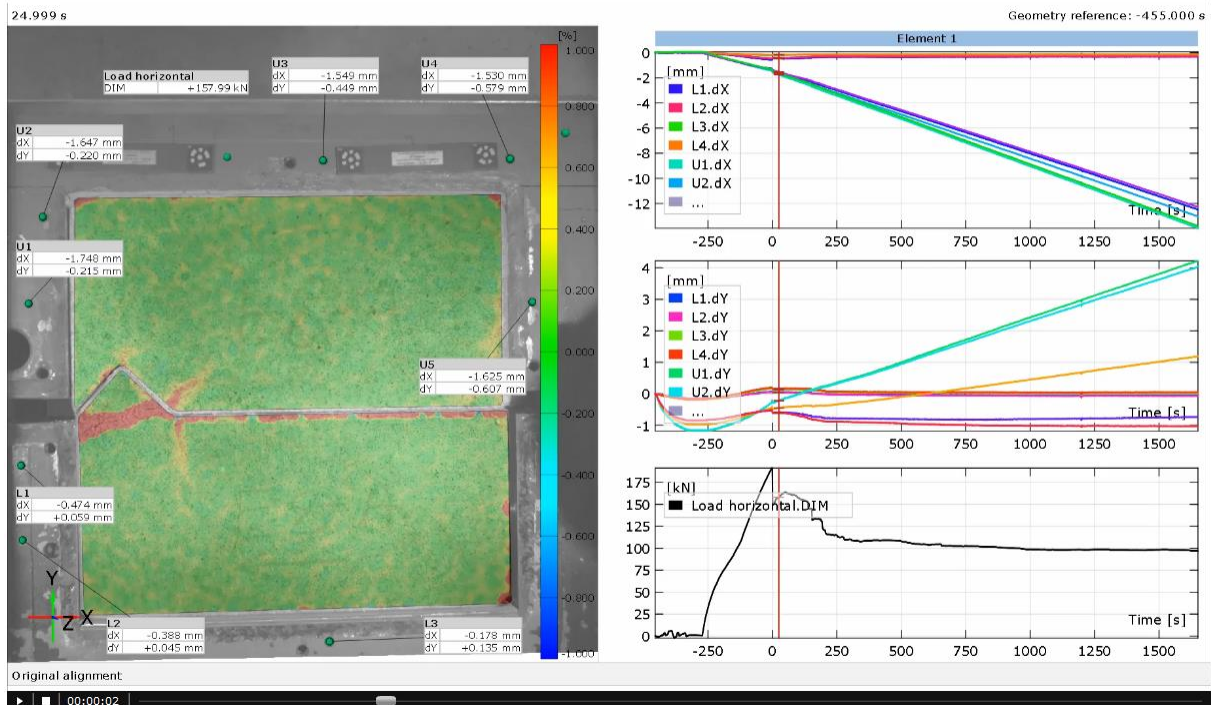


Figure 6.24 Frame displacements of the E8 sample right after peak strength

From figure 6.23 and 6.24 can be seen the displacements for points on the frame. The failure seems to be the same as in the lab test. The degree of rotation can be seen on the diagrams to the right in

the figures, as the difference in displacement between points on the frame. These figures show that the test setup is not as rigid as it was thought. At the time of failure, the difference in vertical displacement is as much as 0.5 mm. This do not seem like much, but consider the hand calculations in section 5, for the difference between sample E8 and E11. As shall be made clear in the next section, this makes a difference, and is a probable reason for the different behavior of the lab test and Atena simulation. Due to the findings regarding the boundary conditions no more effort was put into fitting of sample E8.

6.5.4. Sample E11

The E11 sample is free of rotational constrains. The load is applied 100 mm over the interface, causing a moment.

There are used 1mm elements along the interface, and the recommended stiffness from equation (6.20), $K_{NN}=K_{tt}=10^8 \text{ MN/m}^3$. As with the other eccentric loaded samples, the load is applied 100 mm over the interface. The failure mode is shown in figure 6.25, and is undercutting of the asperity in an angle of approximately 45 degrees from the asperity base.

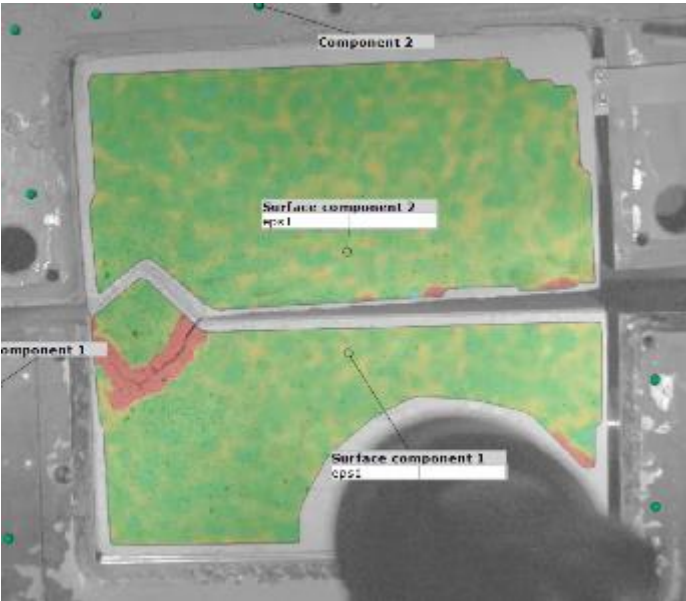


Figure 6.25 The failure modes of the E11 sample from Aramis

The experience from the E8 sample has shown that it is crucial to the result to allow the same degree of rotation as in the lab test. After inspections of the lab setup and conversations with the lab personnel it was concluded that the load cells were not resisting bending or movement in the radial direction. It was discovered that the only thing resisting movement and rotation were four springs used to hold the loading frame for the vertical load. The springs can be seen in figure 4.1. The spring constant was determined by drag tests, as seen in figure 6.26:

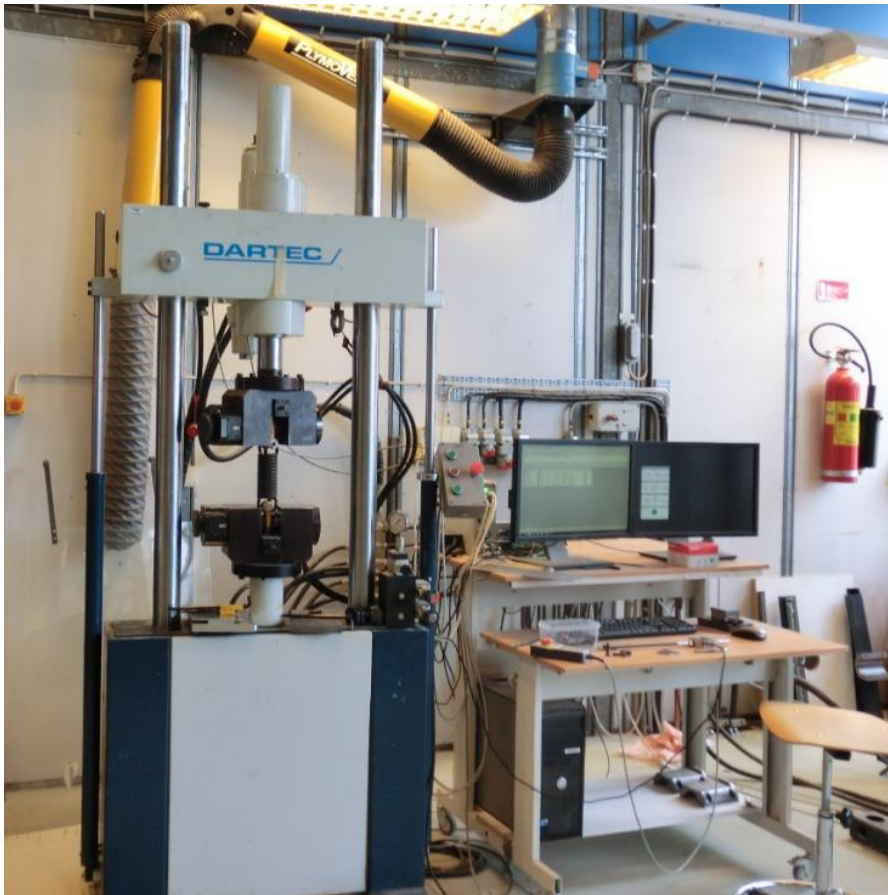


Figure 6.26 The test setup from the drag test to find the spring stiffness

The test gave a spring constant of 70 kN/m. This value is used in the model.

The original model is not wide enough to model the springs, which is shown in figure 4.1, so two arms had to be made to represent the top plate, where the springs are attached. The resulting geometry is shown in figure 6.27:

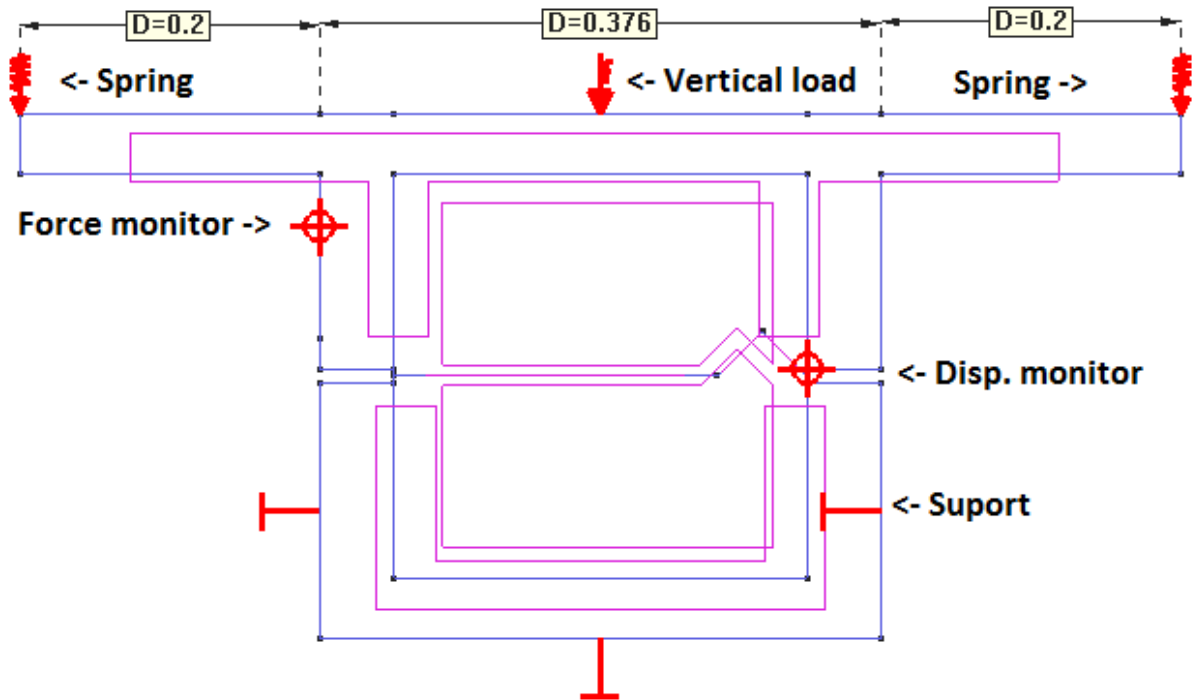


Figure 6.27 The geomtry of the numerical model for the simulation of the E11 sample

When running the model, the capacity was found to 125, compared to 176 in the lab test. The failure mode was undercutting of the asperity as in the lab test. The Crack was initiated at the left corner of the asperity, as shown in figure 6.28:

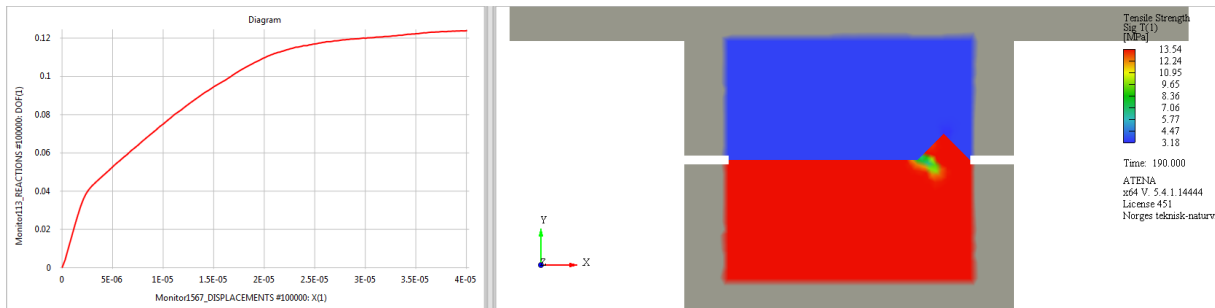


Figure 6.28 The failure mode from the simulation of the E11 sample at peak strength

After some more simulation, a new crack appeared higher up on the asperity, as shown in figure 6.29:

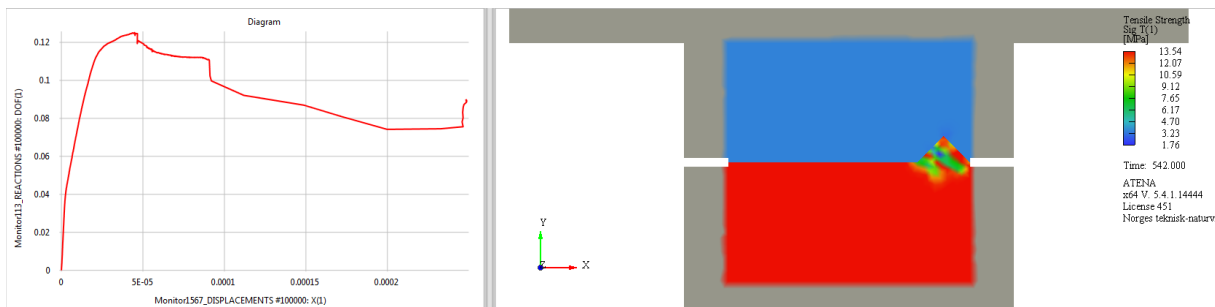


Figure 6.29 The failure modes from the simulation of the E11 sample when the simulation stops.

The failure mode in figure 6.28 is similar to the observed for E11 in figure 6.25. The failure mode in figure 6.29 is almost exactly the same as the failure mode for the E8 sample, as can be seen in figure 6.21.

A similar video was made for the frame displacement as for the E8 sample. It turned out that the frame displacements for the E8 and the E11 samples were similar at the time of failure. That means that the test conditions for the E8 and E11 sample is also similar, even though the post peak behavior of the two samples are very different. This explains the similar peak strength results for the two samples. It seems to be some rim movement in the test setup for the E8 sample, that is not blocked before after peak strength has occurred.

Compared to the lab test result, the simulation of the E11 sample is better than the E8, but it does not fit the lab results in a good way, as can be seen in figure 6.30:

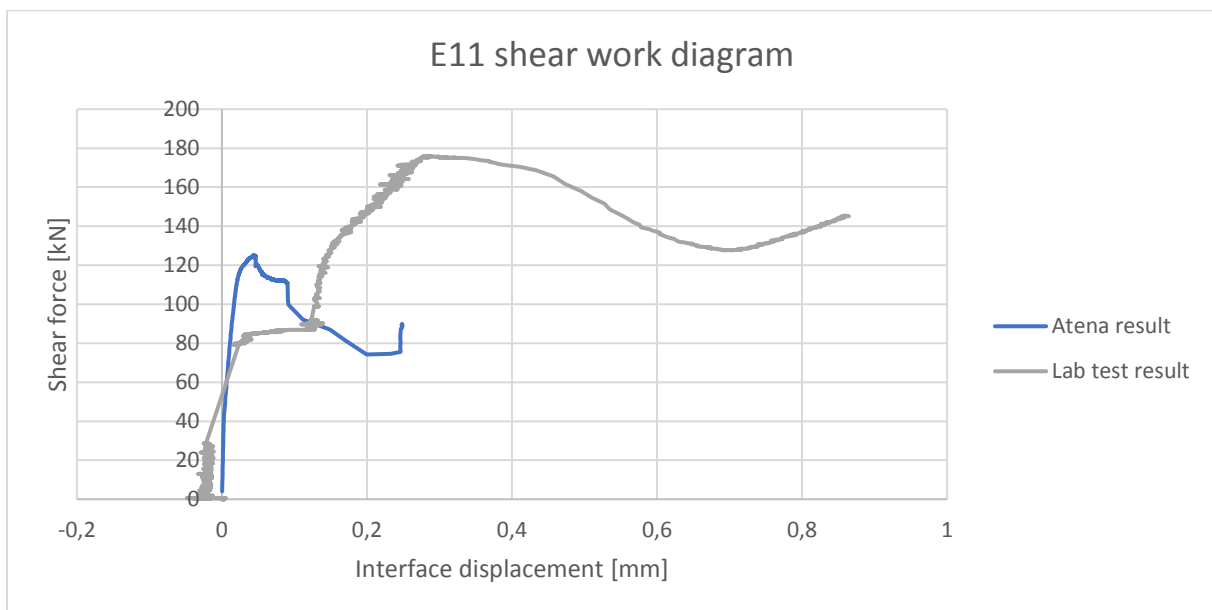


Figure 6.30 The resulting shear work diagram from the simulation of the E11 sample (blue) together with the test results from Aramis (grey)

As can be seen in figure 6.30, the shapes of the work diagrams seem to be quite similar. There are two main differences, the peak strength, and the interface material stiffness. A small parametric study is therefore carried out to see if there can be found a set of parameters in a reasonable range, that can fit the test results.

Investigation of the rock tensile strength

The failure mode is shearing through the rock. It therefore seems reasonable that if the tensile and shear strength of the rock is increased, and the fracture energy increased accordingly, the shear capacity should also increase. In the original model is used a tensile strength of 13.54 MPa, found from test. The tensile capacity was increased to 18 and 30 MPa, and the other parameters adjusted according to this. The resulting work diagrams is shown in figure 6.31:

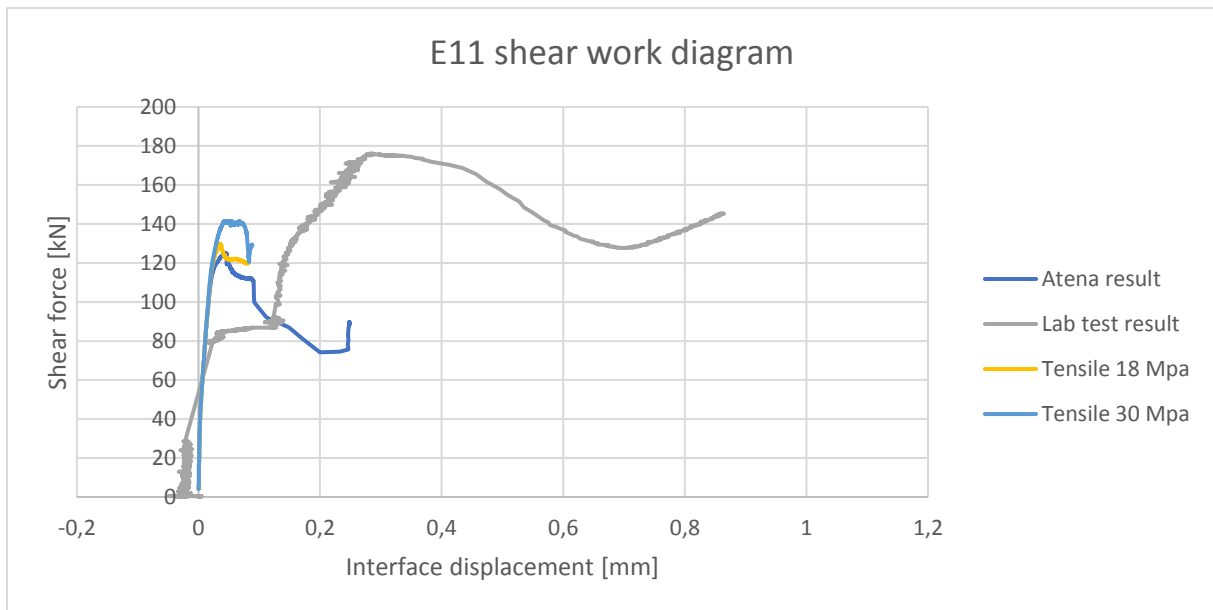


Figure 6.31 Resulting work diagrams from simulations of the E11 sample with higher rock tensile strength

From figure 6.31 can be seen that a doubling of the tensile strength of the rock only increase the shear strength by 15 kN, or 12 %. A tensile strength of 30 MPa is not in a reasonable range. The tensile strength is probably not the problem here.

Investigation of aggregate interlocking.

Aggregate interlocking is a material parameter for the concrete and rock material model. It works on crack surfaces, and prevents sliding on the crack surface. Simulations of the E11 sample shows that use of aggregate interlocking has a prolonging effect on the peak, but little influence on the peak strength:

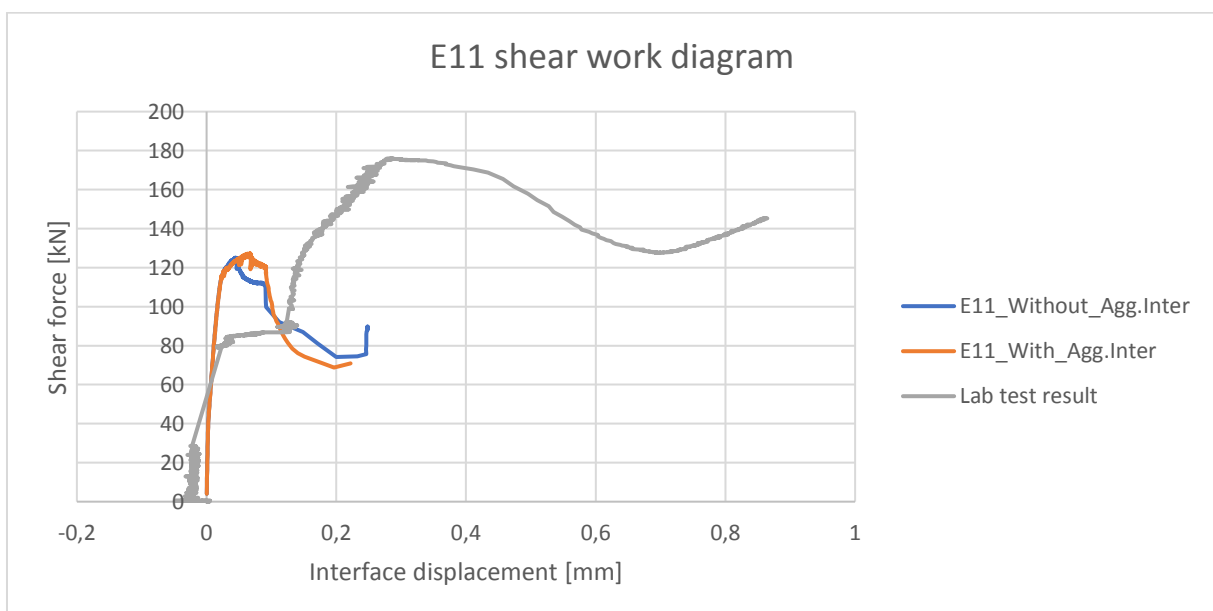


Figure 6.32 Resulting work diagram from the simulation of the E11 sample with the aggregate interlocking parameter turned on

Figure 6.32 indicates that aggregate interlocking brings the simulation work diagram closer to the original, and it should therefore be included. It is used in the further investigations.

Investigation of lab test data

In figure 6.32 can be seen a horizontal sliding of 0.1 mm in the beginning of the lab test work diagram. This can be explained from a gap of 0.1 mm between the concrete and the rock asperity. It would make sense that the model should then behave like the F1 model in the beginning. This is not possible to control, but it is a reasonable assumption. Since it is not possible to put in such a gap in the Atena model, it is reasonable to take away this sliding in the data. The result of this can be seen in figure 6.33:

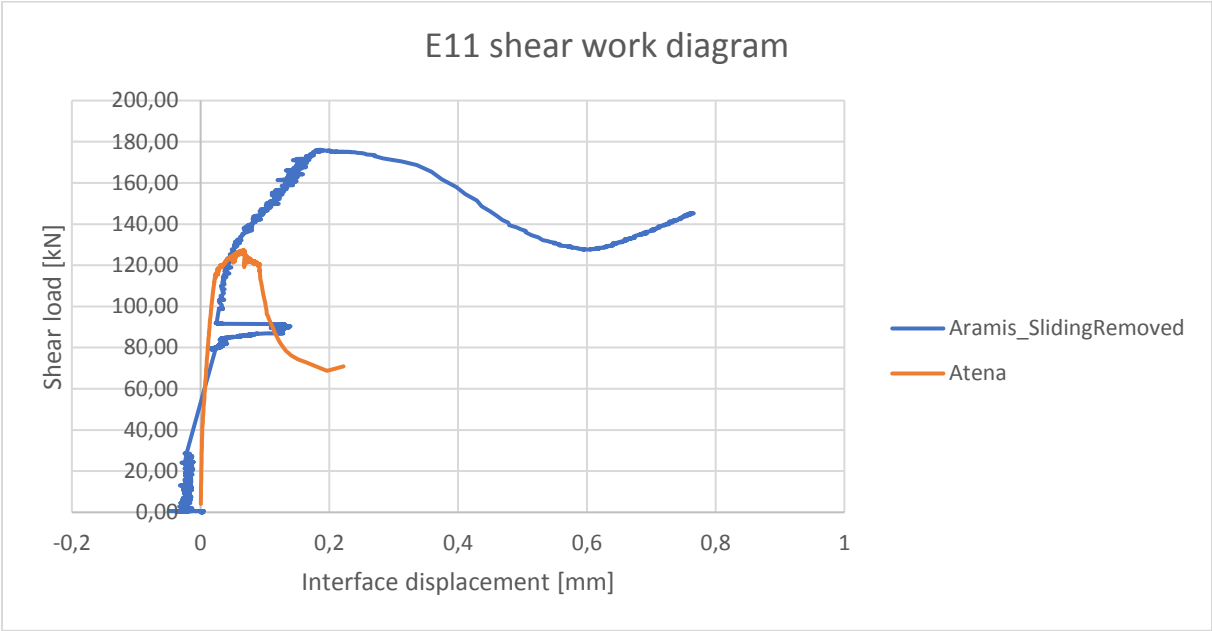


Figure 6.33 Simulation result (orange) and results from Aramis adjusted to take away horizontal sliding part (blue)

Investigation of rotational constrain

The difference in capacity between the FEMs of E8 and E11 can only be explained due to the degree of rotational constrain. Since the lab test result showed results in between, a reasonable explanation would be that they had a rotational constrain in between. To investigate the effect of rotational, constrain, a new model was made of the E11 sample, where the spring stiffness was 10-doubled. Each of the four springs seen in figure # has then a stiffness of 700 kPa, compared to 70 kPa in reality. The result of the model with stiff springs is shown in figure 6.34:

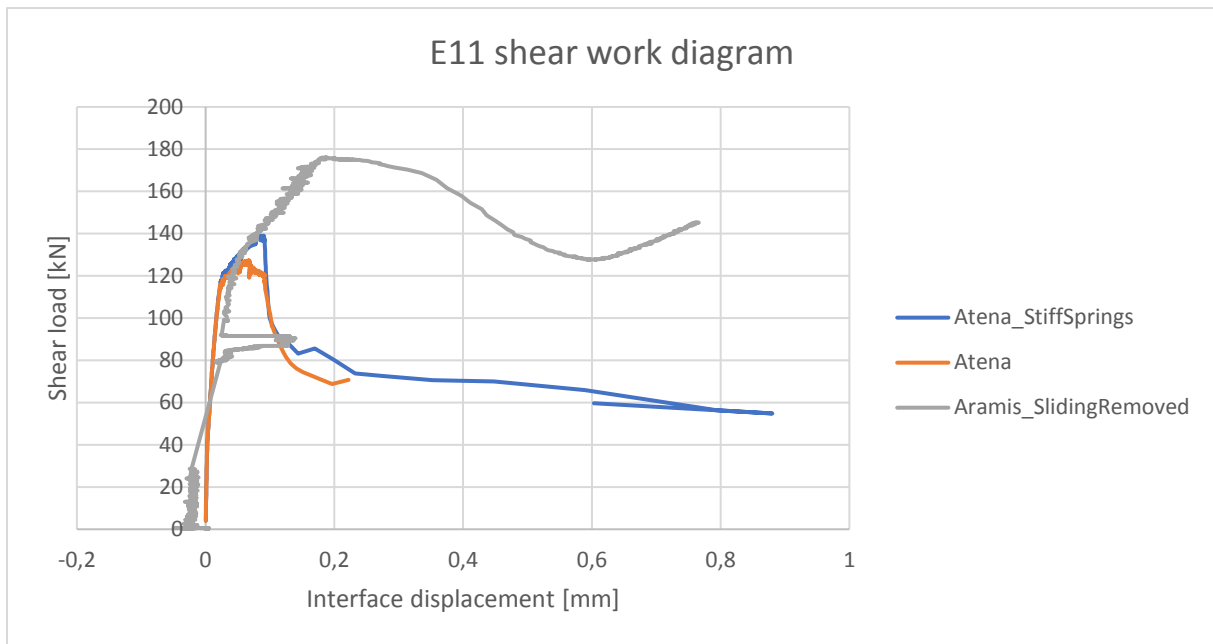


Figure 6.34 Simulation results with 10 times stiffer springs (blue) and adjusted test results (grey)

As can be seen in figure 6.34, the increase in rotational stiffness by 10 times increase of the spring stiffness brings the result closer to the test result. A new model is made, to see if it can be brought even closer with higher rotational stiffness. In figure 6.35 can be seen the result from the model with 50- and 100-doubled spring stiffness:

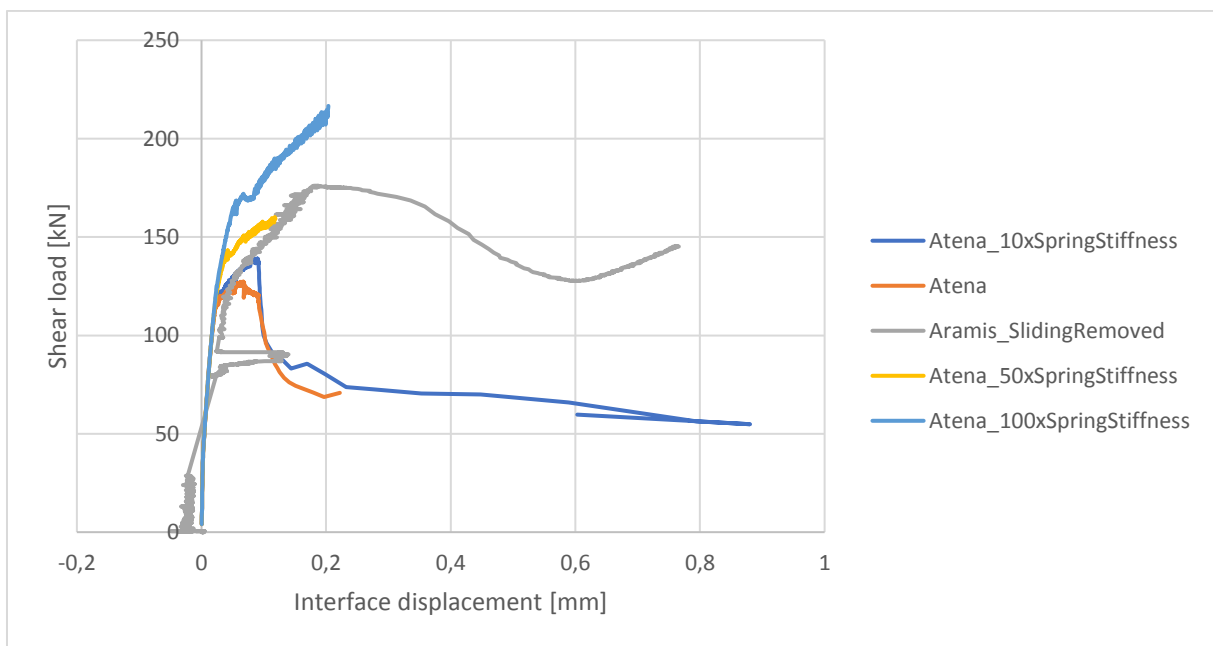


Figure 6.35 Simulation results with 50 (yellow) and 100 (light blue) times higher spring stiffness

In figure 6.35 can be seen that a rotational constrain is a probable reason for the difference in capacity between the E11 lab test and the Atena model. An interpretation of this could be radial resistance at the load pistons. Since it is known that the springs are not the real reason for the difference in rotational constrain, it is not done further attempts of model fitting with the spring stiffness.

Investigation of the model at other normal loads

It is interesting to see how the model of E11 performs for other normal loads. Therefore, the E11 model is modified to model the E12 and the E13 sample with a normal load of respectively 0.6 MPa and 0.2 MPa. There is no Aramis data available for these samples, but the shear capacity, together with the model results is shown in table 6-3:

Table 6-3 Peak shear strength from simulation and tests for the E11, E12 and E13 samples

	E11	E12	E13
Lab test	175 kN	134 kN	40 kN
Atena	125 kN	81 kN	35 kN
Difference	-29%	-40%	-13%

Table 6-3 shows that the Atena model under-predicts the shear capacity for all the models with free rotation and asperity at the end.

6.5.5. Why it is so hard to model post-peak behavior

Tensile failure in brittle materials is in its nature unstable, since the criterion that should be satisfied for a tensile failure to happen is that the release of potential energy in the fracture of a unit area of the structure is higher than the energy needed to break open a unit area of the structure. If a non-reinforced concrete column is loaded in tension until it fails, it is impossible to predict where it is going to fail, given that the material properties varies uniformly over the structure.

When doing non-linear analysis in Atena, it works in the way that the load is applied in load steps, so that when a new small load is applied, the program iterates to find an equilibrium.

When a tensile failure happens, an equilibrium does not exist, since once it is initiated in a small area, the release rate of energy is larger than what the structure can take up. Eventually, in real life a tensile failure stops somewhere, because although it can sound like a black hole, it is not. Unstable tensile failures tend to stop when the failure has reached the edge of that part of the structure. That may not be fatal for the structures ability to carry load but it is most often not possible to carry on the simulation after the local failure, since the program does not manage to converge the energy residual.

7. CASE STUDY DAM KALHOVD

7.1. Introduction

The aim of this case study is to see how use of the real geometry of the foundation will affect the calculated stability of a plate dam pillar compared to a traditional stability assessment with Mohr-Coulomb shear criterion, rigid body displacement and straight shear plain. It is also investigated how different definitions of the factor of safety (FS) against sliding affects the stability.

In this case study, section 59 of Dam Kalhovd is studied. The pillar has an approximate upstream height of 5 m. The geometry has been measured at sight. In figure 7.1 can be seen a picture from sight:

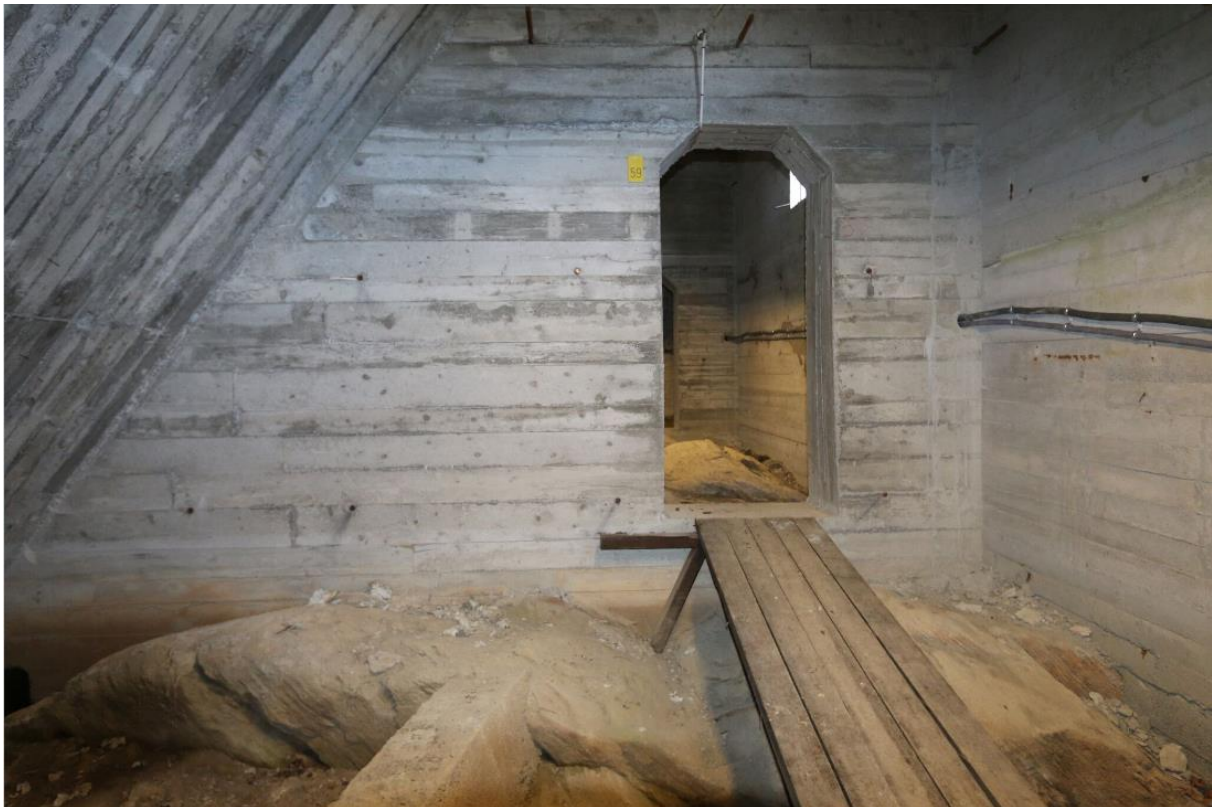


Figure 7.1 Picture of pillar 59 from the Dam Kalhovd

Dam Kalhovd was assessed by Norconsult as part of the reassessment process. As an initial assessment was used the traditional method assuming rigid body displacement and Mohr-Coulomb shear criterion. For pillar 59, this gave a FS against sliding of 1.14.

7.2. Defining the factor of safety

For a FEM, the factor of safety is not so straight forward as for a hand calculation, since the FEA can only find the load situation where the structure fails, meaning that the factor of safety equals one for the applied loads. The factor of safety against sliding is defined as the resistance capacity divided by the acting loads. This means that to find the factor of safety with a FEA, there are two principle ways to go, increase the loads or decrease the resistance capacity. For a traditional calculation, the only resistance is the friction. To reduce the friction factor is a normal procedure (Wyllie and Mah, 2004). But when doing an analysis on the real geometry, the friction is not the only resistance preventing sliding. If the resistance capacity should be reduced, then the material strength of the materials on both sides of the interface should also be reduced. This would lead to an iteration process to find the

factor of safety, were the parameters were adjusted, and the model would need to be re-run to find if the dam is safe with the given factor of safety. For simplicity, it is therefore chosen to put the factor of safety on the water loads (including uplift) and ice loads. This is equivalent to increasing the density of water together with the ice load. Since the calculation is divided into load steps, the factor of safety could then be defined as the load in the load step were the simulation stops divided by the dimensioning loads. The increase in loads are carried out by defining the water- and ice loads in a separate interval, and increase them until failure. The factor of safety is then equal to the resulting loads divided by the dimensioning loads.

7.3. Material parameters

7.3.1. Concrete

There were found a medium compressive cylinder strength of 33.0 MPa and an E-modulus of 25 GPa for the concrete samples from Dam Kalhovd. The tensile strength is set from the eq. (7.1) (Standard Norge, 2010):

$$f_{ctm} = 0.30 * f_{ck}^{\frac{2}{3}} \quad (7.1)$$

$$f_{ck} = f_{cm} - 8 \text{ MPa} \quad (7.2)$$

Applied with a f_{cm} of 33.0 MPa equation (7.1) gives $f_{ctm} = 2.6 \text{ MPa}$

The fracture energy of the concrete is set according to the formula (Westberg and Johansson, 2016):

$$G_f = 73 * f_{cm}^{0.18} \quad (7.3)$$

Applied with a f_{cm} of 41.2 MPa equation (7.3) gives $G_f = 137 \frac{N}{m}$.

7.3.2. Rock

There were done material tests on core samples from Dam Kalhovd. The results from the Concrete were quite reliable, while the results from the rock samples were not consistent, due to limited number of tests and different failure mode observed in compressive tests. Based on a qualitative assessment of the most reliable tests, the compressive strength was set to 100 MPa, and the E-modulus to 60 GPa. The tensile strength was set according to equation (7.1) to 6.1 MPa, and the fracture energy was set to $167 \frac{N}{m}$ according to formula (7.3).

7.3.3. Interface parameters

It was assumed no bonding, i.e. no cohesion, to be able to compare with the results from the spreadsheet calculation. Tests on core samples from Dam Kalhovd showed a friction angle of 69° for a normal pressure of 0.5 MPa. This was considered too high, and it was therefore used a friction angle of 45° , resulting in a friction factor of 1, as recommended in the NVE guidelines (NVE, 2005).

The interface stiffness was set according to equation (6.20), as a function of mesh size.

7.4. Model

7.4.1. Geometry

It is chosen to include the rock foundation in the model, rather than to apply boundary conditions directly on the dam. The rock foundation is modelled to a depth of 8 m and an outcrop of 5 m on both sides of the dam. The rock is modelled with fixed supports on all sides. The thickness of the foundation model is 1m. This is assumed to be the influence zone of the pillar. Unfortunately, the plate has a larger influence zone than the pillar, since its much wider.

It was chosen to model the pillar without the doorway and without reinforcement, to keep the model simple. This can be defended since the aim of the analysis is stability control, not to assess the structural strength. No self-weight is applied to the doorway.

The model is shown in figure 7.2:

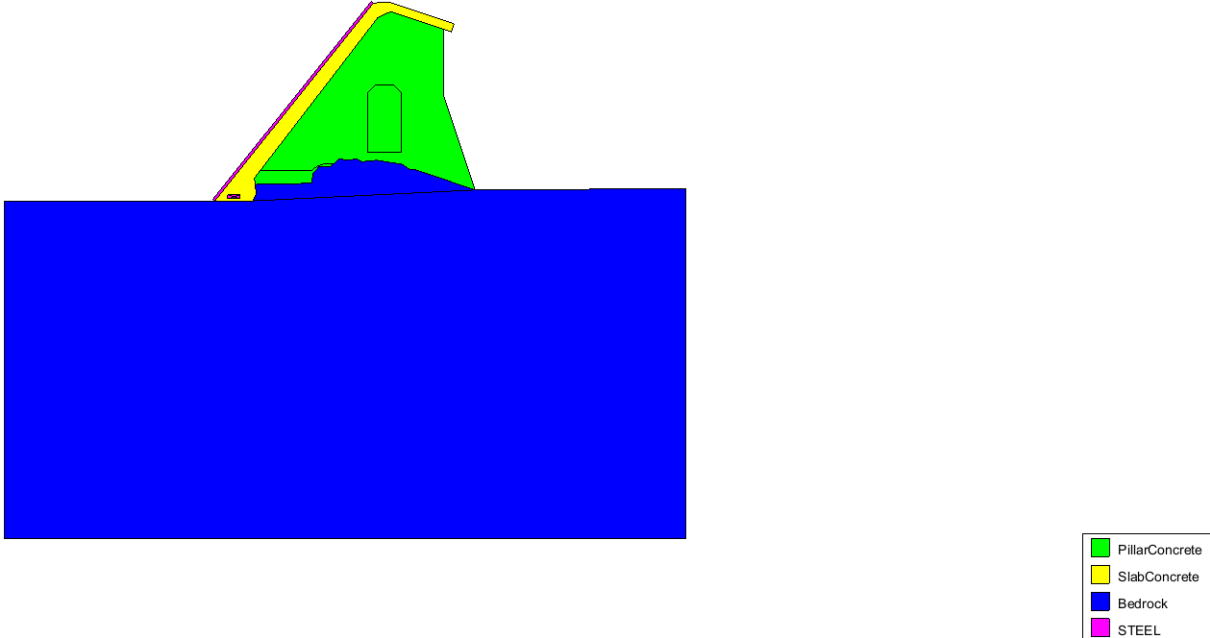


Figure 7.2 The geometry of the numerical model for the simulation of pillar 59 from Dam Kalhovd

In figure 7.2 can be seen that there is a crack in the front of the pillar. Previous experiences have shown that it is difficult to make a model with sliding along two parallel interfaces. It was therefore decided to make two models, one with the interface through the crack, and one with the interface between concrete and rock.

In figure 7.2 can also be seen that the load plate for the application of ice load and hydrostatic load is quite thick. It was therefore decided to reduce its stiffness by a factor of 1000, such that it would be equivalent to a 0.1 mm steel plate, which is assumed to be neglectable.

The geometry of the pillar is not correctly modelled. The real pillar has a top thickness of 0.3 m, increasing to 0.44 m at the bottom. Since the model is made with linear stress elements, which has constant thickness, it is used an average thickness of 0.37 m for the pillar. Since the Mohr Coulomb shear criterion is used for the interface without cohesion, the difference in pillar thickness between the model and reality does not matter for the sliding properties.

7.4.2. Mesh

The geometry is meshed with a mesh size of 0.05 m along the concrete – rock interface, 0.1 m in the concrete parts and 0.5 m in the rock foundation. The mesh together with the quality index is shown in figure 7.3:

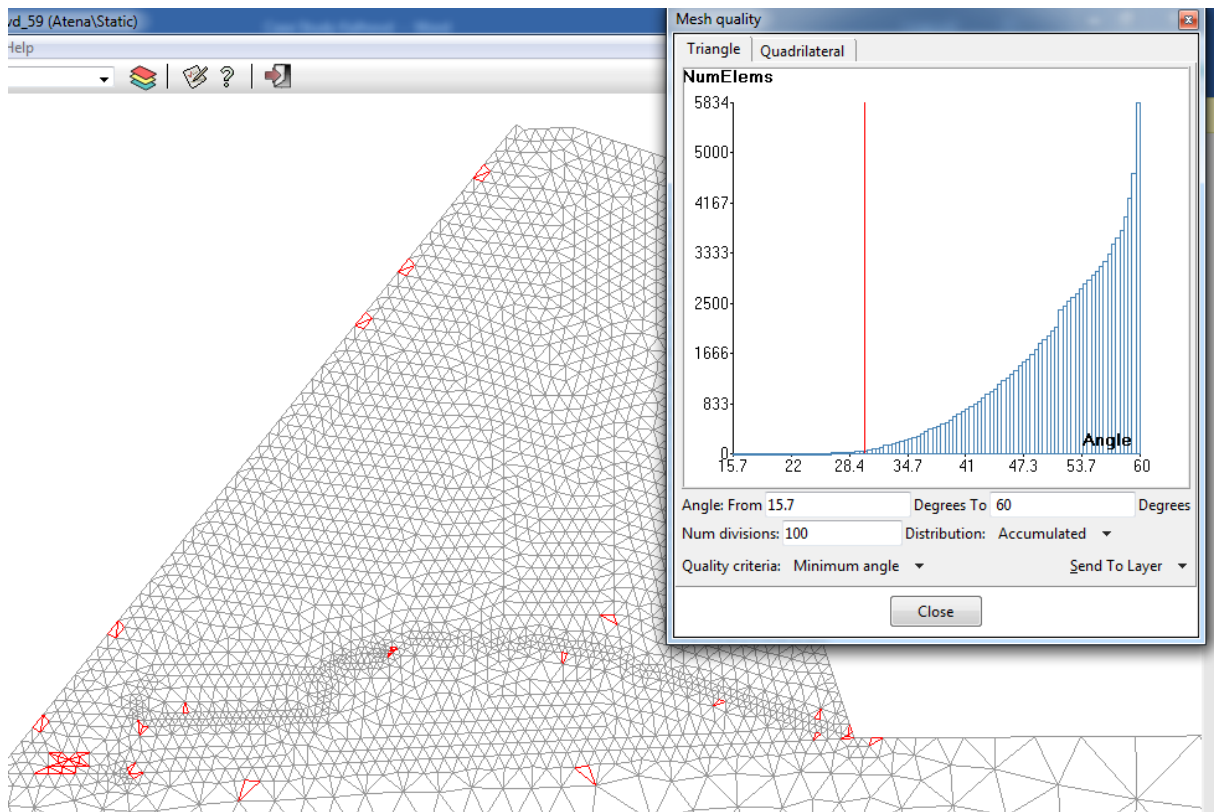


Figure 7.3 The mesh quality for the simulation of pillar 59 from Dam Kalhovd

The best is to have only equilateral elements (angles 60° for triangular elements). Elements with angles less than 30° is considered bad quality (Cervenca et al., 2013). As can be seen from figure 7.3, there are few such elements. There are some where the uplift is applied, but since these are linear elastic and the solution converges it is not believed to have any influence.

7.4.3. Loads

The less beneficial load case is HRW + ice load. The HRW is at elevation 1086.61 mas. The ice load is set to 100 kN/m and the distance between the sections is 5 m, giving an ice load of 500 kN per pillar. The hydrostatic load and ice load is applied on a steel plate with thickness 0.1 mm outside the concrete plate. To get a good mesh, the steel plate had to be made thicker and softer. It is modelled as a 100 mm thick plate with stiffness $E=500$ MPa, which is a thousand of steel stiffness. It is therefore equivalent to a 0.1 mm steel plate for compression, and thinner for bending.

The total height of the section is 4.7 m. Since modelling triangular line loads in Atena is not straight forward, the load is applied as point load in 48 points along the plate, as seen in figure 7.4 and 7.5. The load for each point is calculated as the pressure in the point times the area it represents. Each point represents an area of 0.5 m^2 , except for the outer points representing an area of 0.25 m^2 .

The uplift is modelled as a point load on a steel core inside the concrete plate, as seen in figure 7.4:

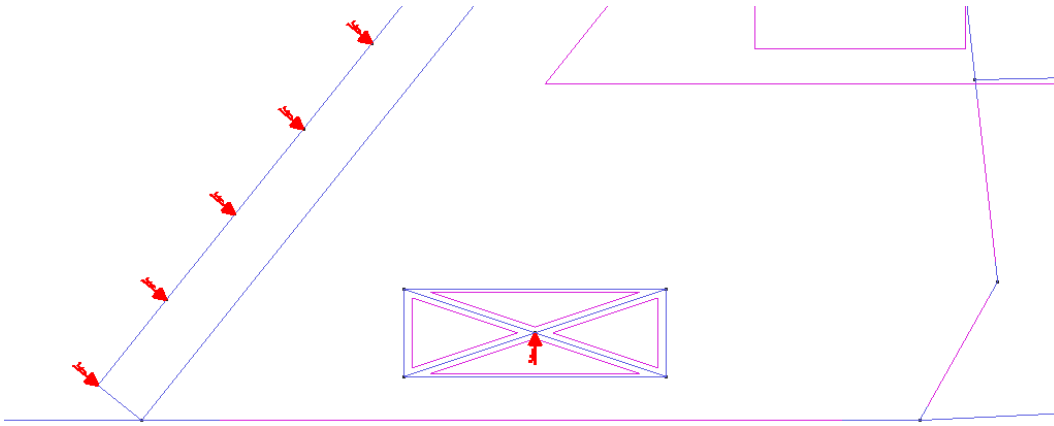


Figure 7.4 Illustration of the load application of the uplift force in the numerical model of pillar 59 from Dam Kalhovd

The uplift force is calculated as the hydrostatic pressure in front of the plate (47 kPa) times the area of the downside of the plate, giving a total load of 211.5 kN.

The self-weight of the structure is applied with a value of $23 \frac{kN}{m^3}$ for the concrete and $27 \frac{kN}{m^3}$ for the rock. No weight is applied for the doorway. The load application is shown in figure 7.5:

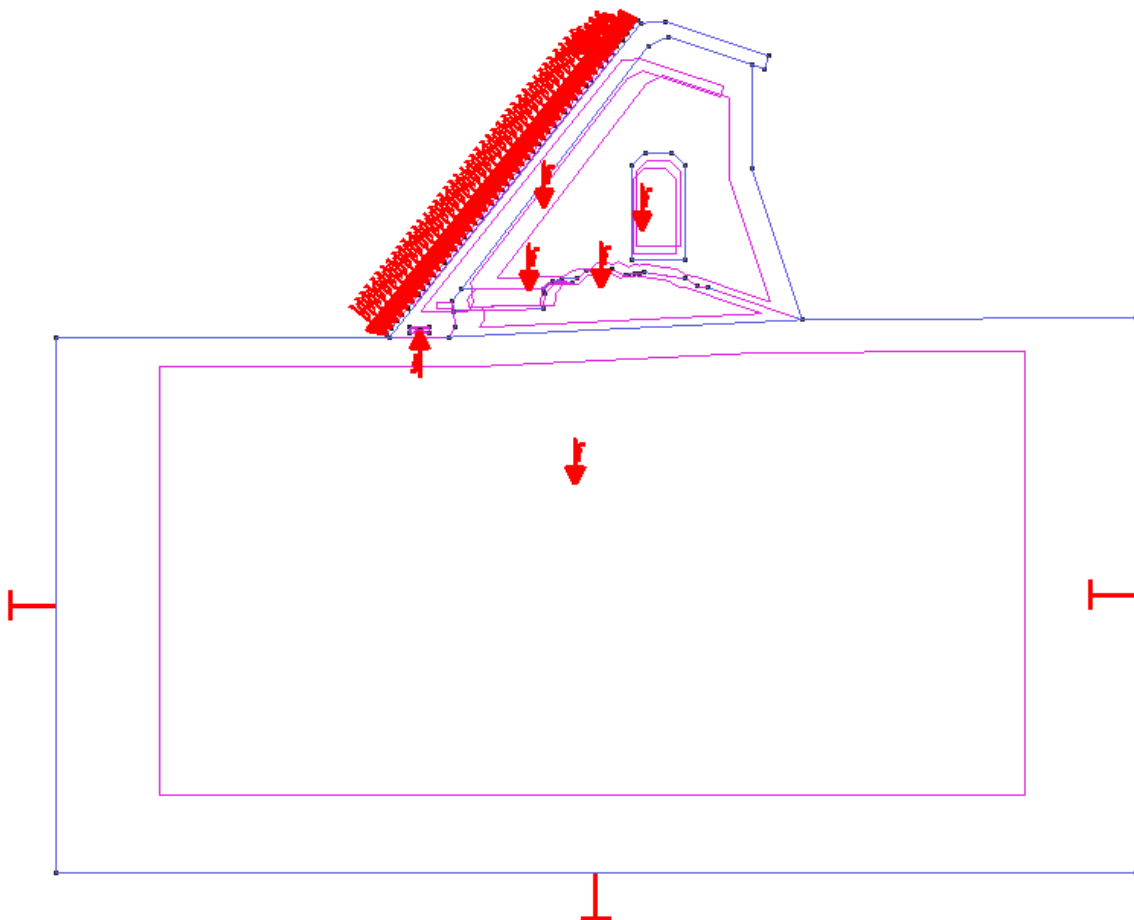


Figure 7.5 The load application in the numerical model of pillar 59 from Dam Kalhovd

The arrows inside the volumes represents surface loads, the up-pointing arrow is the uplift and the loads on the plate is the hydrostatic load and the ice load.

7.5. Results

7.5.1. Model with interface in foundation

First the model was run without the crack, representing the original state. At a load of about 2.4 times the dimensioning, a crack developed similar to the observed crack. After this crack had reached the plate, a new crack started to develop from the tip of the rock asperity towards the plate as shown in figure 7.6:

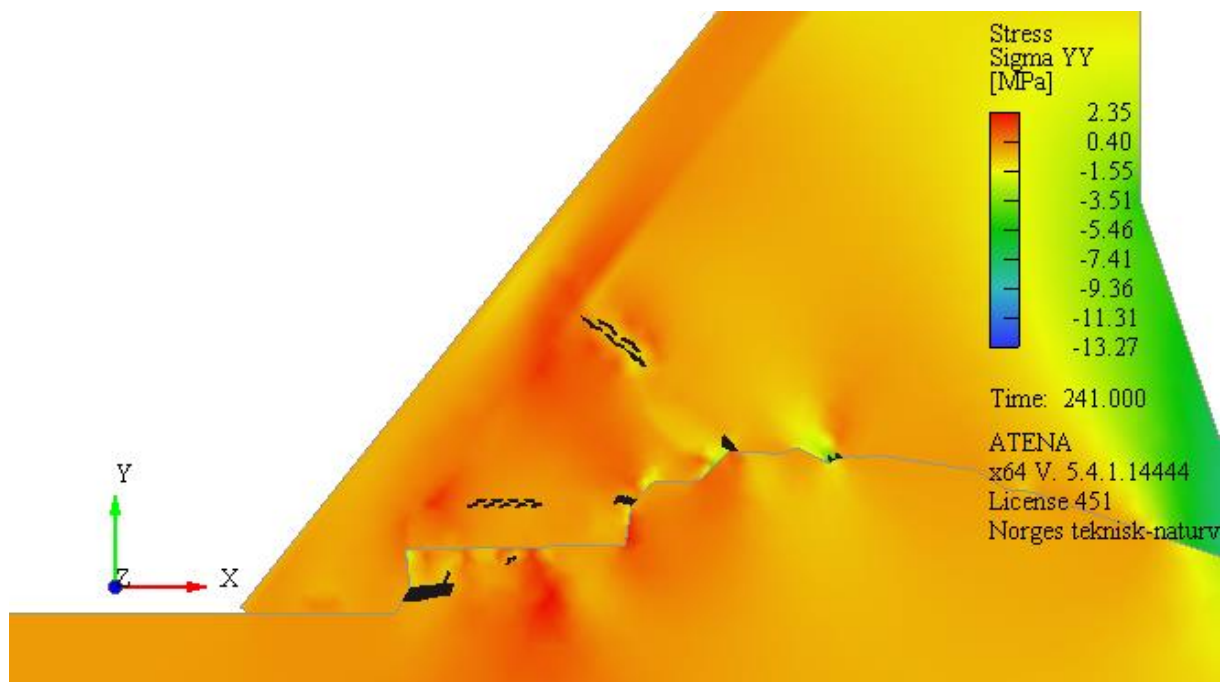


Figure 7.6 Failure modes in the numerical model of pillar 59 from Dam Kalhovd with the interface at the foundation. In the figure is drawn the vertical stresses, and the failure modes are shown as cracks.

Since each load step applies 1% of the dimensioning loads until step 100, and 1% of the water- and ice load from step 101, a simulation until step 240 corresponds to a factor of safety against sliding of 2.4. Since this model do not collapse completely after the development of the first crack, it is assumed to be a valid result to start the simulation without the crack, and let it develop by itself. In the next step, the horizontal concrete crack develops into the plate.

The cracks in the rock is partly a consequence of the assumed influence zone of 1m for the pillar. It is observed that most of the forces in this area comes from the plate. The crack in the front of the rock asperity is therefore not expected to occur on the real dam.

7.5.2. Model with interface in the observed crack

The model with crack through the concrete was run until step 280 before it stopped due to convergence problems. The reason for the lack of convergence was cracking in the rock foundation and through the plate, as shown in figure 7.7:

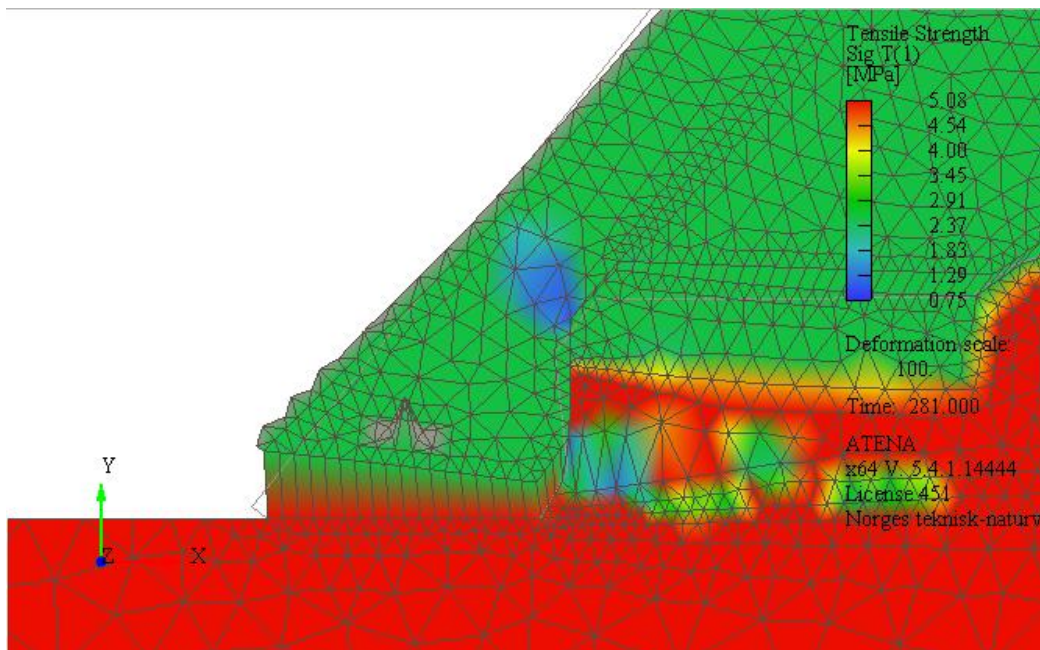


Figure 7.7 Illustration of the failure modes from the simulation of pillar 59 from Dam Kalhovd with an interface in the observed crack. In the figure is drawn the deformed shape over the original shape.

Figure 7.7 shows the deformed shape, with a multiplication factor of 100. It seems like much of the stability against overturning comes from friction between the vertical surfaces of rock and concrete. This would not occur with a straight shear plain, and is one of the main advantages of including the geometry in the model.

280 steps carried out gives $FS=2.8$ for this model. It is observed that there are tensile stresses of 1 MPa in the concrete right over the foundation in the plate front, and this model is therefore not valid. It is not unreasonable that there should be 1 MPa cohesion under the plate, but since this is not documented, this is omitted in the model. It is reasonable to assume that these tensile stresses can explain the difference between the two models.

Based on these considerations, the first model, the one with interface along the foundation, is found to be a good representation of the actual behaviour of the dam. This conclusion is strengthened by the appearance of the same failure mode as is observed on the real dam. This model is therefore used in the parametric study.

7.6. Parametric study

7.6.1. Ice load

A new model was made, where only the ice load was increased. This is done to investigate what happens if the safety factor is only applied to the ice load instead of applying it to both the ice load and the density of water. Then the factor of safety is reduced to 2.1. This means that it is more conservative to only put the factor of safety on the ice loads, than on both the water- and ice loads. The reason for this is the large vertical hydrostatic pressure due to the inclined plate.

Since the ice load is the most uncertain load for Norwegian conditions, this definition of the safety factor is reasonable. This calculation shows that the observed crack can be explained if the ice load has reached 210 kN/m.

7.6.2. Horizontal loads

It is reasonable that the FS should be put on the parameter that contributes to the uncertainty, which is the resistance and the ice load. In the previous section, it was investigated what happens if the FS was put on the ice load. It was stated initially that it is not possible to put the FS on the resistance, since it is very complex with a real geometry. It is also stated that the normal procedure for finding the FS with FEA is to reduce the friction angle. Since the friction angle also represents the geometric roughness when a flat surface is assumed, it is reasonable to put the FS on the resistance as a whole. This can be justified by the large uncertainty in the property of the rock mass. In this section, the FS is therefore put on the horizontal forces. This should be equivalent to putting the FS on the resistance since the resistance equals the horizontal forces at sliding failure.

The hydrostatic pressure is then decomposed into a vertical and a horizontal part, where the horizontal part is increased, while the vertical part is kept constant. Since the uplift is smaller than the vertical hydrostatic pressure on the upside of the plate, this should be a more conservative definition than the initial definition. The ice load is also increased accordingly. The model run to step 199, where it fails, giving a FS=1.98. This is assumed to be the most correct FS. It is also the most conservative. The failure mode is, as before, shearing through the pillar and the plate, as shown in figure 7.8:

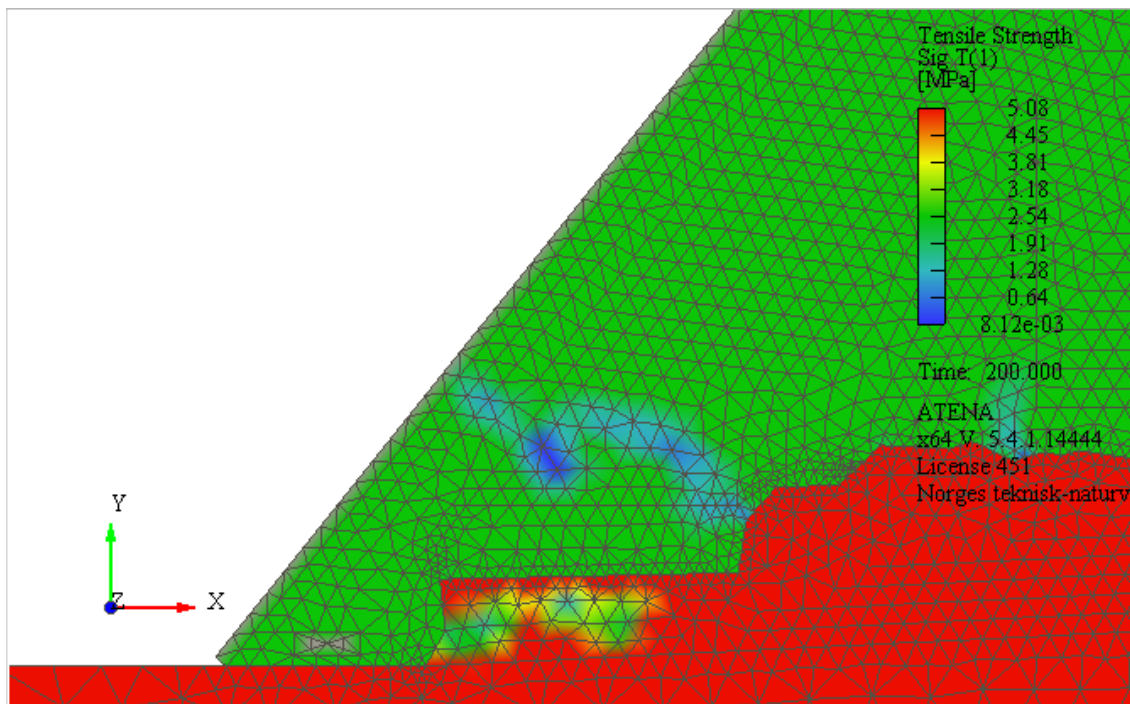


Figure 7.8 The failure modes from the simulation with increasing horizontal loads until failure

At this stage, the model has not converged, but figure 7.8 indicates what happens in the model.

As earlier mentioned, the crack through the rock is un-physical due to geometrical issues. As before, the crack develops at about the same place as the observed crack in the pillar.

7.7. Assessment of scale effects

It is not possible from an empirical point of view to quantify the scale effects in a model, without making scaled versions of the same models. The assessment of scale effect must therefore be set up as a discussion.

One of the nice things about numerical models is that they model distributed forces, which converges to stress as the element size is decreased. Scale effects are in general a force phenomenon, rising from different stress distribution on different scales. When stress is modelled and not force, there should therefore not be any scale effects, in theory. The problem is that the interface where the plastic shear deformation happens is not modelled with high enough resolution. To capture the scale effects, the individual roughness would need to be modelled so that the model would contain the real contact area, since larger surfaces have larger contact areas (Johansson, 2009). The resolution of the geometry in the model presented here is in the order of magnitude 20 cm. To apply the real geometry helps on the scale effect, but it is the authors meaning that the resolution applied here is not high enough to make scale effects disappear.

One way to mitigate this issue without using a very fine geometry would be to use a non-linear failure criterion, describing the post-peak behaviour from shear tests of the same scale as the resolution of the geometry. It was found that the interface displacement in the toe part of the pillar was about 3 mm at the time of failure. Then it is not correct to use a friction angle of 45° . Rather a residual friction angle of 40° should be used in this area. Unfortunately, it is not possible to have a variable friction angle in Atena. A friction angle of 45° can be defended by that the friction angle is higher than this in the parts of the interface that do not have any interface displacements.

8. ADVICE ON THE LARGE-SCALE SHEAR TEST

8.1. Introduction

The large-scale shear test is a part of the Stable Dam project. In the original plan, it should have been carried out in the late summer of 2017, but it has been delayed. When the assignment text for this thesis was made, it was expected that it should be carried out in the summer of 2018. At the delivery date of the thesis, it is expected that the test should be carried out earliest in the autumn of 2018. The purpose of the large-scale test is to be a demonstration of the developed assessment methods, to show that they are competent to be applied on full-scale dams. This leaves two questions to be answered:

- 1) What methods for dam safety assessment should the large-scale test be designed to test.
- 2) How should the large-scale test be carried out in practice.

8.2. Location of the large-scale test

In the Stable Dams project, two main approaches are carried out, to find the shear capacity of idealized surfaces, and to find the capacity of real surfaces. There are two alternatives for the large-scale test, to do it in the lab or in the field. In the lab, it is possible to do the test under controlled conditions. In the field, it is possible to test under much more realistic conditions. To put it on the edge, the choice stands between measuring a realistic sample inaccurately or measuring an unrealistic sample accurately. This should not make much difference, and the difference should be what should be tested. If a natural surface should be tested, it is beneficial to do it in the field, since nature consists of natural surfaces. If a simplified man-made surface should be tested, similar to the shear tests on man-made asperities done at LTU in the spring of 2017, it is better to do it in the lab, since the surfaces would need to be cut out as blocks for preparation. Since the aim of the large-scale test is to show that the developed methods are reliable on real dams with real geometry, I base the further discussion on that the test should be done in the field.

Leif Lia has suggested to do full scale tests on sections of Nåvatn Dam II or Nåvatn dam IV in Åseral municipality in southern Norway. These dams are going to be decommissioned in 2018 in the process of merging the two reservoirs Skjerkevatn and Nåvatn. An air photo of the dams is shown in figure 8.1:



Figure 8.1 Air photo of Dam Nåvatn I, II, III and IV

From the picture in figure 8.1, it looks like dam IV is the best candidate, since this dam has the easiest access. In a brief period in 2018, the water will be drawn down for the decommissioning of the dams. Nåvatn Dam II is a 12 meters high plate dam, and it would therefore be available pillars in all heights below 12 meters. The most interesting would be to test pillars that are deemed unstable by the traditional methods. Norconsults assessment of Dam Kalhovd (appendix C) shows that it is the small pillars (below 6 m) that are most unstable due to ice load. Lower pillars would also require less force at lower heights, and have a longer time window due to rising water.

8.3. Load case

So, what scenario should be tested? How should the pillar be broken? Since it is a low pillar, HRW + ice load will be the dimensioning load case. In the case study on the pillar from Dam Kalhovd, the factor of safety was applied to the resistance, because the model of the resistance was considered most uncertain. This was done by increasing the horizontal forces until failure. For the full-scale test, the model of resistance is not uncertain, since it is a real structure, even if it is not known. The probable cause of failure for the dam is the ice load, and the dam should therefore be broken by increasing the equivalent of the ice load until failure.

8.4. How to apply loads

There would not be enough force to take down more than one pillar at a time. It must therefore be investigated how much cross-bearing there is between neighboring pillars, to find if it is possible to

do the test with the plate. If there is much cross-bearing, the plate would need to be removed or cut off. One approach could be to saw off the plate half way between the pillars, so that a representative part of the plate weight would be assigned to the pillar. But this approach would not be representative of the real state, since we would not apply distributed forces on the plate, and if we do, we would not be able to keep the plate in the correct position and angle at the sides, and therefore, the forces will not be distributed correctly.

The main difficulty with a full-scale test is how to apply the load. The load bearing in a plate dam is highly complex. The most realistic, and therefore also most representative approach would be to test the dam when there is water behind, but this would require the construction of a water retaining structure, since testing the dam with a full reservoir of 120 mill m³ behind is not recommended. To use a water retaining structure would only be representative of the real state if it is found that there is no cross-bearing between the pillars. If such an effect is found, which is very probable, the loads would need to be assigned as concentrated loads.

It should therefore be investigated how the load bearing is distributed between the plate trench and the pillar, so that an equivalent load could be assigned to the plate. After calculating the load and its distribution on the plate, the plate should be removed for the test. The insulating wall should stand to get sideways stability. It would be useful after the test is done to be able to back-calculate to find the equivalent load on a pillar with plate, as a result of the failure load on a pillar without plate. For this purpose, is needed a 3D numerical model of a dam section with the plate trench.

The vertical loads from plate and water could be applied with concrete or steel weights, or by pre-stressing wires between the pillar and rock bolts. The horizontal loads could for example be applied by building a concrete block on the upstream side of the pillar, so that the load could be produced by mechanical or hydraulic jacks, as shown in figure 8.2:

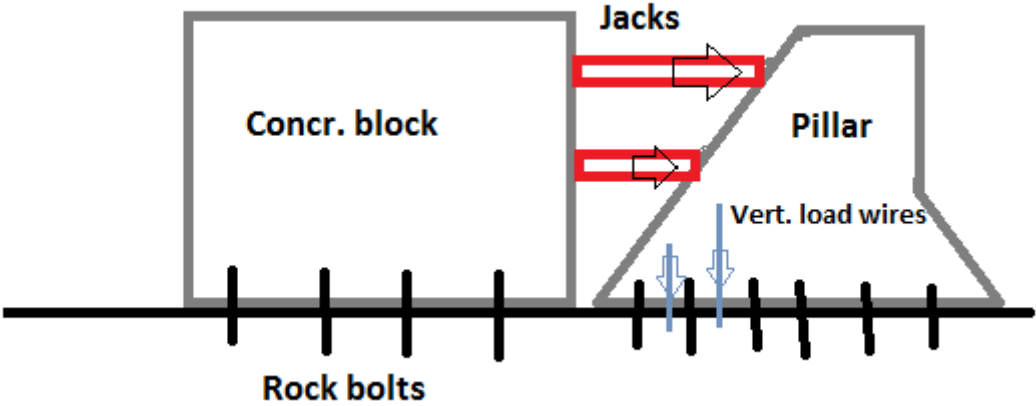


Figure 8.2 Illustration of a possible test setup for the large-scale test

The concrete block would need to have a larger capacity against sliding and overturning than the pillar. A rule of thumb is that it would need to have larger mass than the pillar. The volume of the pillar is approximately 10 m³ (6 m*5m*0.33 m). It would also need to be strengthened with rock bolts, and have the necessary curing time. If there are not enough curing time available, the amount of concrete could be increased to compensate. Concrete costs are in the order of magnitude 3000 NOK/m³ (Norconsult, 2016), so the price for 15 m³ of concrete would come at about 45 000 NOK. The reinforcement, bolts and formwork would amount to at least that much (Norconsult, 2016). The best would be to coordinate this with concrete works for the concrete plinth under the asphalt core on

the new Dam Skjerkevatn, but it would probably not be possible to start that fast. There is also a question of how often the water level in Nyvatn is more than 5 m below the dam crest, but it would hopefully be possible to do the works before the spring flood in 2018.

A simpler alternative for the load application would be to pull the section using a heavy-duty truck, where a dynamometer could measure the force. If this is done during the construction of the new embankment dam Skjerkevatn, there would be lots of available trucks for this purpose. If this method is chosen, a pillar from dam IV must be chosen, due to road access (see figure 8.1). According to (van Daal, 2015), a truck can generate a pull force approximately equal to 50 % of its own weight. According to the authors compendium in plant engineering (Bruland, 2013), a typical size for a wheel loader is 100 tons. If such a wheel loader was equipped for it, it could be approximated from these data that it could pull about 50 tons of force. That is not necessarily enough to pull down a plate dam pillar of 25 tons with favorable foundation geometry, bonding between concrete and rock, and rock bolts. This could be solved by using two trucks, either in parallel or in series. When doing this, it is very important to pull with the correct angle. It can be seen from the photo in figure 8.1 that there is a slope on the downside of the dam IV. From the map, this slope is found to be 65 m long and 14 m high, giving an average inclination of 1:5 or 11° . Since the wires would probably need to be attached to the truck in a height of approximately 2 m, about 3 m more must be added to the height difference due to the height of the dam, giving an inclination of 1:4, or 15° at the best position of the truck. This angle can be very favorable, not only to increase the pulling force, but also for the experiment. A rough calculation shows that for a 5 m high dam with plate inclination 4:5, the load resultant of water and ice will have an inclination of 31° with ice load of 100 kN/m and 17° with an ice load of 200 kN, which were the maximum load for the pillar studied from Dam Kalhovd in the case study. With bonding and rock bolts, the force would probably need to simulate a larger ice load. At 300 kN/m the inclination would be 13° . If the weight of the plate also is included, the angle would be higher. With this angle, there would not be that large need to have vertical forces on the dam, if done right. This is one of the main advantages with the truck alternative.

8.5. Monitoring

The test should be monitored with the Aramis optical measurement system, similar to what is done on the shear tests on man-made asperities, conducted at LTU the spring of 2017. This is important to be able to compare the test to a numerical model. The data from Aramis could also be used to control the loads, by inserting the found displacements into a numerical model, to find the force needed to cause them.

The experience from the spring 2017 shear tests at LTU shows that it is useful to have two independent measurement systems.

8.6. Project risks

There are multiple safety, health and environment risks related to this project. Some of the risks are here listed up:

- Snapping of the pulling wire or load wires, resulting in the wire hitting someone with supersonic speed.
- Bursting of hydraulic cylinders as a result of overloading of machinery.
- The concrete block or pillar overturning sideways and hitting someone.
- Someone getting run over by the truck.

There are also economic risks in the project. One of the main economic risks would be if the project is extended or delayed, for example due to that the applied force is not high enough, or something

breaks down. The measurement devices are probably the most vulnerable component in the project. Most of the mechanical devices can probably be replaced without much delay. SHE issues and delay can hopefully be avoided with proper planning.

9. CONCLUSIONS

9.1. Findings

9.1.1. Theoretical background

- 1) Use of the Mohr-Coulomb shear failure criterion leads to underestimation of the strength for small dams and overestimation of the strength for large dams, since the peak friction angle is decreasing with increased normal load, as shown by Patton (Patton, 1966).
- 2) Use of Patton's criterion requires an advanced model to set the dilatation angle correct. All of these models are rigid body models, meaning that they are unable to take into account the deformation in the dam to find the correct global capacity from the local work diagrams.

9.1.2. Simulation of shear box tests

- 3) The results of the modelling show that simulation these are not straight forward for the shear tests. The main reason for this seems to be that it is hard to replicate the laboratory boundary conditions, especially related to the steel frames and the load pistons. It is possible to fit the model to the result by modifying the rotational stiffness in the boundary conditions. This is not a proof that the rotational stiffness is the difference, but it makes it probable.
- 4) Since it is probable that the main difference between the numerical model and the lab test is due to different rotational constrain in the test setup, and it is possible to calibrate the model using parameters related to the stiffness, the numerical model is assumed to be a good representation of reality. In a real concrete dam, there would not be any problems with the rotational constrains.
- 5) One of the main learning points from modelling of the shear tests is that it is dangerous to calibrate a model with the wrong parameter. Even if a good fit is obtained, the model will not work in other cases.
- 6) It is not straight forward to calibrate the interface material stiffness, since it is both dependent on the mesh size and the shear stress - strain. The best way to set the interface material stiffness seems to be to follow the recommendations in the program manual (Cervenca Consulting, 2017). To have the correct interface material stiffness is most important when cohesion is used.

9.1.3. Case study

- 7) A factor of safety is not a good way to assess the safety of a concrete dam, since it does not differentiate between parameters with small and large variation. In the case study, the FS was applied to the horizontal loads, which is equivalent to applying it to the sliding resistance. When this definition is applied to dam section 59 of Dam Kalhovd, it obtains a factor of safety against sliding of 1.98, compared to 1.14 with the traditional approach. The reason for this is that the failure mode is no longer sliding on a straight shear plain, but material failure in rock and concrete. Of the FS definitions investigated, this was the most conservative.
- 8) The method with finite element analysis with real geometry seems to be a better representation of reality, and shows more capacity than the traditional method. It would not provide additional capacity for all sections, only on those with beneficial geometry. But it could mean the difference between decommissioning the whole dam and only doing strengthening of the worst sections. This would lead to a large gain for both the economy and the environment without violating society safety.
- 9) The contribution from the slab trench seems to be very large. This effect should be taken into consideration also in traditional sliding analysis, for example by including the shear capacity of the plate in the shear resistance.

- 10) The stabilizing moment from the vertical component of friction between rock asperities and concrete is a major contribution to the stability against overturning for rough geometries. In a FEA, this contribution is included, but it is not recognized in the traditional method.

9.1.4. Conclusions on the large-scale test

- 11) The test should be done in the field to have a realistic foundation. Dam Náváttn II and IV are good candidates. Dam IV is the best due to easiest access.
- 12) A 3D model must be made to determine if there is cross-bearing between the pillars, and if it is, to find the equivalent loads on the pillar, so that it could be determined what loads should be applied. If there is cross-bearing, the plate must be removed.
- 13) The load case should be HRW + ice load, and the pillar should be broken by increasing the ice load, since that is the most realistic scenario.
- 14) The pillar could be simulated by a 2D plain stress model, similar to what is done in the case study in this thesis.
- 15) An optical measurement system should be used to control the loads, and the result from the numerical model. It should be two independent measurement systems.
- 16) Two methods for load application is presented. The cheapest and most realistic is probably the alternative with pulling the pillar with a heavy truck. The best way to choose would be to contact the entrepreneur working on the dam, and ask what can be delivered to which price.

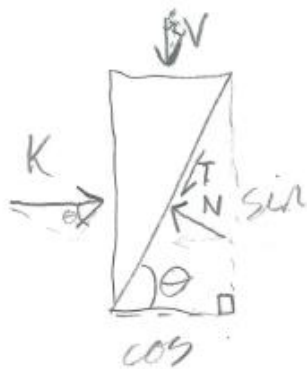
9.2. Suggestions for future work

- 1) A Finite Element Model of a dam should be made where the roughness is represented through a spatial distributed, advanced failure criterion that includes the post-peak behavior. This failure criterion must be calculated for each element along the dam from the actual roughness at the foundation. The idea is to combine the FEMs ability to handle distributed stress and displacements, and its ability to iterate to find a solution, with an advanced, empirical shear failure criterion based on the real geometry. This should be combined with shear tests documenting the interface post-peak behavior at different normal stress levels, so that the peak friction angle is reduced to the residual friction angle during a given shear deformation of the interface. The failure criterion should be connected with the interface material stiffness, for example through the contact area. This approach would favor Grasselli's criterion (Grasselli, 2001), since it includes the contact area. It is not possible to use advanced shear criteria in Atena – GiD in the standard form, but it could be made possible by programming a new module.
- 2) An analytical method should be determined to find the contribution from the vertical friction component on the overturning stability. By hand calculation on sample M5 was found that for asperities with sum of friction angle and asperity angle larger than 90 degrees, this effect would be beneficial for the overturning stability. If this effect is quantified, it could be used for foundations with rough geometry and good rock quality.

10. SOURCES

- BANDIS, S. 1980. *Experimental studies of scale effects on shear strength, and deformation of rock joints*. University of Leeds.
- BARTON, N. 1973. Review of a new shear-strength criterion for rock joints. *Engineering Geology*, 7, 287-332.
- BARTON, N. & BANDIS, S. 1982. Effects Of Block Size On The Shear Behavior Of Jointed Rock. American Rock Mechanics Association.
- BARTON, N. & CHOUBEY, V. 1977. The shear strength of rock joints in theory and practice. *Rock mechanics*, 10, 1-54.
- BAŽANT, Z. & OH, B. 1983. Crack band theory for fracture of concrete. *Matériaux et Construction*, 16, 155-177.
- BRULAND, A. 2013. *Anleggsteknikk GK: Kompendium*, Institute of Civil Engineering, NTNU.
- CERVENCA CONSULTING 2017. Atena Science. 5.4.1 ed. Prague.
- CERVENCA, V., JENDELE, L. & CERVENCA, J. 2013. ATENA Program Documentation. In: CERVENCA CONSULTING (ed.). Prague.
- CIMNE 2017. GiD. 13 ed.
- ELTERVAAG, Ø. 2013. *Sliding Stability of Lightweight Concrete Dams - Development of Numerical Models*. Master thesis, NTNU.
- GRASELLI, G. 2001. *Shear strength of rock joints based on quantified surface description*. Ecole Polytechnique Fédérale de Lausanne.
- HIBBELER, R. C. & FAN, S. C. 2011. *Mechanics of materials*, Singapore, Prentice Hall.
- JENSEN, V. & SKOGLUND, M. 2000. *Spørreundersøkelse vedrørende tilstanden til norske betongdammer, fyllingsdammer og kraftverk*, Trondheim, SINTEF, Bygg og miljøteknikk, Sement og betong.
- JOHANSSON, F. 2009. Shear Strength of Unfilled and Rough Rock Joints in Sliding Stability Analyses of Concrete Dams.
- KONOW, T. 2017. Eksisterende betong- og murdammer, evaluering av sikkerhet - Utkast for diskusjon. Dr. Tech Olav Olsen.
- KULATILAKE, P. H. S. W., SHOU, G., HUANG, T. H. & MORGAN, R. M. 1995. New peak shear strength criteria for anisotropic rock joints. *International Journal of Rock Mechanics and Mining Sciences & Geomechanics Abstracts*, 32, 673-697.
- LADANYI, B. & ARCHAMBAULT, G. 1969. Simulation Of Shear Behavior Of A Jointed Rock Mass. American Rock Mechanics Association.
- LIAHAGEN, S. A. 2012. *Stabilitet av betongdammer - Ruhetens påvirkning på skjærkapasiteten mellom betong og berg ; Stability of concrete dams The influence from roughness on the shear capacity between concrete and rock*. Master thesis, NTNU.
- NORCONSULT 2016. *Kostnadsgrunnlag for vannkraftanlegg : prisnivå 01.01.2015*, Oslo, Norges vassdrags- og energidirektorat.
- NVE 2005. Retningslinjer for betongdammer.
- NYMO, A. 2016. *Buttresses on Flat-Slab Dams - Planning of Shear Tests*. Master thesis, NTNU.
- PATTON, F. D. 1966. *Multiple modes of shear failure in rock and related materials*. University of Illinois.
- STANDARD NORGE 2010. *Eurokode 2: Prosjektering av betongkonstruksjoner = Eurocode 2: Design of concrete structures : concrete bridges : design and detailing rules : Del 2 : Bruer, Lysaker*, Standard Norge.
- STØLEN, P. 2012. *Målsetdammen - Sikkerhet mot glidning i platedam ; Målsetdammen - Safety against Sliding in Plate Dam*. Master thesis, NTNU.
- VAN DAAL, M. 2015. *The knowledge: Pull force* [Online]. heavyliftnews.com. [Accessed 05.06. 2017].
- WESTBERG, M. & JOHANSSON, F. 2016. Probabilistic model code for concrete dams. Energiforsk.
- WYLLIE, D. C. & MAH, C. 2004. *Rock slope engineering*, CRC Press.

Appendix A – Derivation of the Mohr-Coulomb formula for inclined sliding



$$N = K \cdot \sin(\theta) + V \cdot \cos(\theta)$$

$$T = N \cdot \tan(\phi)$$

$$\begin{aligned} \Sigma F_x &= K - N \cdot \sin(\theta) - T \cdot \cos(\theta) \\ &= K - K \sin^2(\theta) - V \cos(\theta) \sin(\theta) - K \sin(\theta) \cos(\theta) \tan(\phi) - V \cos^2(\theta) \tan(\phi) \\ &= K (1 - \sin^2(\theta) - \cos(\theta) \sin(\theta) \tan(\phi)) - V (\cos(\theta) \sin(\theta) + \cos^2(\theta) \tan(\phi)) \end{aligned}$$

$$\Sigma F_y = N \cdot \cos(\theta) - T \cdot \sin(\theta) - V = N \cdot (\cos(\theta) - \sin(\theta) \tan(\phi)) - V$$

$$= (K \cdot \sin(\theta) + V \cdot \cos(\theta)) (\cos(\theta) - \sin(\theta) \tan(\phi)) - V$$

$$= K (\cos(\theta) \sin(\theta) - \sin^2(\theta) \tan(\phi)) - V (1 + \cos(\theta) \sin(\theta) \tan(\phi) - \cos^2(\theta))$$

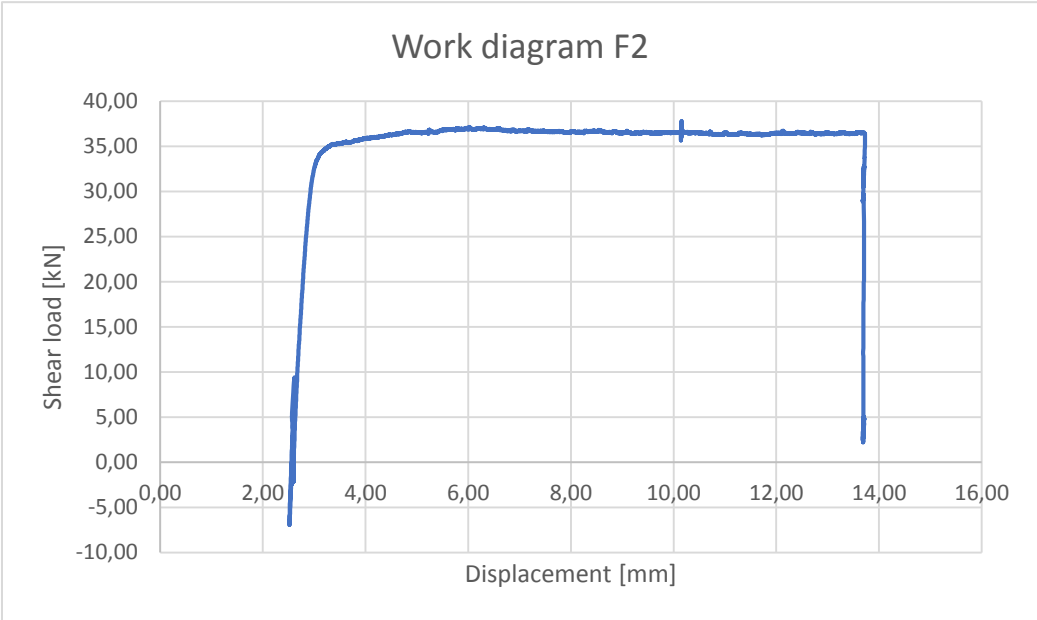
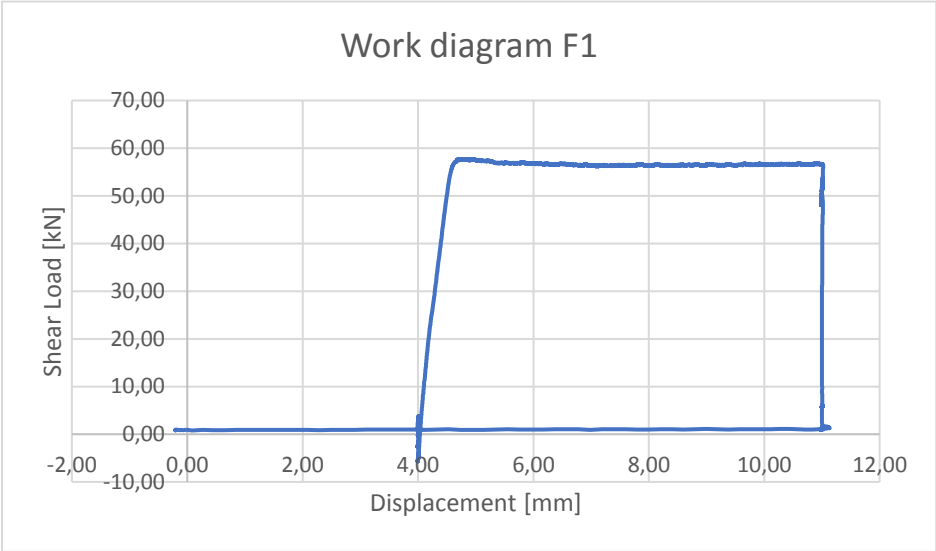
$$\Sigma F_x = 0 \Rightarrow K = V \cdot \frac{\cos(\theta) \sin(\theta) + \cos^2(\theta) \tan(\phi)}{1 - \sin^2(\theta) - \cos(\theta) \sin(\theta) \tan(\phi)} = V \cdot \frac{\sin(\theta) + \cos(\theta) \tan(\phi)}{\cos(\theta) - \sin(\theta) \tan(\phi)}$$

$$\Sigma F_y = 0 = K = V \cdot \frac{1 + \cos(\theta) \sin(\theta) \tan(\phi) - \cos^2(\theta)}{\cos(\theta) \sin(\theta) - \sin^2(\theta) \tan(\phi)} = V \cdot \frac{\cos(\theta) \tan(\phi) + \sin(\theta)}{\cos(\theta) - \sin(\theta) \tan(\phi)}$$

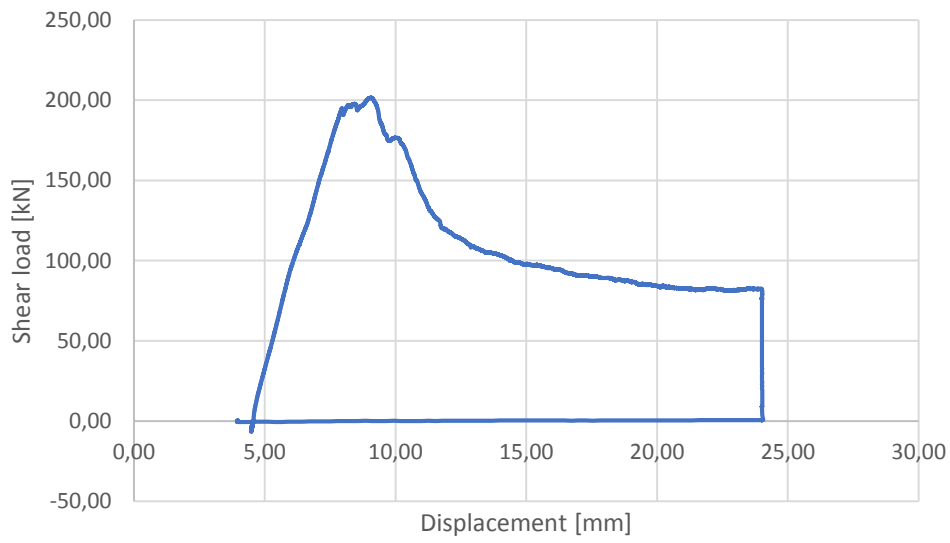
$$\theta = 45^\circ, \phi = 39^\circ \Rightarrow K = V \cdot 9,5$$

Appendix B – Work diagrams based on LVDT measurements

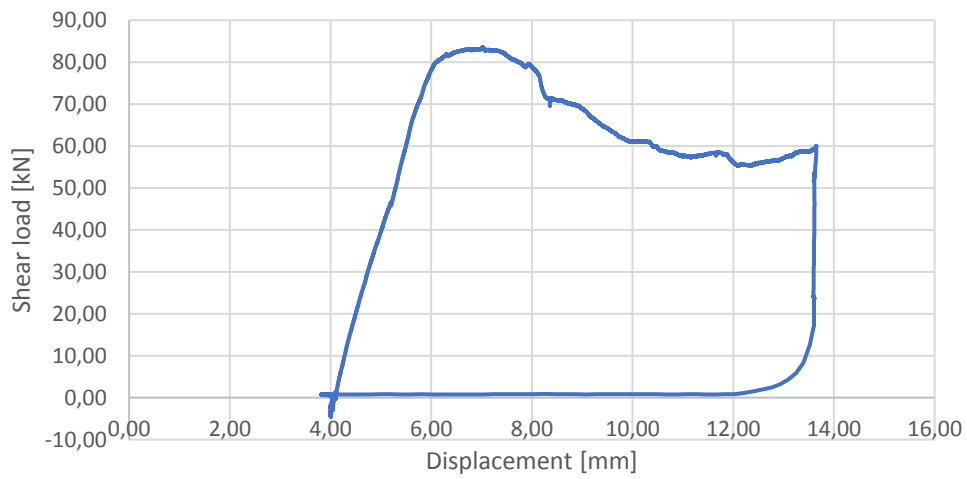
Pure shear samples



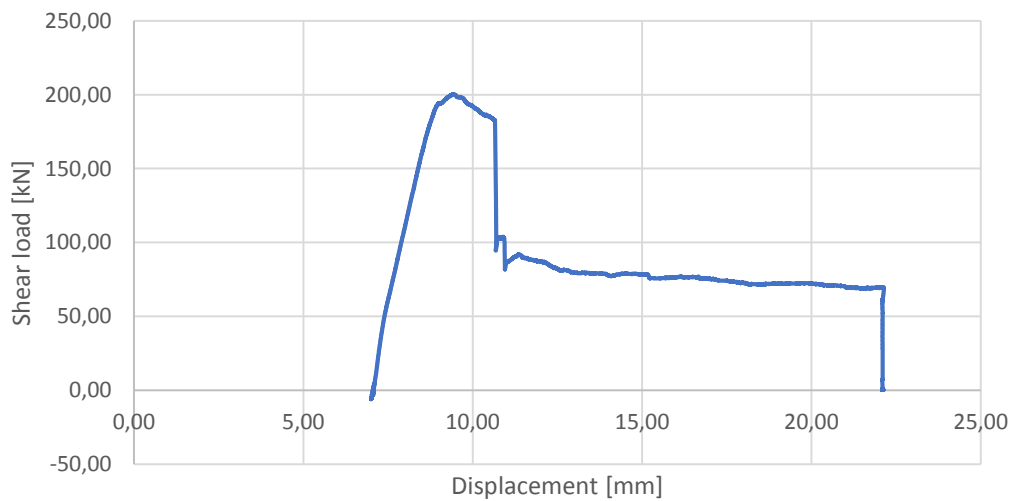
Work diagram M2



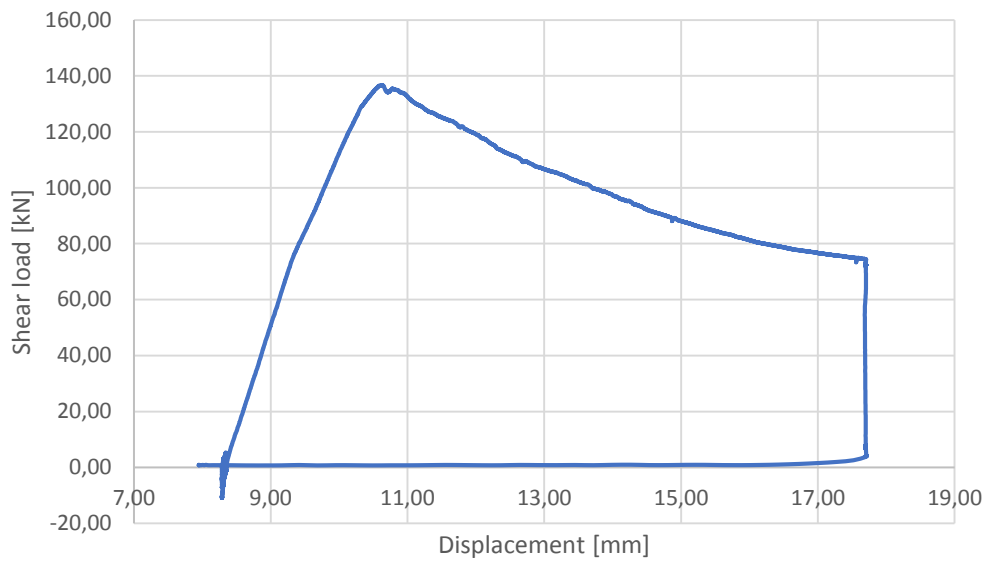
Work diagram M3



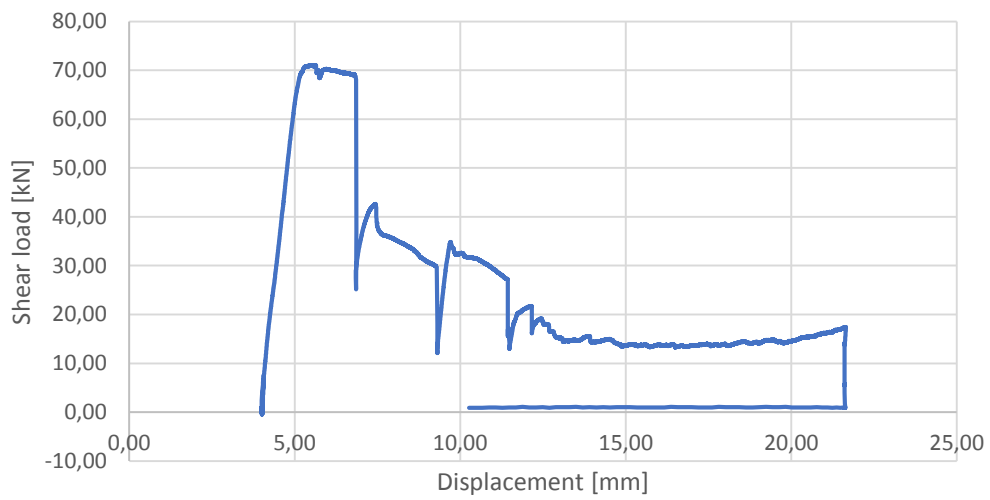
Work diagram E1



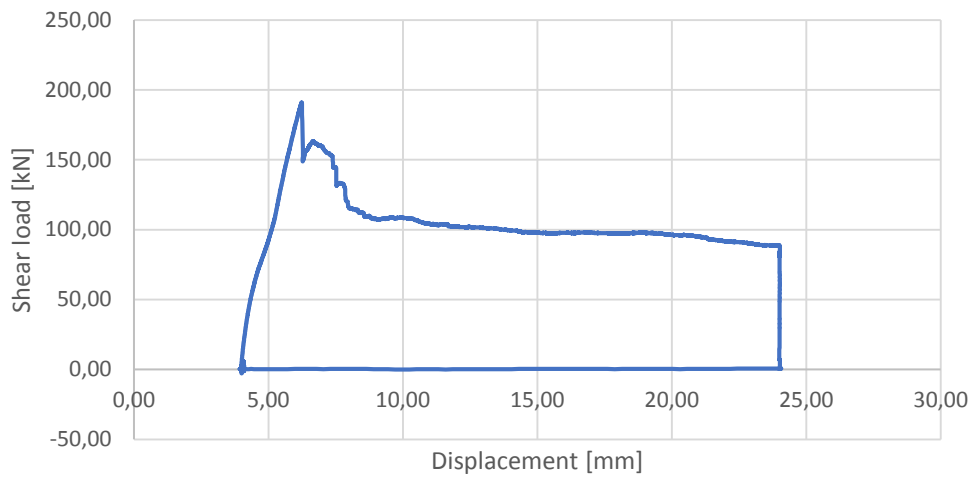
Work diagram E2



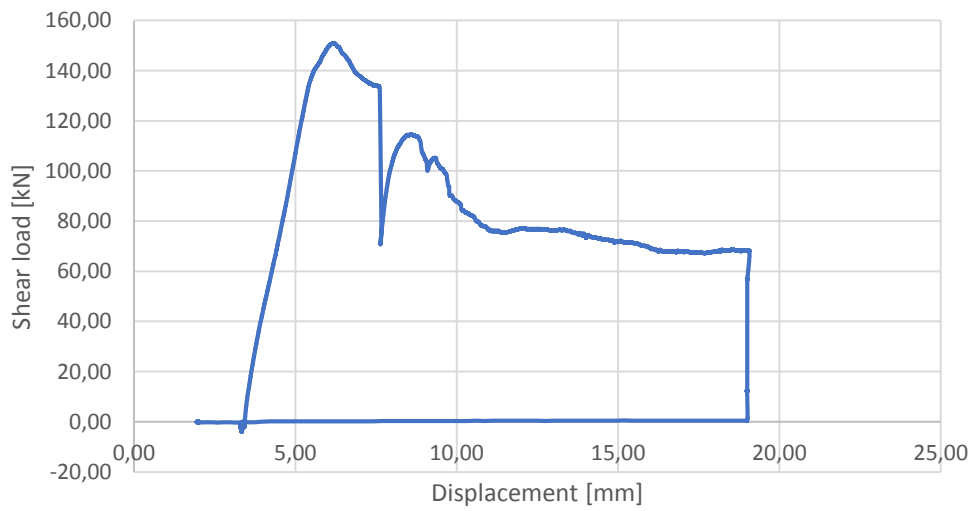
Work diagram E3



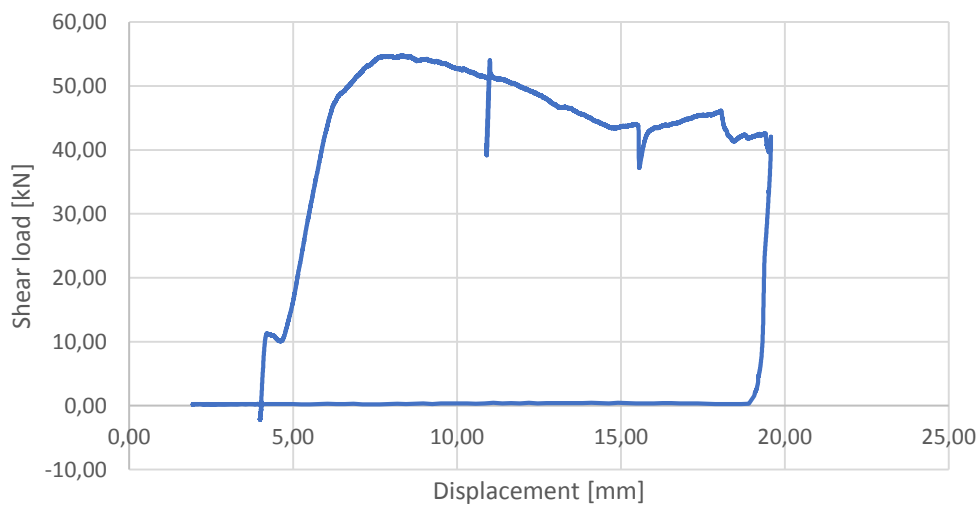
Work diagram E8



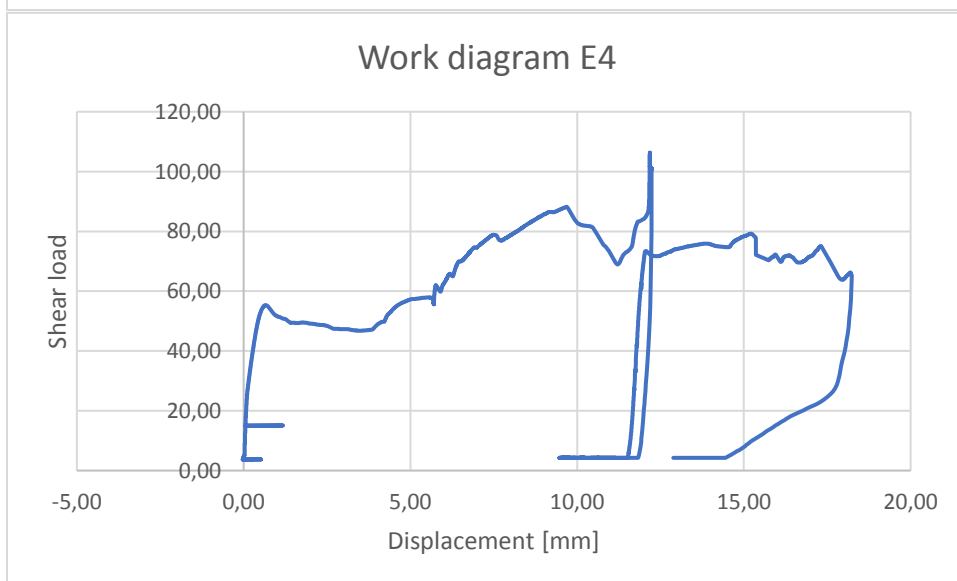
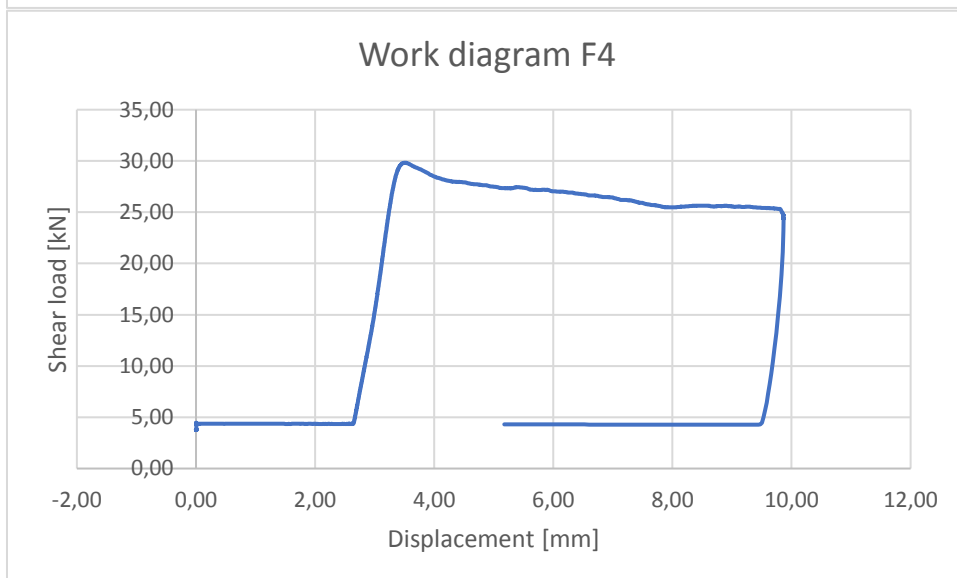
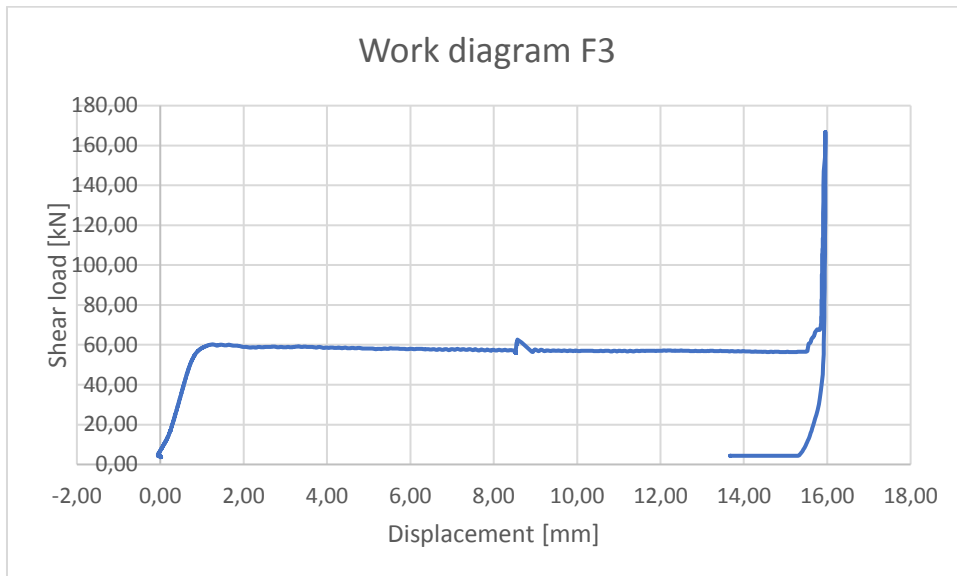
Work diagram E9



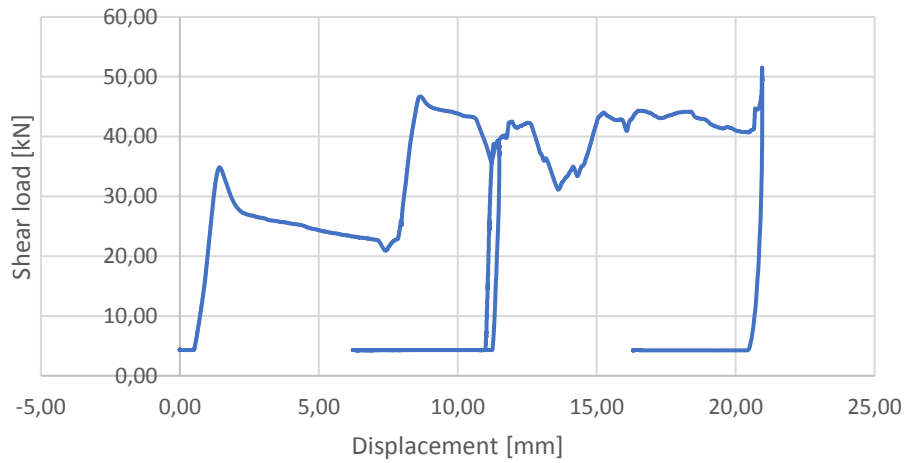
Work diagram E10



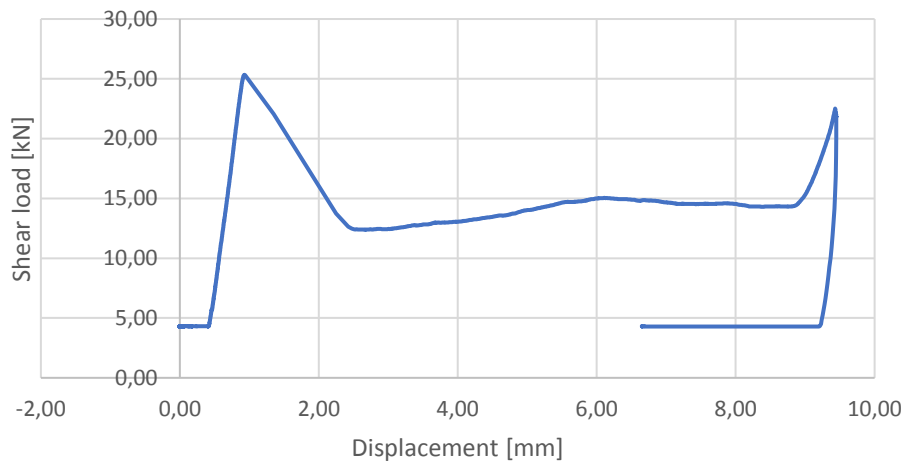
Shear + moment samples



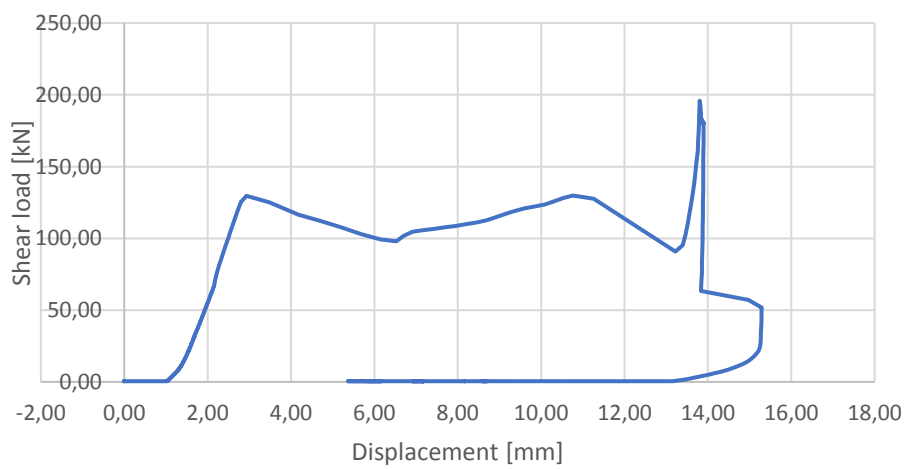
Work diagram E5



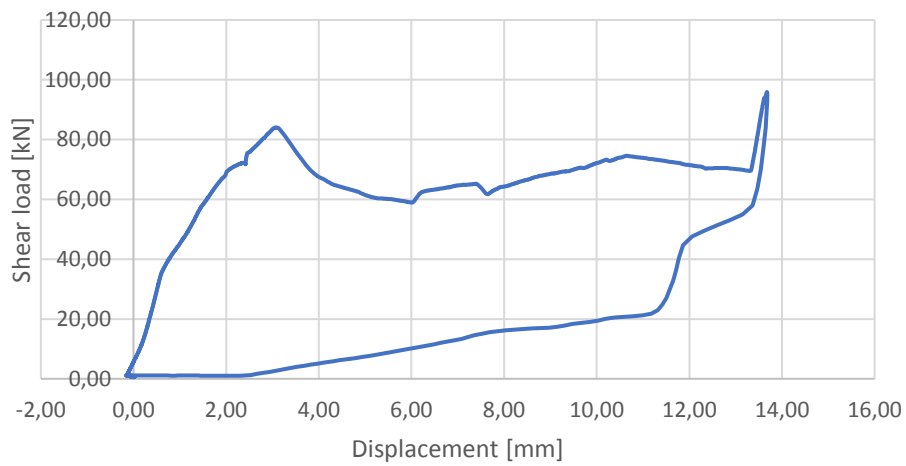
Work diagram E6



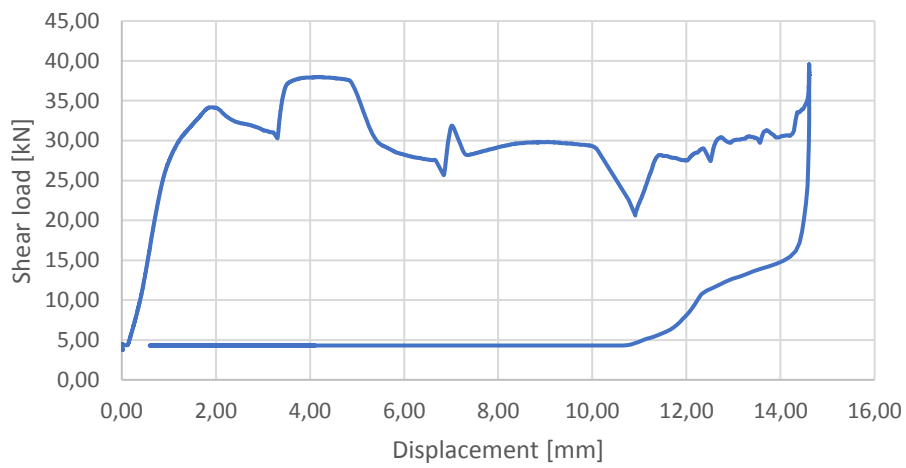
Work diagram M4



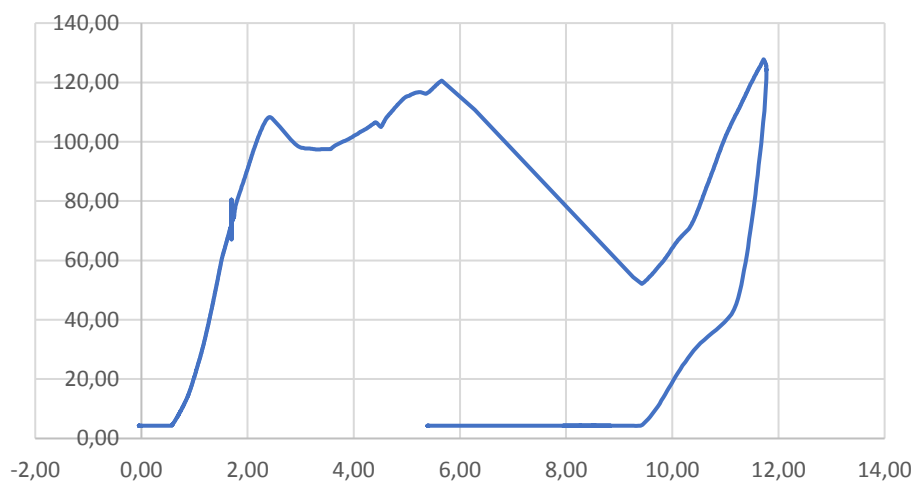
Work diagram M5



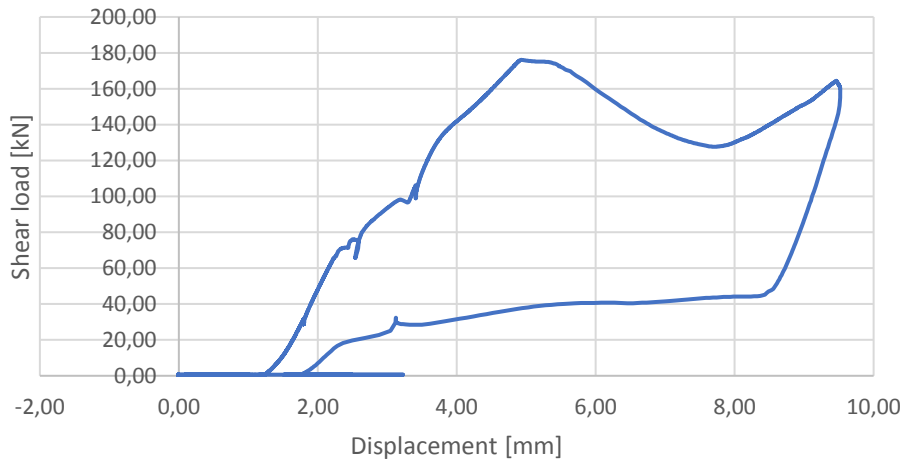
Work diagram M6



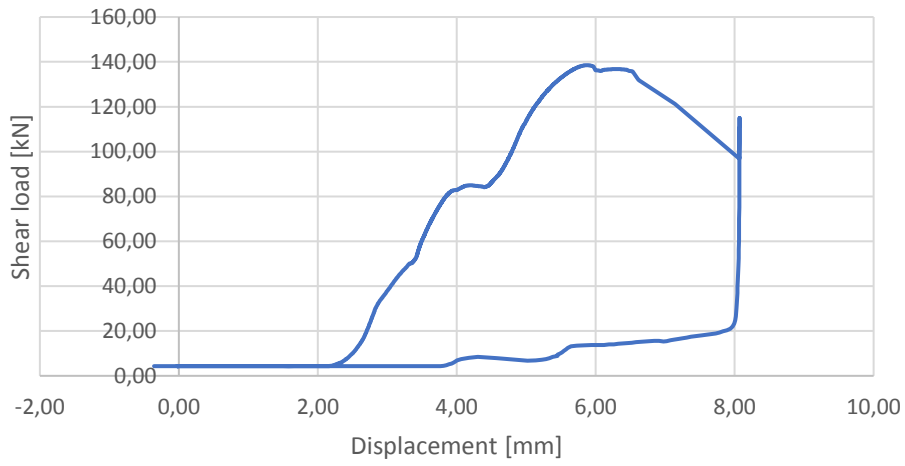
Work diagram M7



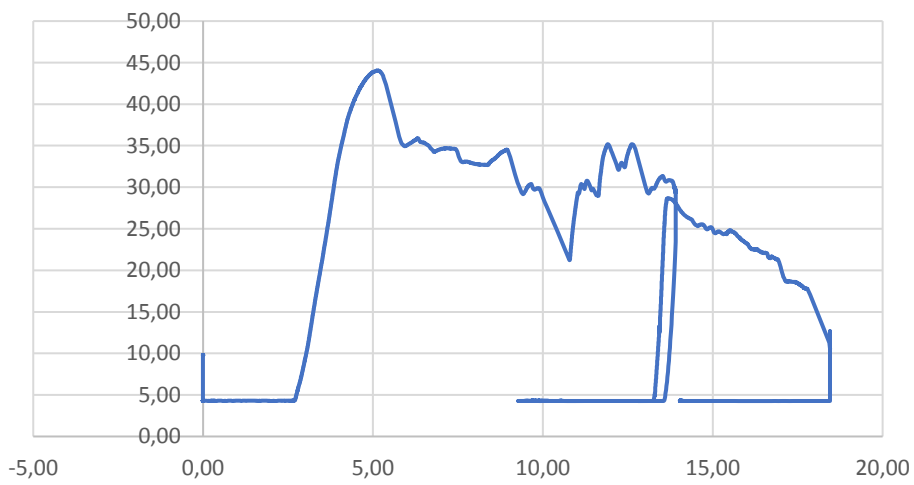
Work diagram E11



Work diagram E12



Work diagram E13



Appendix C – Results from stability assessment of Dam Kalhovd

The results presented here are carried out by Norconsult for Statkraft, who is the dam owner. These results are only a rough estimate of the strength capacity, for use in an early phase of the re-assessment. They are found with the traditional method from the guidelines from the height of the pillars, the inclination of the foundation and a general pillar shape.

Dam Kalhovd - Geometri, stabilitet

Revidert:
2016-09-02



Damseksjon	Oppmåling ¹	Damhøyde ² (m)	Vinkel på glideplan ³ (grader)	Status iht. NVEs krav	Stabilitet glidning/ HRV + Is, S = 1,4	Stabilitet velting/ HRV + Is, S = 1,4	Kommentar
NN. Vederlag	Nei						
Pilar U	Delvis	1,5	15,0	ikke ok	0,57	0,40	Grafisk metode kan vurderes
Pilar 1	Delvis	3	20,0	ikke ok	1,39	0,65	Grafisk metode kan vurderes
Pilar 2	Delvis	4	15,0	ikke ok	1,39	0,85	Grafisk metode kan vurderes
Pilar 3	Delvis	5	5,0	ikke ok	1,09	1,03	
Pilar 4	Delvis	5,0	0,0	ikke ok	0,91	1,03	
Pilar 5	Delvis	4,0	5,0	ikke ok	0,93	0,85	
Pilar 6	Delvis	4,0	5,0	ikke ok	0,93	0,85	
Pilar 7	Delvis	6,0	0,0	ikke ok	1,01	1,20	
Pilar 8	Delvis	6,0	0,0	ikke ok	1,01	1,20	
Pilar 9	Delvis	8,0	20,0	Ok	2,65	1,48	
Pilar 10	Delvis	8,0	0,0	ikke ok	1,15	1,48	
Pilar 11	Delvis	8,0	5,0	≈ Ok	1,38	1,48	
Pilar 12	Delvis	8,0	5,0	≈ Ok	1,38	1,48	
Pilar 13	Delvis	8,0	0,0	ikke ok	1,15	1,48	
Pilar 14	Delvis	8,0	5,0	≈ Ok	1,38	1,48	
Pilar 15	Delvis	7,0	20,0	≈ Ok	2,51	1,35	Grafisk metode kan vurderes
Pilar 16	Delvis	5,0	10,0	ikke ok	1,32	1,03	Grafisk metode kan vurderes
Pilar 17	Delvis	4,0	15,0	ikke ok	1,39	0,85	Grafisk metode kan vurderes
Pilar 18	Delvis	5,0	20,0	ikke ok	2,10	1,03	Grafisk metode kan vurderes
Pilar 19	Delvis	5,0	20,0	ikke ok	2,10	1,03	Grafisk metode kan vurderes
Pilar 20	Delvis	5,0	15,0	ikke ok	1,64	1,03	Grafisk metode kan vurderes
Pilar 21	Delvis	5,0	5,0	ikke ok	1,09	1,03	
Pilar 22	Delvis	5,0	10,0	ikke ok	1,32	1,03	Grafisk metode kan vurderes
Pilar 23	Delvis	5,0	20,0	ikke ok	2,10	1,03	Grafisk metode kan vurderes
Pilar 24	Delvis	5,0	15,0	ikke ok	1,64	1,03	Grafisk metode kan vurderes
Pilar 25	Delvis	6,0	10,0	ikke ok	1,47	1,20	Grafisk metode kan vurderes
Pilar 26	Delvis	6,0	5,0	ikke ok	1,21	1,20	
Pilar 27	Delvis	6,0	10,0	ikke ok	1,47	1,20	Grafisk metode kan vurderes
Pilar 28	Delvis	6,0	0,0	ikke ok	1,01	1,20	
Pilar 29	Delvis	7,0	15,0	≈ Ok	1,96	1,35	Grafisk metode kan vurderes
Pilar 30	Delvis	10,0	10,0	Ok	1,80	2,41	Grafisk kontroll (arbeidstegn.)
Pilar 31	Delvis	8,0	-5,0	ikke bestemt			Bunntappeløp, må vurderes
Pilar 32	Delvis	10,0	-5,0	ikke bestemt			Bunntappeløp, må vurderes
Pilar 33	Delvis	9,0	-10,0	ikke ok	0,85	1,60	
Pilar 34	Delvis	7,5	-15,0	ikke ok	0,67	1,43	
Pilar 35	Delvis	6,0	-10,0	ikke ok	0,73	1,22	
Pilar 36	Delvis	5,0	5,0	ikke ok	1,14	1,06	
Pilar 37	Delvis	5,0	5,0	ikke ok	1,14	1,06	
Pilar 38	Delvis	5,0	0,0	ikke ok	0,95	1,06	
Pilar 39	Delvis	5,0	5,0	ikke ok	1,14	1,06	Arbeidstegning framlagt
Pilar 40	Delvis	6,0	0,0	ikke ok	1,06	1,26	Arbeidstegning framlagt
Pilar 41	Delvis	6,0	15,0	ikke ok	1,88	1,22	Grafisk metode kan vurderes
Pilar 42	Delvis	6,0	0,0	ikke ok	1,04	1,22	
Pilar 43	Delvis	6,0	0,0	ikke ok	1,04	1,22	
Pilar 44	Delvis	6,0	0,0	ikke ok	1,04	1,22	
Pilar 45	Delvis	7,0	-5,0	ikke ok	0,93	1,37	
Pilar 46	Delvis	8,0	0,0	ikke ok	1,16	1,49	
Pilar 47	Delvis	7,0	5,0	ikke ok	1,33	1,37	
Pilar 48	Delvis	6,0	15,0	ikke ok	1,88	1,22	Grafisk metode kan vurderes
Pilar 49	Delvis	6,0	5,0	ikke ok	1,25	1,22	
Pilar 50	Delvis	5,5	-5,0	ikke ok	2,31	1,14	

Pilar 51	Delvis	5,5	20,0	ikke ok	2,31	1,14	Grafisk metode kan vurderes
Pilar 52	Delvis	5,5	20,0	ikke ok	2,31	1,14	Grafisk metode kan vurderes
Pilar 53	Delvis	6,0	10,0	ikke ok	1,52	1,22	Grafisk metode kan vurderes
Pilar 54	Delvis	6,0	5,0	ikke ok	1,25	1,22	
Pilar 55	Delvis	5,0	-5,0	ikke ok	0,80	1,06	
Pilar 56	Delvis	5,0	-5,0	ikke ok	0,80	1,06	
Pilar 57	Delvis	5,0	5,0	ikke ok	1,14	1,06	
Pilar 58	Delvis	5,0	-10,0	ikke ok	0,67	1,06	
Pilar 59	Delvis	5,0	5,0	ikke ok	1,14	1,06	
Pilar 60	Delvis	5,0	5,0	ikke ok	1,14	1,06	
Pilar 61	Delvis	5,0	5,0	ikke ok	1,14	1,06	
Pilar 62	Delvis	5,0	5,0	ikke ok	1,14	1,06	
Pilar 63	Delvis	4,0	0,0	ikke ok	0,84	0,87	
Pilar 64	Delvis	4,0	-5,0	ikke ok	0,70	0,87	
Pilar 65	Delvis	4,0	5,0	ikke ok	1,00	0,87	
Pilar 66	Delvis	4,0	20,0	ikke ok	1,93	0,87	Grafisk metode kan vurderes
NN Vederlag	Nei						

1) Visuell vurdering av glideplan (revurderingsbefaring 28/9-2015)

2) Høyde er avstand fra damkrone kt. +1086,60/+1086,90 til fjell ved oppstrøms eller nedstr. damtå.

3) Glideplan mot berg, 0 grader er horisontalt, - betyr fall fra magasinet og + betyr fall mot magasin.